

# **A New Compact Broadband Radial Power Combiner**

vorgelegt von  
M.Sc.  
**Mehdi Ghanadi**  
aus Teheran

Von der Fakultät IV – Elektrotechnik und Informatik  
der Technischen Universität Berlin  
zur Erlangung des akademischen Grades

Doktor der Ingenieurwissenschaften  
Dr.-Ing.

genehmigte Dissertation

Promotionsausschuss:  
Vorsitzender: Prof. Dr.-Ing. W. Heinrich  
Berichter: Prof. Dr.-Ing. H. Henke  
Berichter: Prof. Dr. A. Banai

Tag der wissenschaftlichen Aussprache: 30.11.2011

Berlin 2012

D83



## **Zusammenfassung**

Die vorliegende Doktorarbeit beschreibt das Design und den Aufbau eines neu entwickelten N-Wege Radial-Power-Combiners in Mikrostreifenleitungstechnik. Die Verwendung von Mikrostreifenleitungen auf dünnen Substraten führt zu einem kompakten Aufbau, geringem Gewicht und niedrigen Herstellungskosten und damit zu signifikanten Vorteilen gegenüber axialen Leistungsummierern. Der N-Wege Radial-Power-Combiner summiert die Leistung der N-Eingangsports ohne Zwischenstufen direkt in einem Schritt. Hieraus resultiert ein hoher Wirkungsgrad und eine sehr kompakte Bauweise.

Im Rahmen der Arbeit wurde ein vollständiges analytisches Modell für einen 8-Wege-Breitband-Combiner entwickelt und die Ergebnisse für den Frequenzbereich 2-17GHz vorgestellt. Zum Vergleich wurde eine numerische Simulation mit der Software HFSS durchgeführt und die ursprünglichen Ergebnisse für den Frequenzbereich 2-17GHz auf beste Performance optimiert.

Zwei 8-Wege Radial-Power-Combiner wurden aufgebaut und vermessen. Über die gesamte Bandbreite war die erzielte Rückflussdämpfung besser als 10dB und die Einfügedämpfung kleiner als 1.5dB.

Als Funktionstest wurde mit diesen Combinern die Leistung von 8 Breitbandverstärkern zu je 0.12W zu einer Gesamtausgangsleistung von 0.7W summiert. Die Ergebnisse sind auf Gesamtausgangsleistungen bis 100W übertragbar. Die durchgeführten Messungen stimmten mit den theoretischen Ergebnissen überein und bestätigten somit die Genauigkeit des Design- und Optimierungsprozesses.



## **Abstract**

The N-way radial power combiner sums the power of N devices directly in one step without having to proceed through several combining stages. This results in high combining efficiencies and in a compact mechanical form.

This dissertation presents a technique for the design of an N-way wideband microstrip radial power combiner which offers some advantages over axial power combiners. Thin microstrip lines in the combiner structure lead to low manufacturing costs and compact size and weight. A full analytical study is done and results are presented for an 8-way broadband microstrip radial power combiner operating from 2GHz to 17GHz. Also a full wave simulation using HFSS is done and the initial results are optimized for best performance.

A couple of radial power combiners were built and measured: The achieved return loss is above 10dB and the insertion loss is below 1.5dB over the full bandwidth. These combiners were used to combine the outputs of 8 broadband amplifiers to produce a total output power of around 0.7W.

For both passive and active stages, the obtained measurement results well validate the design and optimization processes.



## Table of contents:

1 Overview of N-Way Power Combining Techniques .....	1
1.1 TWTs and SSPAs .....	2
1.2 Power combining techniques .....	3
1.2.1 Multi step power combiners.....	8
1.2.1.1 Chain combiner.....	8
1.2.1.2 Corporate combiners.....	9
1.2.2 N-way combining strategies.....	11
1.3 Radial power combiners.....	17
1.3.1 Cavity-based radial combiners.....	18
1.3.2 Non-resonant radial power combiners .....	19
1.3.2.1 Axially conical symmetric combiners. ....	19
1.3.2.2 Microstrip line combiners.....	20
1.4 Spatial power combining architectures.....	26
1.4.1 Tile amplifiers .....	28
1.4.2 Tray amplifiers.....	29
1.4.2.1 Waveguide spatial power combining.....	30
1.4.2.2 Coaxial waveguide spatial power combiner.....	31
1.5 Comparison between N-way combining methods.....	35
2 Radial Power Combining Modeling Methods.....	37
2.1 Scattering matrix properties of lossless N-way power combiner.....	37
2.2 Eigenvalue equation analysis.....	39
2.3 Planar analysis for microstrip radial power combiner.....	44
2.4 Equivalent model analysis for junction.....	47
2.5 Cavity type combiner analysis methods.....	47
3 Design and Optimization of Microstrip 8-Way Radial Power Combiner.....	49
3.1 8-way radial power combiner scattering matrix properties.....	50
3.2 Design method for microstrip radial power combiner.....	53

3.2.1	Splitting/combining pad design.....	55
3.2.2	The junction analysis.....	60
3.2.3	Design of output matching network.....	68
3.3	Total structure simulation.....	70
3.4	Mechanical structure.....	75
3.5	Measurement results.....	80
4	Integration of Broadband Amplifiers into the Radial Power Combiner .....	85
4.1	Theory of combination.....	85
4.2	Simulations.....	90
5	Conclusion.....	95
	Appendix.....	96
	References.....	98

**List of figures:**

Fig1.1. Average output power of tube Amplifiers and SSPA [1], [2]... 3

Fig1.2. A view of device level combining in a power transistor chip. 16 FET cells are combined in a parallel configuration.....3

Fig1.3. Combining techniques classification diagram. ....4

Fig1.4. Combining loss versus RMS phase error for a 4-way power combiner.....7

Fig1.5. A chain combining structure .....9

Fig1.6. Combining efficiency for the chain combining structure. Loss in decibels refers to the loss in each power path in each stage’s coupler. ....9

Fig1.7. The corporate combiner architecture. The amplifiers are successively combined using two-way combiners .....10

Fig1.8. General 2 way corporate (binary) combining.....10

Fig1.9. Combining efficiency for a corporate combining structure (“Loss” indicates loss per stage).....11

Fig1.10. Efficiency comparison between typical N-way combiner and typical corporate combiner.....12

Fig1.11. A general scheme of resonant cavity combiners.....13

Fig1.12. An S-band 32 port coaxial cavity combiner [4]. N symmetrical ports with the identical probes are located around the internal cavity. ....13

Fig1.13. A scheme and photo of 32-way waveguide cavity combiner [5]. ....14

Fig1.14. Wilkinson N-way combiner. ....15

Fig1.15. A microstrip radial power combiner. Microstrip ports are located symmetrically around the central port [10].....16

Fig1.16. Examples of non-radial power combiner. Some structures have used holes that are etched in the middle of the conductor pattern to equalize the signal path lengths from the input port to the output ports [11]. ....16

Fig1.17. Rucker’s 5-way combiner. In this combiner five diode oscillators are combined in a radial structure [12]. ....17

Fig1.18. The first type of radial power combiners, which is a 12-way microstrip radial power combiner that contains some isolation resistors. Central port is connected to a coaxial connector at the other side of the structure[14]. ....18

Fig1.19. Basic configuration of the conical power combiner [16]. ....20

Fig1.20. Measured insertion loss and simulated and measured reflection coefficient at the central output port for the conical power combiner [16]. ....20

Fig1.21.	The 4-way radial microstrip combiner that was presented by Abouzahra in [17]. .....	21
Fig1.22.	Theoretical results for the Abouzahra 4-way power combiner [17].	21
Fig1.23.	An 8- way microstrip power combiner [18].	22
Fig1.24.	Simulated and measured results of the 8-way microstrip power combiner in[18] .....	22
Fig1.25.	Fathy’s 30-way microstrip radial power combiner with isolation resistors [10].	23
Fig1.26.	Central port measurement and simulation results for Fathy microstrip radial power combiner [10]. The large microstrip circular matching patch reduces the combiner’s bandwidths. ....	23
Fig1.27.	A general scheme of radial two step power combiner. ....	24
Fig1.28.	Calculated and measured $S_{11}$ and $S_{21}$ for the 14-way two step power combiner presented in [19]. ....	24
Fig1.29.	The structure of Haifeng radial two step power combiner [20]. ....	25
Fig1.30.	Spatial power combining concept, each element consists of one amplifier, the input and the output antenna. ....	26
Fig1.31.	Spatial power combining architectures. In the tile approach the elements are located in one plate and in the tray method the elements are located in the parallel plates [23].	27
Fig1.32.	Spatial power combiner classification.....	27
Fig1.33.	In grid approach devices are integrated at the vertical and horizontal intersections [23].....	28
Fig1.34.	In array approach separate antenna elements are integrated directly with active devices and each element acts as an independent device [23]. ....	29
Fig1.35.	Waveguide spatial combiner [24]. The power combiner consists of several active arrays that are inserted in a standard waveguide. ....	30
Fig1.36.	The concept of a coaxial waveguide spatial N-way power combining[21]. ....	31
Fig1.37.	Schematic of an oversized coaxial waveguide combiner [21]. ....	32
Fig1.38.	Tray design for the modular spatial coaxial combining system [21]. ....	32
Fig1.39.	Some pictures of coaxial waveguide spatially power combining [21].	33
Fig1.40.	Dissipative loss for 16- and 32-tray combiners with 50-Ohm microstrip through line in place of the active device [21]. ....	33
Fig1.41.	Output return loss measurement for 16- and 32-tray combiner [21]. ....	34

Fig2.1.	A general N-way radial power combiner, (a) Top view (b) Side view. $R_1$ is the $360/N$ degree rotational operator .....	39
Fig2.2.	General N-way microstrip disc junction with the central axial port. ....	45
Fig2.3.	Parameters of the circumferential ports. ....	46
Fig2.4.	Theoretical and experimental results for the ten-way radial power combiner [17]. .....	46
Fig2.5.	N-way radial cavity power divider/combiner. ....	47
Fig3.1.	Bulky coaxial waveguide combiner (left) [21] and not fully wideband conical radial power (right) [16]. ....	49
Fig3.2.	General 8-way radial power combiner and its port configuration. Ports are spaced 45 degrees apart. ....	50
Fig3.3.	The equivalent circuit model for the junction of coaxial and microstrip patch. ....	53
Fig3.4.	A model for the coaxial/radial line structure. Each microstrip radial power combiner consists of three main sections: the common port transition or launcher, the non-planar junction and the N-way planar splitter/combiner. ....	54
Fig3.5.	A transmission line N-Way power combiner. ....	55
Fig3.6.	A linear matching network in a two port microstrip line. ....	56
Fig3.7.	Simulation results for linear microstrip impedance transformer (50 ohm to 100 ohm) for three different lengths. ....	57
Fig3.8.	Eight taper lines that are connected to the junction point. ....	58
Fig3.9.	AWR Microwave Office simulation results for ideally connected taper lines. ....	58
Fig3.10.	A simple 8 way combiner with the output matching. ....	59
Fig3.11.	Simulation results for a simple 8-way combiner with output matching section (Fig3.10 ) and without matching section ( Fig3.8 ). ....	60
Fig3.12.	The junction and coaxial contact, “p” is the circular radius and “h” is the substrate thickness ,”b” and “a” are the outer and inner radius of coaxial conductors respectively. .....	60
Fig3.13.	The equivalent model for the junction. ....	61
Fig3.14.	Equivalent values of the junction for $b=2.1\text{mm}$ and $1.5\text{mm}<a<2\text{mm}$ . ....	63
Fig3.15.	Ratio of imaginary part over real part of $Z_{cj}$ versus frequency for $Z_j = 1$ .....	64

Fig3.16.	Combiner response with and without junction effect. The junction is modeled by equivalent circuit model without optimization. ....	65
Fig3.17.	HFSS model for the junction (left) Radial combiner top view (right).....	66
Fig3.18.	Full wave simulation results for 8 way junction. Port (1) is considered as central port. ....	66
Fig3.19.	Full wave junction model is inserted in Fig3.10 circuit. ....	67
Fig3.20.	Comparison between the ideal junction combiner and the combiner with full wave junction model.....	67
Fig3.21.	Linear taper coaxial matching network. ....	68
Fig3.22.	Multi section impedance matching network. ....	69
Fig3.23.	linearly tapered and step tapered coaxial line with 30mm length. ....	69
Fig3.24.	Comparison between equal length linear and multi step taper coaxial lines. ....	69
Fig3.25.	A drawing of microstrip power combiner with its important parameters. ....	70
Fig3.26.	Microstrip radial power combiner model in HFSS. ....	72
Fig3.27.	Simplified structure using H-planes symmetry. ....	72
Fig3.28.	HFSS simulation results for the simplified structure using H-plane symmetry.....	73
Fig3.29.	Complete structure simulation results. ....	73
Fig3.30.	Common port to other port coupling simulation results. ....	73
Fig3.31.	Ports isolation simulation results ( $ S_{23} $ , $ S_{34} $ , $ S_{45} $ , $ S_{56} $ , $ S_{67} $ , $ S_{78} $ , $ S_{89} $ ). ....	74
Fig3.32.	Port isolation simulation results ( $ S_{24} $ $ S_{25} $ $S_{26}$ ). ....	74
Fig3.33.	The magnitude of the electric field in the combiner at 10GHz.....	75
Fig3.34.	A view of radial power combiner and its mechanical structure. ....	76
Fig3.35.	A cut view of the radial power combiner. ....	76
Fig3.36.	Modified SMA connector contact to microstrip transition. ....	77
Fig3.37.	HFSS simulation results for the modified SMA connector to microstrip transition. ....	77
Fig3.38.	Walls in the upper housing. This walls help in better attachment, create more spatial isolation between ports and decrease unwanted resonance frequencies. ....	78
Fig3.39.	Top view of the manufactured microstrip radial power combiner. Holes around the junction are provided to send out extra solder or epoxy in the attachment process. ....	78
Fig3.40.	Bottom side of the manufactured microstrip radial power combiner. ....	79
Fig3.41.	Tapered coaxial center conductor used for output matching. ....	79
Fig3.42.	Common port measured $ S_{11} $ in the epoxy attachment method. ....	80
Fig3.43.	Common port measured $ S_{11} $ in soldering attachment method. ....	81

Fig3.44.	Comparison between simulated and measured combiner response. ....	81
Fig3.45.	Two combiners are connected back to back to measure the combiner loss. ....	83
Fig3.46.	MMIC placement in combiner. ....	83
Fig3.47.	Measured insertion loss for two back to back combiners. ....	84
Fig4.1.	General radial power combiner network .....	85
Fig4.2.	Output power and harmonics and definition of IP3.....	87
Fig4.3.	Linearity analysis for the MMIC amplifier and the combiner.....	88
Fig4.4.	Gain and return loss for HMC463 (die).....	90
Fig4.5.	Measured response for HMC463 with connectors.....	90
Fig4.6.	The measured gain (Amplitude and phase) for eight amplifiers .....	91
Fig4.7.	Eight amplifiers are combined with 3D model of radial power combiner.....	92
Fig4.8.	Simulation results for the combined amplifiers.....	92
Fig4.9.	Eight amplifiers are integrated into radial power combiner. The divider is placed behind the combiner .....	93
Fig4.10.	Comparison between simulated and measured results for eight combined amplifier .....	94
Fig4.11.	Measured maximum output power for the combined amplifiers.....	94
Fig5.1.	The original conical radial power combiner [16] .....	96
Fig5.2.	The modified conical radial power combiner .....	96
Fig5.3.	Simulation results for the original and the modified conical radial power combiner.....	97

**List of tables:**

Table 1.1	Summarizes the specifications of tray and tile architectures. ....	35
Table 1.2	Comparison table between various types of power combiners. ....	36

## **Preface**

High power broadband amplifiers are a crucial element for a variety of electronic and telecommunication systems. However, the product of power and bandwidth is fixed for a specific amplifying device, that is, the broader the bandwidth, the less the output power. Hence, a variety of broadband power combining techniques has been developed for achieving higher output power than is available from a single device.

The conventional staged combining techniques are not efficient for more than eight amplifiers, but the N-way combining structure sums the power of the N devices directly in one step without having to proceed through several combining stages. This opens the possibility to achieve high combining efficiencies.

Large numbers of compact N-way power-combiners have been presented in recent years but many of them are designed for narrowband applications. The intent of this research is to extend the radial power combiner to a broadband application, high efficiency and compact size while maintaining a low cost.

The thesis is organized in the following way. Chapter 1 describes various types of N-way power combiners and their advantages over conventional combining techniques.

Chapter 2 follows with the modeling of radial power combiners. Several methods are presented for analyzing the combiner. One is finally applied to the microstrip radial power combiner as the chosen type for our ultimate purpose.

Chapter 3 develops a practical design method for the microstrip radial power combiner. Finally it is simulated and optimized using HFSS software and measurements are compared with simulated results.

In Chapter 4, eight amplifiers are integrated into the combiner. 15 GHz bandwidth (2 GHz to 17 GHz) is achieved with near 0.7 watt of output power. Chapter 5 concludes the work and presents potential improvements.

# 1 Overview of N-Way Power Combining Techniques

Power amplifiers are one of the most important parts of microwave systems. In the past years, the Traveling Wave Tube (TWT) has become an important part of microwave systems for radar, satellite communication and wireless communication. However, by the development of solid state power amplifiers, the attractiveness of TWT's decreases and high power SSPA's become interesting candidates in high power application.

Power, bandwidth, efficiency, linearity and noise are the most important features in high power amplifier design. Perfect realization of all these features in one amplifier- especially a high power amplifier- is a difficult task for RF engineers. On the other hand by the development of the broad band application, demand of broadband amplifier and power combiner has increased. Commercially available broadband MMIC (Microwave Monolithic Integrated Circuit) chips offer about 1 Watt power levels. For example, HMC797 from Hittite and TGA2509 from Triquint, have 28dBm, and 29dBm output power in a bandwidth of 2 ~20 GHz, respectively. Other devices like travelling-wave tube amplifiers provide high power but are limited in bandwidth. So there is a need for ways to overcome this kind of limitation and develop new techniques for broadband power amplifiers.

Broadband power combining techniques as a solution for broadband power amplifiers are introduced for combining the output power of a large quantity of lower power amplifier circuits in a broadband environment. In this chapter, various methods of combining the output power of a large number of MMIC amplifiers will be presented and their efficiency and bandwidths will be compared.

## **1.1 TWTs and SSPAs**

Vacuum electronic amplifiers are used in a wide variety of military and commercial microwave systems and applications which require high power at high frequency such as millimetre wave band. Klystron, magnetron, and crossed field amplifier (CFA) are the primary products of today's industry.

The advance in tube technology has improved the efficiency of the TWT amplifier up to 70% for narrow band and 50% for broadband, which is the current best solution for space satellite transponders. However, the drawbacks of the TWT amplifiers are also obvious, such as considerable size and weight. Tube amplifiers also need the high voltage drive - Electronic Power Conditioner (EPC) that requires additional complex accessory circuit and involves high voltage risk. Moreover, the tube amplifier is always rated with saturation power, which leads to bad linearity and is not good for broadband communication. To work linearly, the TWT amplifier is normally backed off from its saturated output power or additional linearization circuits are added. On the other hand, linearization circuitry results in dramatic increase of system complexity and cost, therefore each small increase in efficiency is very expensive. A high efficiency high power TWT amplifier in satellite may cost up to half a million dollars [1].

On other side, improvements in solid-state material and amplifier have pushed the output power level of a single MMIC to the watt level. For instance, there is a commercially available MMIC amplifier that can output more than 10 Watts over X band. However, with the advent of high-power solid-state devices, it is still difficult and costly at the present time to realize significant RF output power at a single device.

Fig1.1 shows the availability of power amplifiers and TWTs versus frequency and power[2]. In summary, the advantages and disadvantages of TWAT and SSPA are as follow:

### **TWT's advantages:**

Higher power, higher efficiency, smaller size and lower weight

### **TWT disadvantages:**

Lower bandwidths, lower life time, noise, need to additional high voltage circuits, poor linearity

### SSPA advantages:

Higher Reliability and longer lifetime, easier manufacturability, better noise performance and higher bandwidth

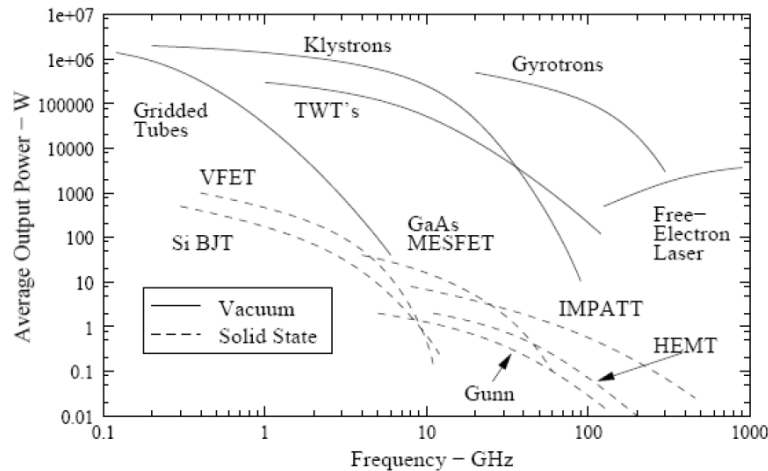


Fig1.1. Average output power of tube Amplifiers and SSPA [1], [2].

## 1.2 Power combining techniques

Power combining can be considered on two general levels: the device level and the circuit level [3]. In device level combining approach, a group of active devices are arranged (for example in a parallel configuration) in small region compared with a wavelength. Device level combining is generally limited in the number of devices that can be efficiently combined. Fig1.2 shows the device level combining in a power transistor.

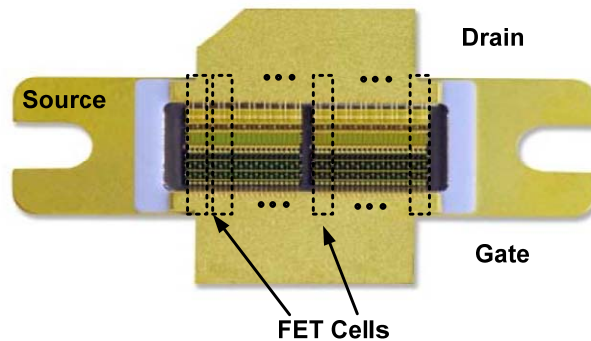


Fig1.2. A view of device level combining in a power transistor chip. 16 FET cells are combined in a parallel configuration.

In the circuit level, devices can be combined by various types of combining methods like Wilkinson combiner. Although the number of combining ports in circuit level are limited, but by selecting the proper strategy higher output power is achievable.

Circuit level combining approaches can be separated into two general categories, those which combine the output of N devices in a single step and those which do not. The former are called N-way combiners and will be further discussed in this section. The latter category of combiner is simpler and more widely used. It includes the chain (serial) and tree (corporate) combining structures [3].

In the circuit level combining method the output of N amplifiers are combined in a medium such as a microstrip, coaxial or a waveguide. In another method, known as spatial power combining, the outputs of amplifiers are combined in the space. However this method can be placed in N-way combining group. The N-way combiners also can be divided into cavity resonant and non-resonant combining structures. Fig1.3 shows the various combining methods in a simple chart.

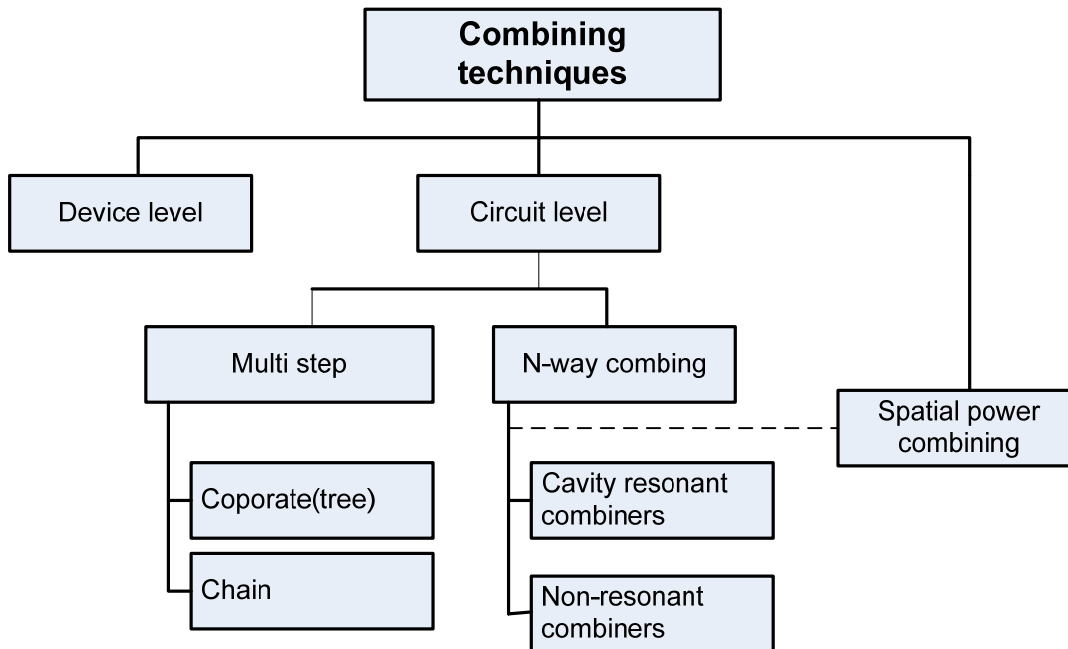


Fig1.3. Combining techniques classification diagram.

### **Some consideration for combiner design**

Some parameters should be considered as a key specification in combiner/divider design.

These parameters are described below :

**Bandwidth:** The bandwidth of many schemes is very narrow, and in some cases this is not important. But for wideband applications, this parameter becomes a main criterion for many circuit designs.

**Efficiency:** Maintaining low loss in a combiner is very important especially when output power is high.

**Size:** The size of combiner will be a function of the technique, as well as the medium. For example, a radial combiner using microstrip lines will be much smaller than a waveguide radial combiner.

**Isolation:** Isolation is one of the most important specifications of a combiner network. Ideally we don't want any of the amplifiers to "see" each other. In practice, it is often difficult to achieve 20dB isolation between all branches, which might be enough. The most common problem due to poor isolation in a combiner is that spurious oscillations can occur.

**Graceful degradation:** When power sources are combined (power amplifiers driven at the same phase angle), if the isolation is enough, an amplifier can fail in the network and output power of the network will degrade gracefully. However, it isn't as simple as calculating the fraction of power amplifiers that are left operating. In an N-way combiner, if one or more amplifiers fail, the output power will (ideally) be reduced by the square of the fraction of working amplifiers. For example, one failure out of eight results in 76.6 % power. One failure out of four results in 56.3% power. If one amplifier fails in a two-way combiner, you only have 25% of the original combined power.

Amplitude errors: Variations in amplitude also cause a loss in power in a SSPA.

Phase errors: A power-combined amplifier will have phase errors, and these will cause loss of power. Phase errors can occur within the power splitter, the individual amplifiers, or the power combiner.

To calculate the effect of phase error on the combiner efficiency, consider a two-way power combiner with the combined signal as follow:

$$E(t) = e_1 \cos(\omega t + \phi_1) + e_2 \cos(\omega t + \phi_2) \quad (1-1)$$

Where  $e_1, e_2$  are the maximum amplitude of the individual signals and  $\phi_1, \phi_2$  are their phases. We are concerned about the effects of phase errors, so for simplicity let  $e_1 = e_2 = e$ . The average power of  $E(t)$  can be written as follow:

$$p = \overline{E(t)^2} / Z_0 = (e^2 / Z_0) [1 + \cos(\phi_1 - \phi_2)] \quad (1-2)$$

Where,  $Z_0$  is the characteristic impedance. Now assume that the phase error  $\delta\phi = \phi_2 - \phi_1$  is a normally distributed, zero mean random variable with variance  $\sigma^2 = \langle \delta\phi^2 \rangle$ . Then the expected value of the power density is

$$\langle P \rangle = (e^2 / Z_0) (1 + \langle \cos \delta\phi \rangle) = (e^2 / Z_0) (1 + e^{-\sigma^2/2}) \quad (1-3)$$

Where we have used the identity  $\langle \cos x \rangle = e^{-\sigma_x^2/2}$  where  $\sigma_x$  is the standard deviation of  $x$ . Since the maximum value of  $\langle P \rangle$  is  $P_{\max} = 2e^2 / Z_0$  then

$$\langle P \rangle / P_{\max} = \frac{1}{2} (1 + e^{-\sigma^2/2}) \quad (1-4)$$

More generally, the phase combining loss factor for  $N$  identical inputs in an  $N$ -way power combiner is given by [35]

$$\langle P \rangle / P_{\max} = \frac{1}{N^2} \sum_k \sum_m e^{-\sigma_{km}^2/2} \quad (1-5)$$

Where  $k$  and  $m$  range over the  $N$  inputs and  $\sigma_{km}^2$  is the variance of the phase difference at the output port of the signals from inputs  $k$  and  $m$ .

In the special case that each combiner input has a phase error independent of the others and all errors are identically distributed with variance  $\sigma_0^2$ , the variances of the phase differences (relative to the baseline) are all  $\sigma_{km}^2 = 2\sigma_0^2$  when  $k \neq m$ . Then

$$\langle P \rangle / P_{\max} = \frac{1}{N^2} [N + \sum_k \sum_{m \neq k} e^{-\sigma_0^2}] = \frac{1 - e^{-\sigma_0^2}}{N} + e^{-\sigma_0^2} \quad (1-6)$$

For example Fig1.4 is a plot of the loss for a 4-way power combiner as a function of the RMS phase error of each input port.

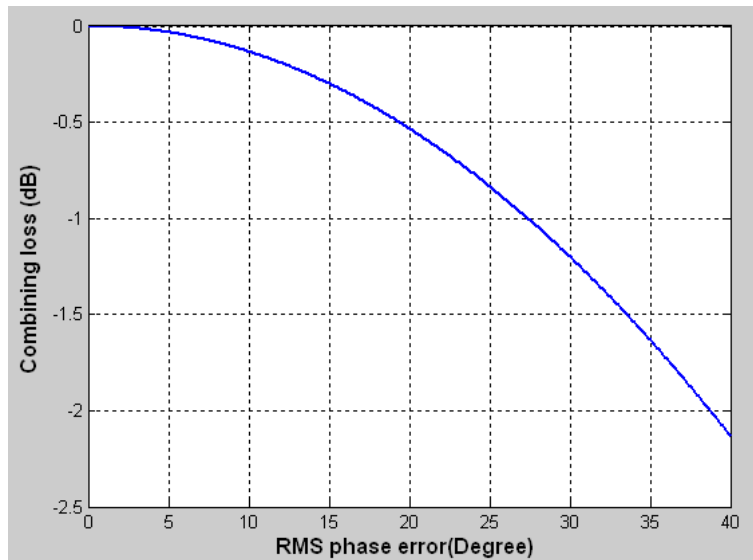


Fig1.4. Combining loss versus RMS phase error for a 4-way power combiner.

## 1.2.1 Multi step power combiners

### 1.2.1.1 Chain combiners

A chain or serial combiner is shown in Fig1.5. Here, for an N-stage combiner each successive stage or coupler adds 1/N of the output power to the output. The number of the stage determines the required coupling coefficient for that stage, as indicated in the Fig1.5. The choice of coupling coefficients is also affected by the loss in the coupler. Neglecting losses, the necessary coupling coefficient for the  $N_{th}$  stage is  $10 \log N$  in decibels [3]. One advantage of the chain configuration is that another stage can be added by simply connecting the new source to the line after the  $N_{th}$  stage through a coupler with  $10 \log(N + 1)$  coupling coefficient. The chain combining approach is non-binary, and, in principal, any number could be combined. Losses in the couplers reduce the combining efficiency and bandwidth attainable with this approach. Also, it is difficult to build the couplers with the high coupling coefficients necessary when larger numbers of devices are to be combined. The combining efficiency  $E_c$  can be estimated by assuming that the losses in each coupler are divided equally between the two paths of power flow through the coupler. A coupler, when viewed as a power splitter, divides the input power equally or unequally, depending on its design, into two output ports. The roles of input and output ports are interchanged when the coupler is used as an adder, but the two paths of power flow are the same although the direction of flow is reversed. The following equation shows the combining efficiency [3]:

$$E_c = \frac{1}{N} \left[ 10^{(N-1)L/10} + \sum_{k=0}^{N-2} 10^{(1+k)L/10} \right] \quad (1-7)$$

Where L is loss of couplers in dB and N is number of stages. This relation is plotted in Fig1.6 for several values of loss L per path. It is obvious that the combining efficiency decreases by an increase in the number of devices.

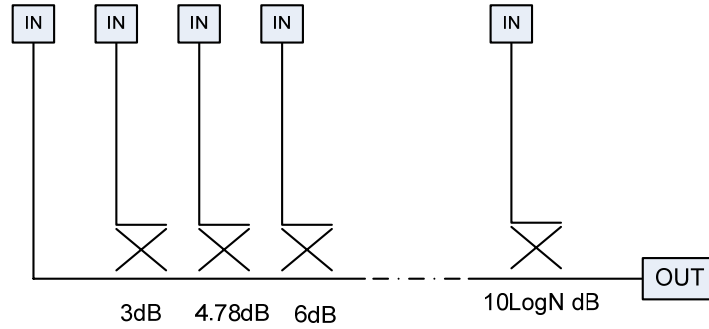


Fig1.5. A chain combining structure.

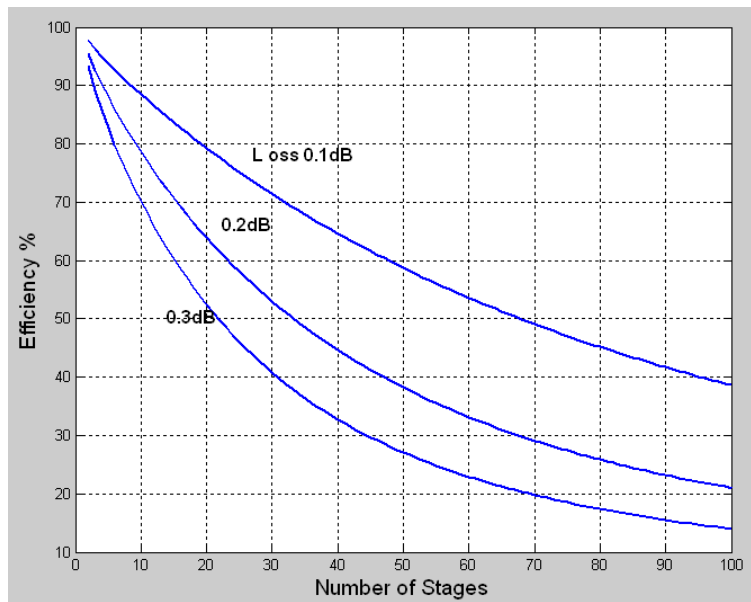


Fig1.6. Combining efficiency for the chain combining structure. Loss in decibels refers to the loss in each power path in each stage's coupler.

### 1.2.1.2 Corporate combiners

Other type of circuit level combiners is corporate or binary combiner. The general scheme of corporate combiners is shown in Fig1.7. To satisfy system requirements, power from many individual devices must be added coherently. As shown in Fig1.8, the outputs from multiple circuits are successively combined using two-way adders such as Wilkinson combiners. The number of individual devices is  $2^N$ , where N is the number of stages. The combining efficiency is therefore  $E_c = L^N$ , where L is the insertion loss of

each stage. Note that the physical layout of the corporate combiners with many elements causes the transmission line length in the last stages of combining to become very long. As the number of devices increases, the losses in these lines become insurmountable. As shown in Fig1.9, loss of the combining circuit will increase dramatically and consequently the output power decreases.

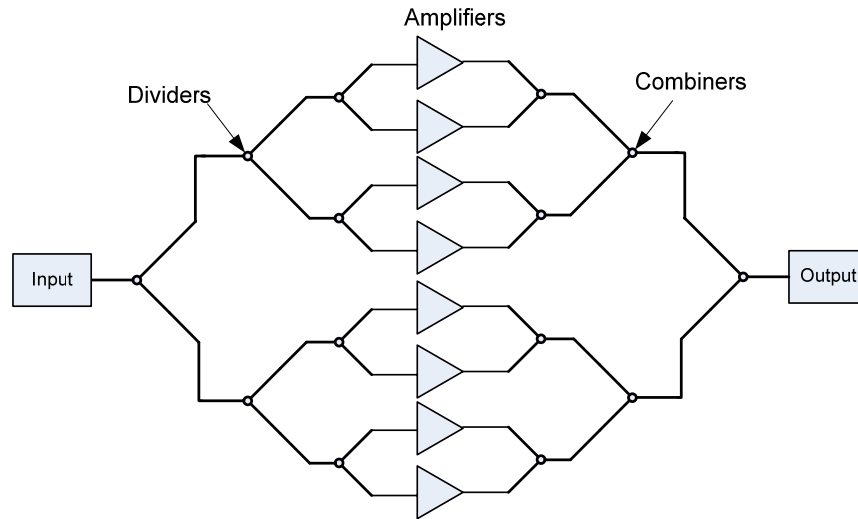


Fig1.7. The corporate combiner architecture. The amplifiers are successively combined using two-way combiners.

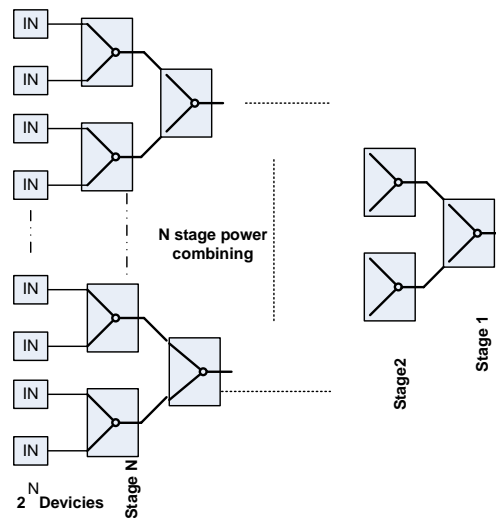


Fig1.8. General  $2^N$  - way corporate (binary) combining.

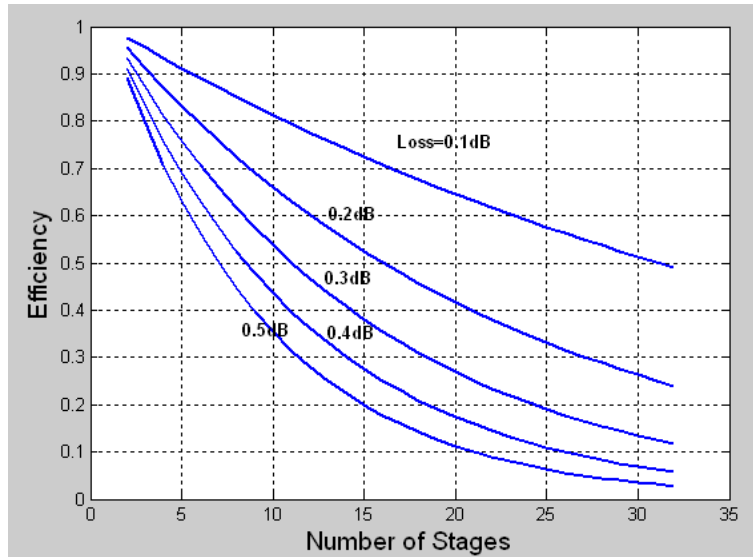


Fig1.9. Combining efficiency for a corporate combining structure (“Loss” indicates loss per stage)

The chain or tree combining structures can be realized in a number of different transmission media such as microstrip, coaxial line, or waveguide. The choice of the transmission media heavily impacts the resulting size and circuit losses. With microstrip, combiners are the most compact and with waveguide, they have the lowest loss.

### 1.2.2 N-way combining strategies

High losses associated with circuit combining schemes can be avoided with the N-way or spatial combining technique since the power is combined in a low loss electric medium or in a lossless space.

The N-way combining structure sums the power of the N devices directly in one step without having to proceed through several combining stages. This opens the possibility of such structures having high combining efficiencies since the power does not have to pass through several stages of combiners. Fig1.10 shows a comparison between typical binary and typical N-way combiners.

The N-way combiners can be further divided into two categories, cavity resonant and non-resonant combining structures.

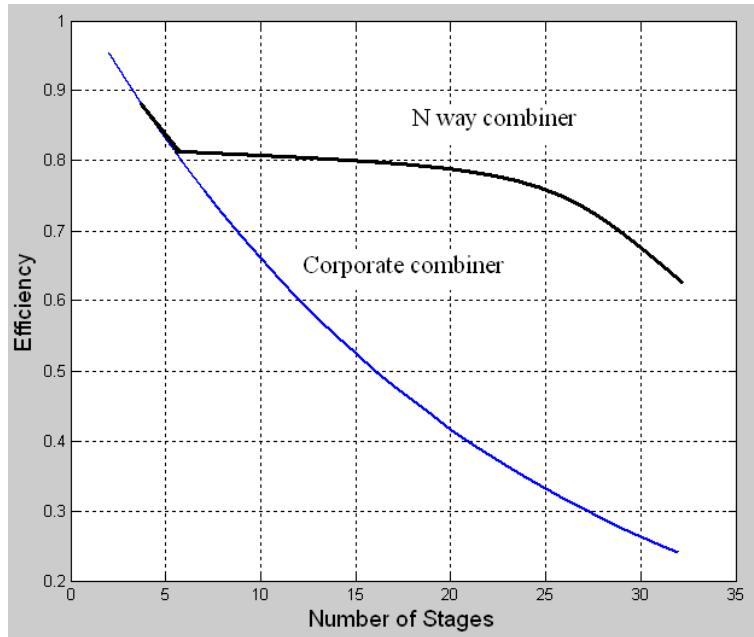


Fig1.10. Efficiency comparison between typical N-way combiner and typical corporate combiner.

#### A. Cavity combining structures

In this category of power combiners, the sum of output powers from a number of devices is obtained by coupling their outputs to a single resonator (see Fig1.11 ). Because of their resonant nature, these types of combiners have narrow bandwidths. The medium of the cavity can be a coaxial or a waveguide, but in both of them N input ports excite a single cavity.

A coaxial cavity combiner is shown in Fig1.12 . It is built around a planar radial cavity which comprises of one central and N symmetrically located peripheral probes. The peripheral probes are identical in shape and size. However, the dimensions of the central probe may differ from those of the peripheral probes. The probe configurations may be in the form of posts loaded with discs. The probes are energized from coaxial entries or from equivalent gaps in the ports.

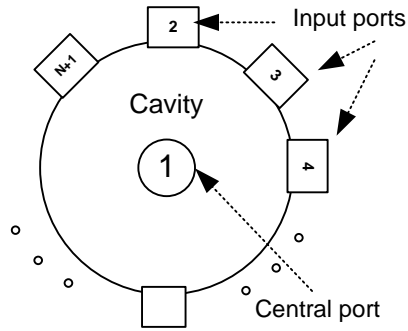


Fig1.11. A general scheme of resonant cavity combiners.

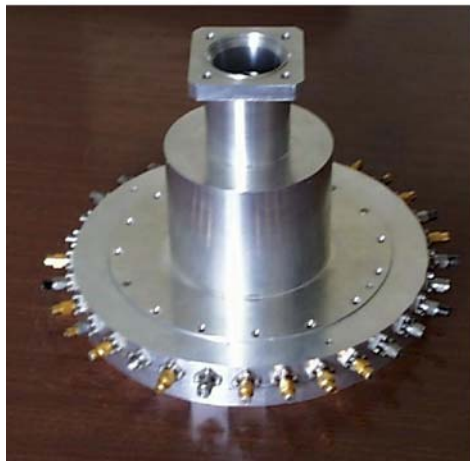
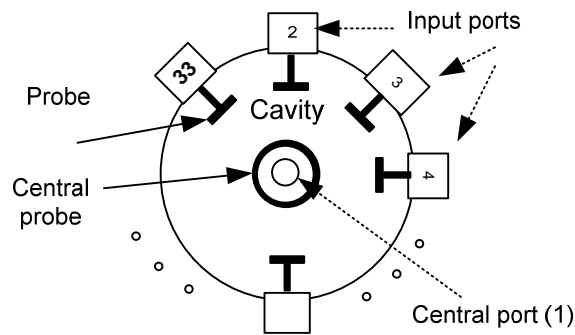


Fig1.12. An S-band 32 port coaxial cavity combiner [4].  $N$  symmetrical ports with the identical probes are located around the internal cavity.

A scheme of waveguide cavity combiner is presented in Fig1.13. In this combiner  $N$  symmetrical input waveguide ports excite the internal cavity. Because of symmetrical shape, a circular waveguide port is located in the center of cavity as output port. Waveguide combiners are known as bulky structures especially for low frequency bands and so they are more common in upper frequency band like Ku, K, Ka.

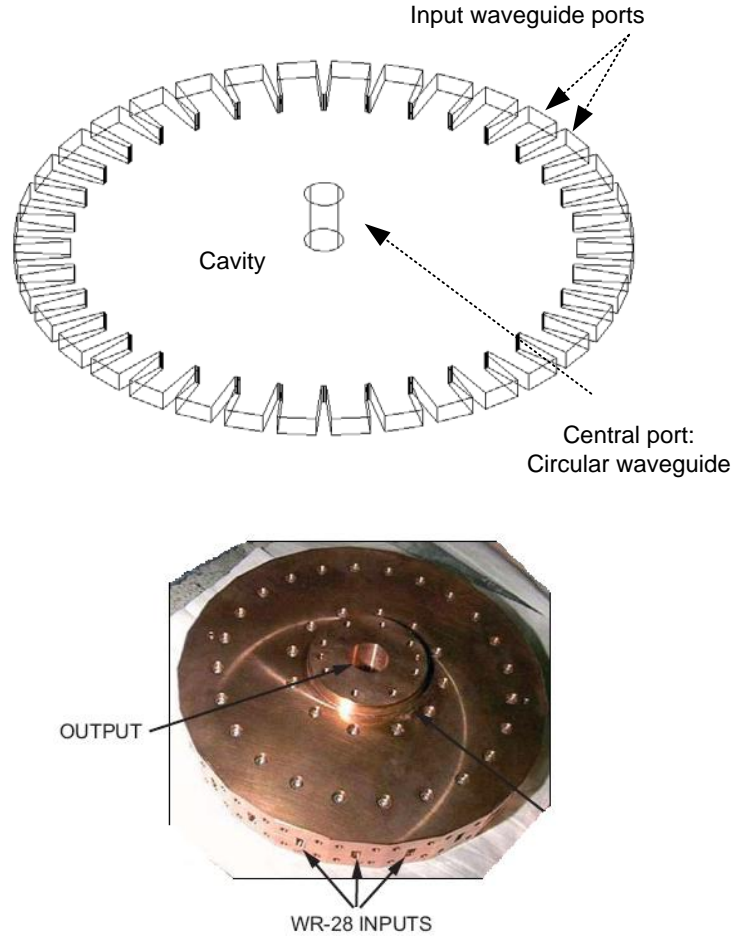


Fig1.13. A scheme and photo of 32-way waveguide cavity combiner [5].

### B. Non-resonant combining structures

Non-resonant combining techniques usually use transmission lines in their combining path. Because of their non-resonant structure, they offer the wide-band operation. One of the oldest and best known of these structures is the Wilkinson N-way combiner [6]. The concept for the combiner is illustrated in Fig1.14. The input ports (of impedance  $Z_0$ ) feed into N output lines of characteristic impedance  $\sqrt{N}Z_0$  which are one-quarter-wavelength long. Isolation between the N-ports is accomplished by means of the resistive star connected to the N-ports. The best known version of the Wilkinson circuit is the two-way combiner. The principal problem with the Wilkinson approach at high frequencies is that

it is generally not possible to connect sufficiently powerful isolation resistors in the manner shown when  $N > 2$ . Nor can the resistors be connected as shown when planar circuits are used (except for the two-way Wilkinson). Accordingly, a number of modifications of the concept have been suggested over the years [7]–[9].

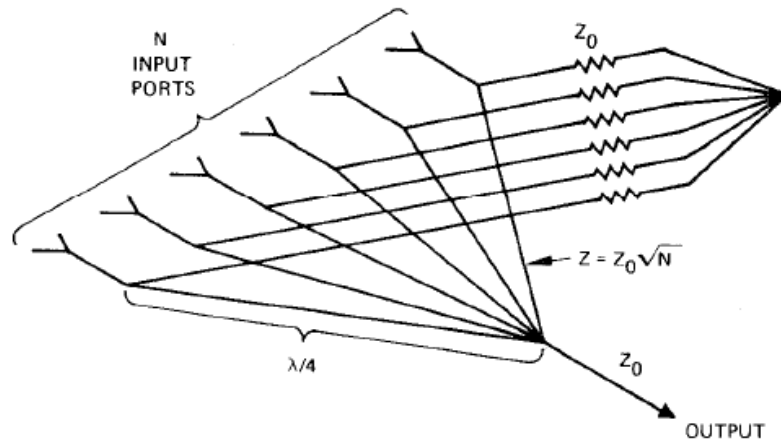


Fig1.14. Wilkinson N-way combiner.

N-way combiners can be radial or non-radial. Fig1.15 and Fig1.16 show some radial and non-radial planar N-way combiners respectively. In radial configuration, N ports are located symmetrically around the central port, while in the non-radial combiners there is no symmetry between the input ports.

One type of non-radial microstrip combiners is presented in [11] (see Fig1.16 e). This power combiner was simulated with parametric analysis and a working prototype at 25–31 GHz is designed and fabricated with four amplifier units. For this combiner a combining efficiency of 79.5% is achieved at 25 GHz.

But most of N-way combiners are radial combiners. Because in a radial structure, there is more space for combining higher number of amplifiers and the symmetry between all input ports is more convenient. Regardless of choosing resonant cavity combining or non-resonant combining, in most cases, radial structures are preferred over other types, due to their simple design and easily achievable phase balancing between their ports.

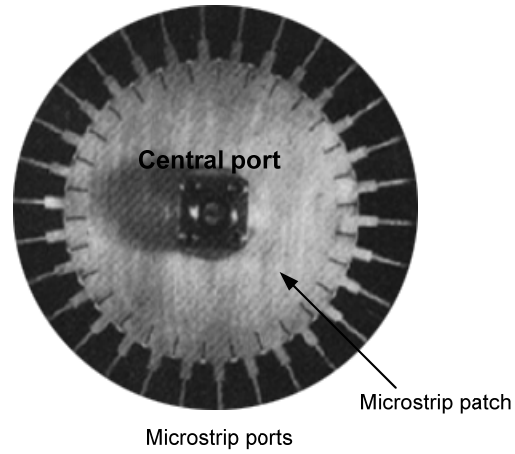


Fig1.15. A microstrip radial power combiner. Microstrip ports are located symmetrically around the central port [10].

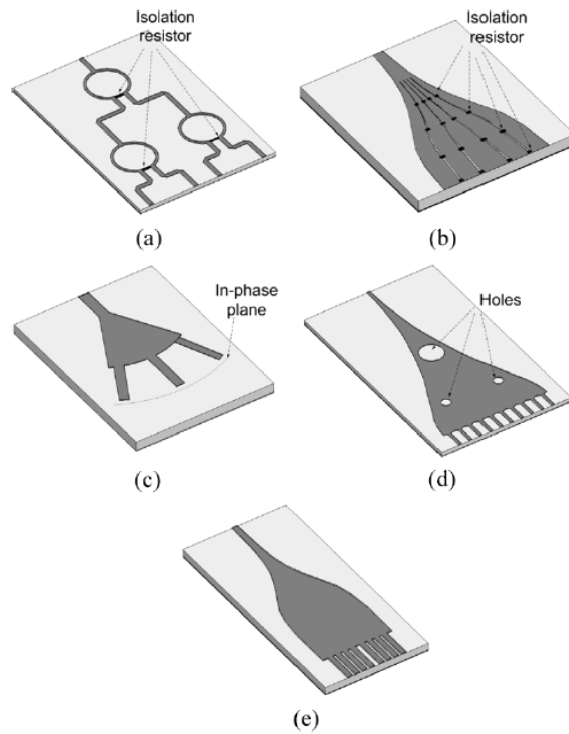


Fig1.16. Examples of non-radial power combiner. Some structures have used holes that are etched in the middle of the conductor pattern to equalize the signal path lengths from the input port to the output ports [11].

### 1.3 Radial power combiners:

In a radial power combiner,  $N$  input ports are located symmetrically around the central part of the combiner, which sums the power of the  $N$  ports directly in one step and delivers the total power to the central port. “One step combining” has shorter distances, hence lower combining loss, between  $N$  ports and the central port. This method also increases the bandwidth because signals don’t have to pass through several combining stages.

Radial power combiners can have two categories, cavity or non-resonant, similar to the categorization of  $N$ -way combiners, as mentioned before.

Another classification for  $N$ -way power combiners is based on their medium, which can be a microstrip, strip line or a waveguide. In the microstrip medium, the propagation mode is TEM but in the waveguide medium non-TEM modes are excited. In comparison with a non-TEM combiner, TEM combiner can provide wider RF bandwidths.

One of the oldest and best known radial power combiner structure is the Wilkinson  $N$ -way combiner [6]. Another traditional radial combining structure was introduced by Rucker [12] and later analyzed by Kurokawa [13]. In that technique, 5-diode oscillators with coaxial transmission lines, each approximately one-quarter-wavelength long, were radially combined (see Fig1.17).

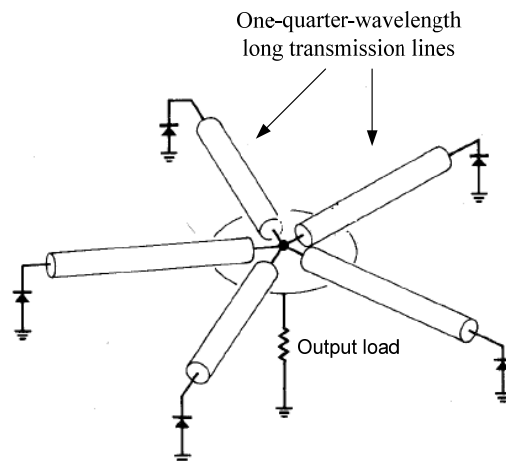


Fig1.17. Rucker’s 5-way combiner. In this combiner five diode oscillators are combined in a radial structure[12].

An example of X-band 12-way radial combiner was reported in [14]. Fig1.18 shows this type of combiner. The combiner uses radially sectored dielectric-filled transmission lines for the power divider/combiner structures. The combiner has demonstrated a combining efficiency of 87.4 percent with a 1-dB bandwidth greater than 2GHz at 8.5 GHz (23%). By using resistors, the isolation between the peripheral ports ranged from 13dB (for the nearest neighbors) to 22dB depending upon the relative ports positions.

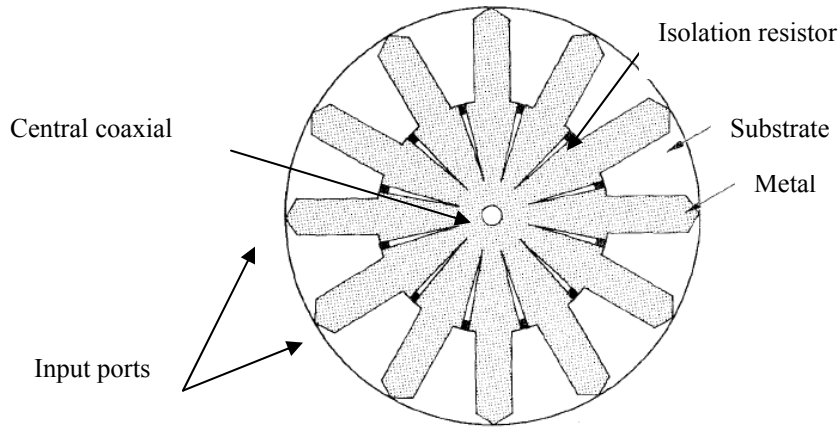


Fig1.18. The first type of radial power combiners, which is a 12-way microstrip radial power combiner that contains some isolation resistors. Central port is connected to a coaxial connector at the other side of the structure[14].

### 1.3.1 Cavity-based radial combiners

Cavity-based radial power combiners are usually used in narrowband applications and present low insertion loss in their bandwidths. Two examples of cavity-based combiners are waveguide and substrate integrated waveguide (SIW) radial power combiners. A Ka-band waveguide combiner is presented in [5]. The proposed architecture can combine 32 individual monolithic microwave integrated circuits (MMICs) with 80 percent combining efficiency in frequency band from 31GHz to 36 GHz.

A compact radial cavity power combiner based on the substrate integrated waveguide (SIW) technology is also presented in [15]. The measured insertion loss is approximately 0.2 dB in 500 MHz bandwidths.

Because of their limited bandwidths, we are not interested in waveguide and SIW radial power combiners.

### **1.3.2 Non-resonant radial combiners**

A number of non-resonant combining techniques have been proposed in previous years. Because of their non-resonant structure, they offer wider bandwidths and can be connected to wide-band amplifiers. In these combiners, the energy travels in a radial direction between a central port and axially symmetric peripheral ports. The final structure of each combiner depends on the type of the in-between transmission lines. Several examples of non-resonant radial power combiners will be discussed in the following sections.

#### **1.3.2.1 Axially conical symmetric combiners**

A conical power combiner is one type of transmission line combiners. In the first glance this combiner is similar to a cavity radial combiner but in fact it uses the conical transmission lines. These transmission lines have a significant advantage over cavities because they support a transverse electromagnetic (TEM) mode and, therefore, have constant characteristic transmission line impedance along propagation direction. This greatly simplifies the simulation and design of the structure for broadband applications. It also allows for a simpler broadband coaxial-to-conical line transition.

An axially symmetric power combiner, which utilizes a tapered conical impedance matching network to transform ten 50- Ohm inputs to a central coaxial line over the X-band was build in [16]. Fig1.19 shows the structure of this combiner. The combiner is fed by ten axially symmetric peripheral coaxial lines, each connected to a probe which couple energy magnetically into a conical transmission line. This conical transmission line terminates to a coaxial air line at its apex. Stepped impedance matching networks were incorporated into the central and peripheral feeding coaxial lines. The bandwidth of 47% was achieved with a minimum return loss of 18.5 dB from 7.7 to 12.4 GHz. The maximum loss in the operating band is 0.28 dB, and the average loss is only 0.18 dB. Fig1.20 shows the measurement results.

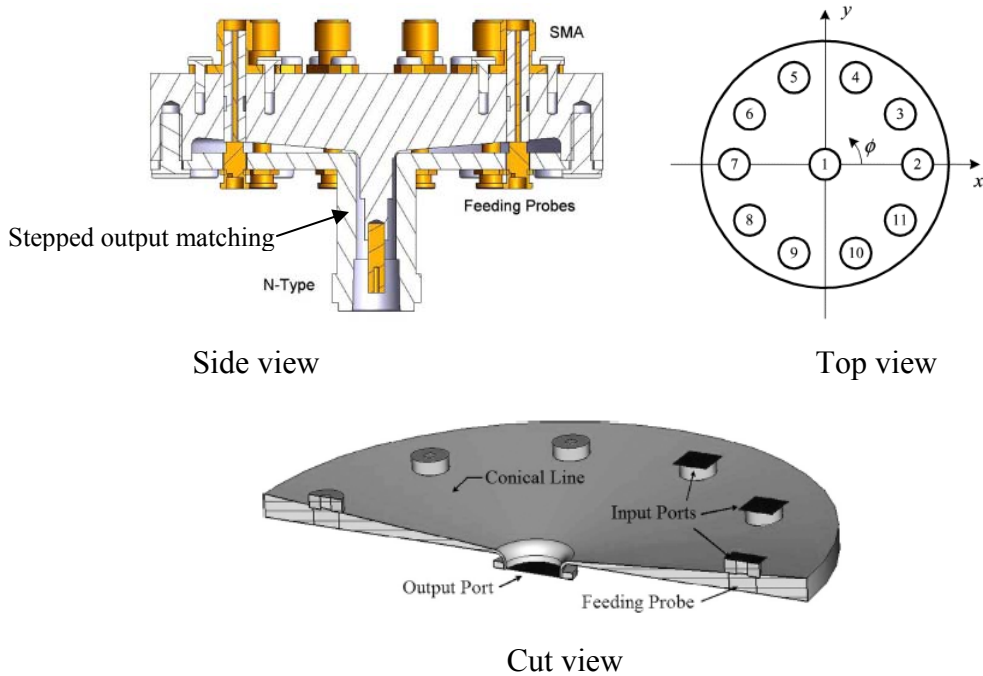


Fig1.19. Basic configuration of the conical power combiner [16].

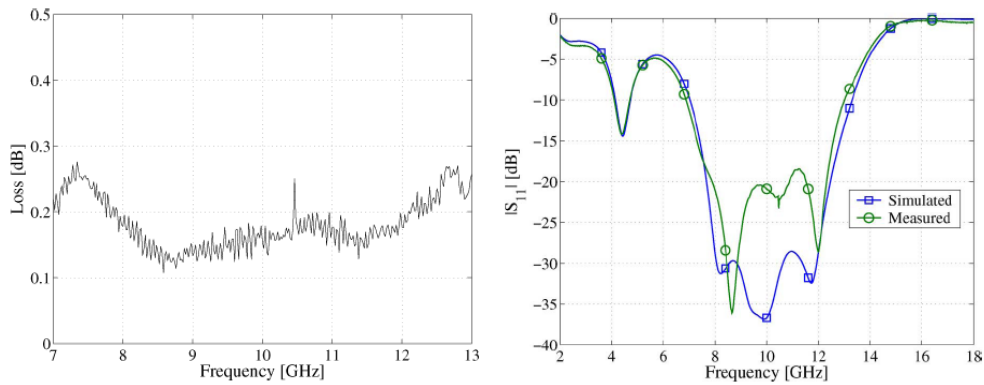


Fig1.20. Measured insertion loss and simulated and measured reflection coefficient at the central output port for the conical power combiner [16].

### 1.3.2.2 Microstrip line combiners

Various types of microstrip combiners have been introduced in the past years. Because of simple structure and low cost manufacturing, this kind of combiners is favorable in many designs. Moreover simple integration capability with MMICs is another advantage of microstrip combiners. In this section common types of microstrip radial power combiner will be presented.

A simple 4-way radial microstrip combiner was presented by Abouzahra in [17] as shown in Fig1.21. A design method using Green function was developed in this work, which was based on the planar circuit approach. In this approach the two- dimensional Green's function for the circular segment is used to derive the impedance matrix of the circuit. This method will be presented in the next chapter.

The design method is verified for 4-way combiner; however this method can be implemented to N-way combiner design. The bandwidth of this combiner is 4GHz at 14~18GHz with the 0.3dB insertion loss. Fig1.22 shows the measurement results.

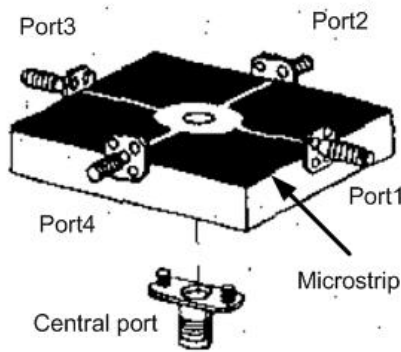


Fig1.21. The 4-way radial microstrip combiner that was presented by Abouzahra in [17].

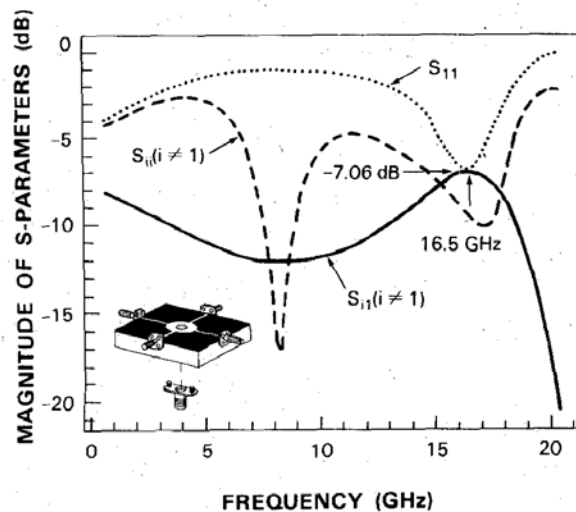


Fig1.22. Theoretical results for the Abouzahra 4-way power combiner [17].

Another type of microstrip radial divider/combiner was presented in [18]. Fig1.23 and Fig1.24 show the structure and response of this divider/combiner. The common port of this divider/combiner is also a microstrip line that causes additional loss in the structure. On the other hand the 90 degree transition between central cylinder and common port microstrip line and also the large circular patch in upper side that increases the parasitic capacitance, limits the structure bandwidth. This type of 8-way combiner has narrow bandwidth (16% at 5 GHz) and its insertion loss is about 1 dB. These combiners are preferred in narrowband and low frequency applications.

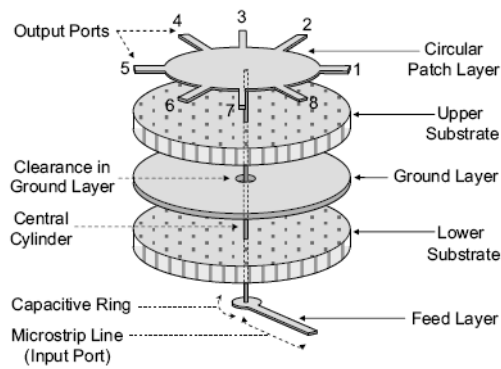


Fig1.23. An 8- way microstrip power combiner[18].

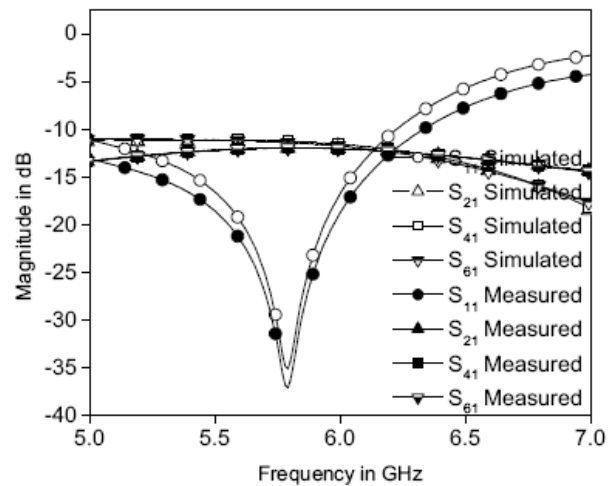


Fig1.24. Simulated and measured results of the 8-way microstrip power combiner in[18].

A 30-way radial microstrip power combiner was presented by Fathy [10] as shown in Fig1.25. Fathy presents a simple and general technique to design this type of radial power combiners with a highly predictable performance. This technique will be investigated in the next chapter. The output port is perpendicular to microstrip surface and has one 90 degree transition. There is also a large microstrip circular patch that reduces the combiner's bandwidth. However, this combiner has good isolation between its input ports. This isolation is created by thin resistors between each two ports. Proposed combiner works in X-band with 25% bandwidths and 0.55dB insertion loss. The measured isolation between ports is also better than 15 dB.

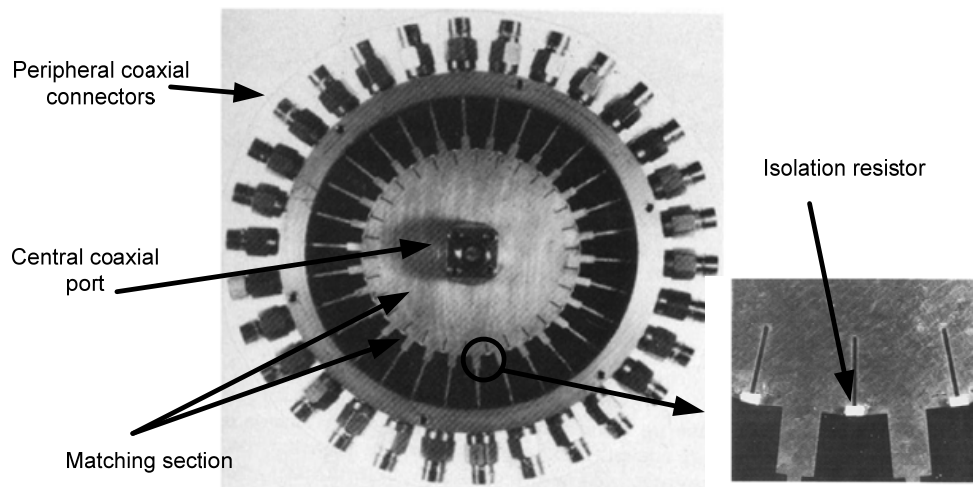


Fig1.25. Fathy's 30-way microstrip radial power combiner with isolation resistors [10].

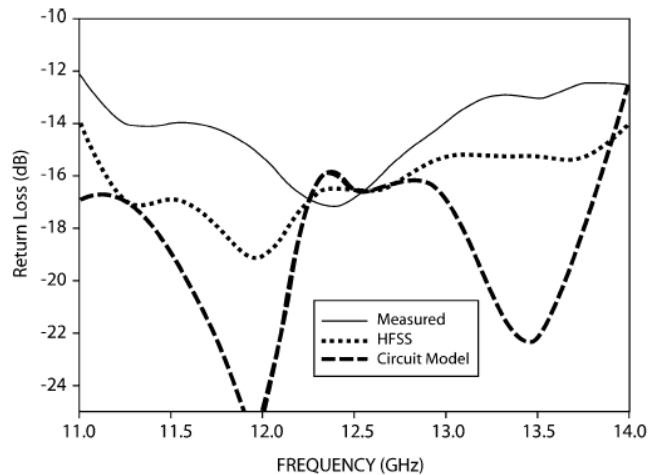


Fig1.26. Central port measurement and simulation results for Fathy microstrip radial power combiner [10]. The large microstrip circular matching patch reduces the combiner's bandwidths.

### Radial two step power combiners

Although N-way power combiner is a term for combining with one step but there is another type of combiner that include both N-way and binary combiner as shown in Fig1.27 . A radial two step topology is proposed in [19] to design a 14-way planar power combiner. The achievable bandwidth is 15 % for the power combiner. Fig1.28 shows the topology and measurement results of the 14-way power combiner. The return loss of the output port and the isolation between input ports are better than 13 dB.

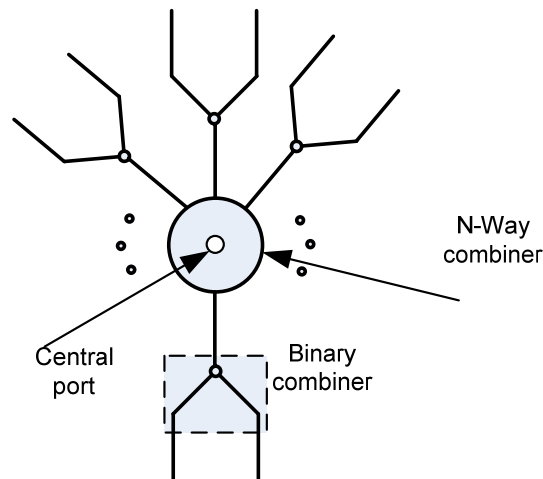


Fig1.27. A general scheme of radial two step power combiner.

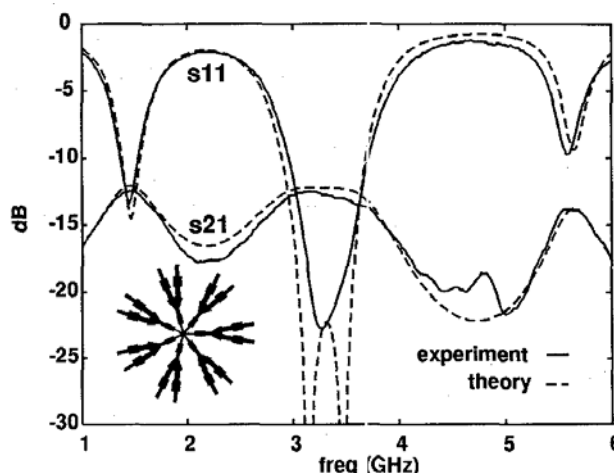


Fig1.28. Calculated and measured  $S_{11}$  and  $S_{21}$  for the 14-way two step power combiner presented in [19].

Another 16-way improved two step radial power combiner with isolation resistor worked at 5-6GHz is presented by Haifeng [20]. This combiner integrates a binary Wilkinson combiner and eight-way radial power combiner. The combiner efficiency is near 90%. The structure of the Haifeng combiner is shown in Fig1.29.

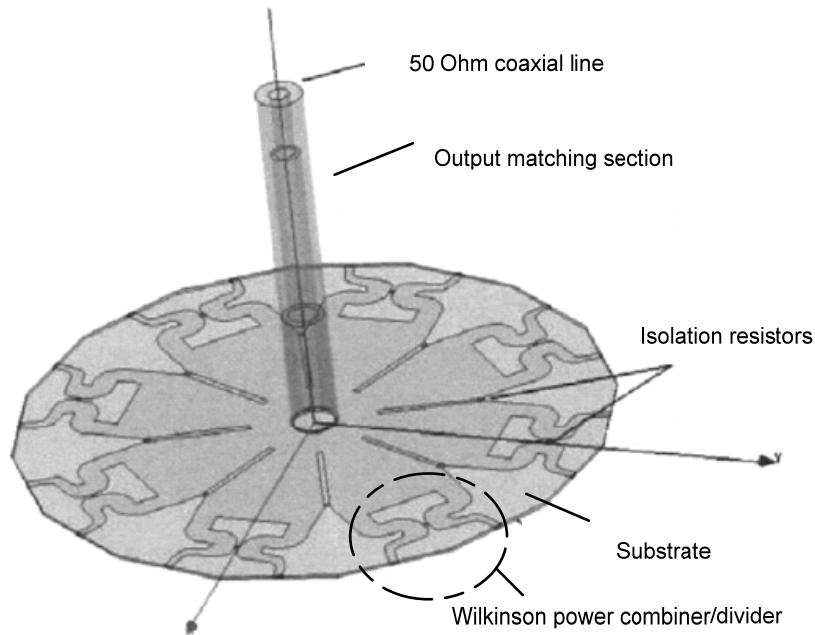


Fig1.29. The structure of Haifeng radial two step power combiner [20].

## 1.4 Spatial power combining architectures

As mentioned in section 1.2.1, if amplifiers or MMIC components are combined using transmission line circuits, there is an upper limit to the number of elements which exerts a limit on the power. N-way transmission line radial power combiners also have some disadvantages especially when N is increased. It is clear that for a small number of amplifier elements (and, hence, small levels of output power) planar corporate combining architectures are more efficient, but, as the number of amplifiers increases, it becomes necessary to use a spatially combined architecture. Fig1.30 shows the spatial power combining concept [21].

In summary spatial power combining advantages are:

- Higher bandwidths (in comparison with corporate and chain)
- Higher efficiency
- Failure tolerance

Spatial power combining disadvantages are:

- Complicated mechanical assembling
- Difficult packaging issues
- Bulky
- Heat transfer

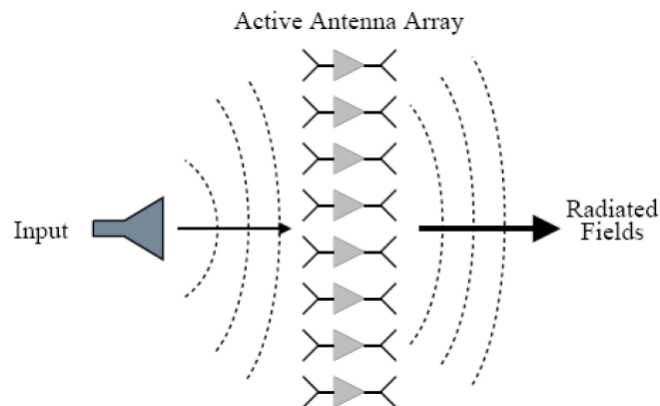


Fig1.30. Spatial power combining concept, each element consists of one amplifier, the input and the output antenna.

Spatial power combining in the first time was reported at 1968 with the construction of a 100-element spatially combined array; each element operated between a pair of monopole antennas [22].

**Various types of spatial power combining**

Active arrays for spatial combining systems have been demonstrated in the two classic array topologies tile and tray. In the tile approach the elements are located in one plane while in the tray method the elements are in parallel plates as shown in Fig1.31. In the case of the tile approach, two distinct design approaches have been developed, grid and array. The tray method can also be divided in two various structures, waveguide and coaxial. Fig1.32 shows a diagram for the spatial combining classification.

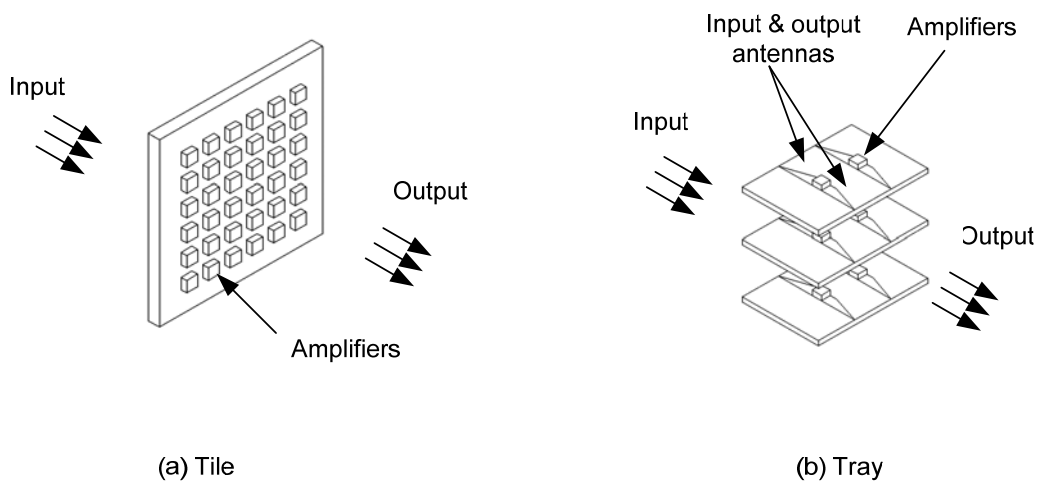


Fig1.31. Spatial power combining architectures. In the tile approach the elements are located in one plate and in the tray method the elements are located in the parallel plates

[23].

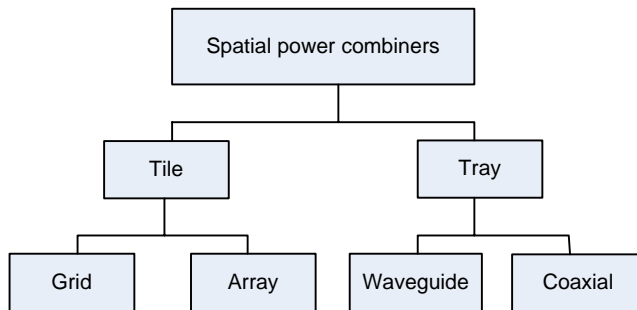


Fig1.32. Spatial power combiner classification.

### 1.4.1 Tile Amplifiers

As mentioned, the tile approach can be divided into two categories, grid and array. In the “grid” category, active devices are integrated at the vertical and horizontal intersections of a metallic mesh as shown in Fig1.33 [23]. The vertical wires connect either the input circuits or the output circuits of the amplifiers, while the horizontal wires connect the other circuit. An incoming wave can thus be polarized to interact only with the amplifiers’ input circuits, while the outgoing wave will be orthogonally polarized. Polarizer grids on either side of the structure ensure isolation between input and output circuits. In the grid topology, the active elements are generally spaced much closer than half a wavelength. The entire length of the grid wires acts as single antenna elements. The drawback of grid method is that the small cell sizes limit the gain and power per cell. Moreover, because the active devices are very dense, the grid amplifier can only be monolithically fabricated.

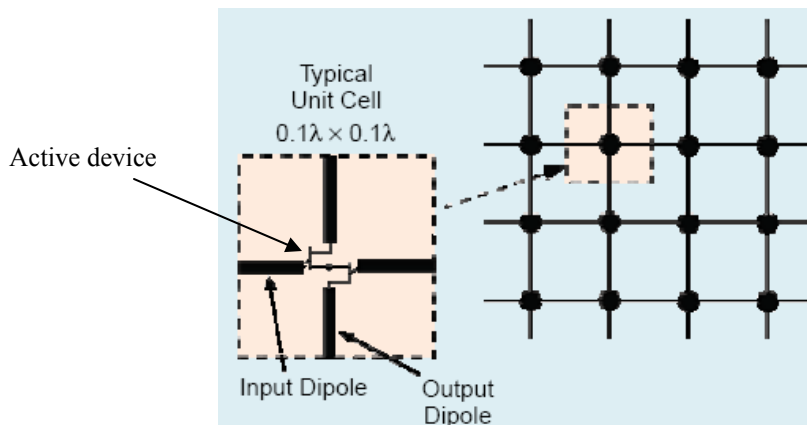


Fig1.33. In grid approach devices are integrated at the vertical and horizontal intersections [23].

In the “array” category, separate antenna elements are integrated directly with active devices or MMIC amplifiers, with each element acting as an independent cell as shown in Fig1.34 [23]. The array acts as a periodic antenna array with the elements spaced at roughly half wavelength intervals. The electromagnetic waves are received on one side of the array, active devices can be placed on either or both sides of the array, and the array radiates on the other side.

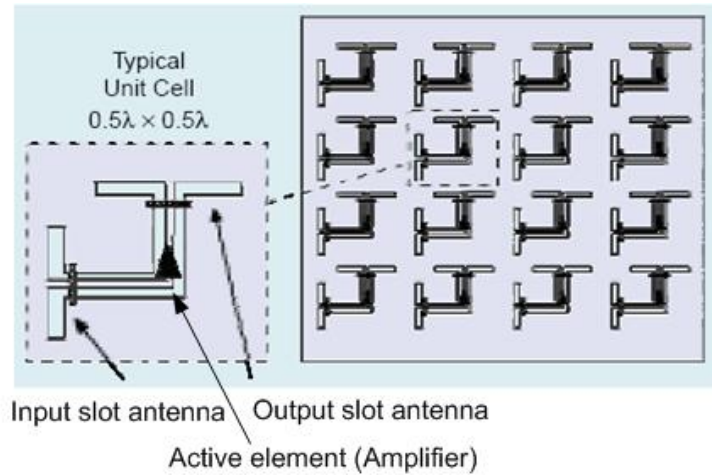


Fig1.34. In array approach separate antenna elements are integrated directly with active devices and each element acts as an independent device [23].

### 1.4.2 Tray amplifiers

The tray approach, illustrated in Fig1.31 (b), uses a tray of end-fire antenna elements with multiple trays stacked to provide a two-dimensional array. The tray then acts to receive an input signal to excite an electrical circuit that runs perpendicular to the plane of the antenna array, and to radiate from the other side of the trays. Several tray approaches have been introduced but in general it can be divided into two groups, depending on the output medium; either a rectangular or an oversized coaxial waveguide. Description of each category is as follows.

### 1.4.2.1 Waveguide spatial power combining

In the spatial power combiners the output of amplifiers are combined in the space. In some applications like phase array systems, amplifiers are combined in free space, however, they can be combined in waveguide in more efficient way.

The surrounding waveguide provides an excellent performance for the power devices and is an optimum choice for most high-power applications [24]. In this structure the power combiner is comprised of several arrays of active antennas, which consist of tapered slotline antenna sections and high power MMIC amplifiers, as shown in Fig1.35. These arrays were mounted onto a small metal fixture, for both mechanical support and heat removal, and inserted into a standard X-band waveguides. This architecture also provides more space for the RF circuitry and active devices. Another advantage of this configuration is that the metal carrier of each circuit tray permits good heat conduction. This structure has some disadvantages like bandwidth limitation. In fact dominant  $TE_{10}$  mode inside rectangular waveguide causes a non-uniform excitation of amplifiers inside the waveguide resulting in bandwidth reduction. Another disadvantage of the tray approach is the length of the system. An X-band 120W power amplifier is reported in [24] by this method, which had about 75% power combining efficiency.

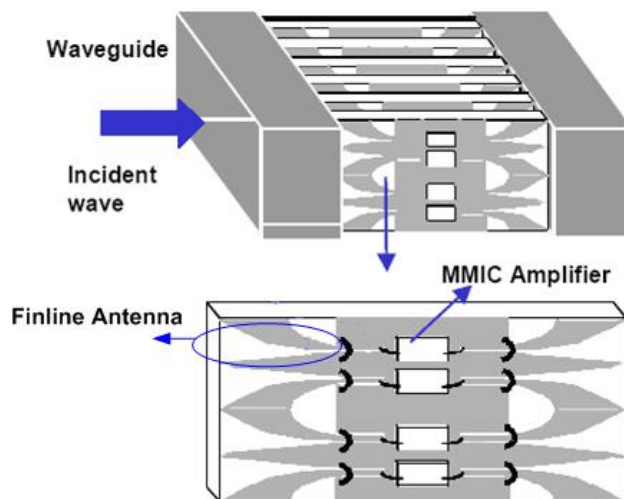


Fig1.35. Waveguide spatial combiner [24]. The power combiner consists of several active arrays that are inserted in a standard waveguide.

### 1.4.2.2 Coaxial waveguide spatial power combiner

The rectangular waveguide combiner is easier to be fabricated and also better for thermal management, but the rectangular waveguide dominant  $TE_{10}$  mode will lead to non-uniform illumination of the antenna trays inside the waveguide and therefore will reduce the bandwidth and efficiency and distort the saturation characteristics of the system [24].

These difficulties with waveguide spatial power combiners can be addressed by adapting the approach to a TEM waveguide environment, such as a coaxial waveguide. Fig1.36 illustrates how this might be done by using radial tapered-slotline (finline) structures distributed uniformly in the annular aperture of an oversized coax [21]. The compact finline array helps suppress higher modes in the coaxial waveguide. The bandwidth of the transformer can be fully exploited because the TEM mode in a coaxial waveguide does not have a cut-off frequency, as  $TE_{10}$  in a rectangular waveguide.

As shown in Fig1.37 the combiner is fed by an oversized coaxial line, tapering to standard coaxial connectors at either end. This structure can accommodate a large number of amplifiers, provide uniform illumination of the array, and can be designed for ultra-wide-band operation.

Traditionally coaxial waveguide combiner was exploited as the cylindrical resonant cavity combiners in the 70s [3]. Angelos Alexanian [21] first applied the coaxial structure to spatial power combiner field with a preliminary demonstration of the idea using passive elements.

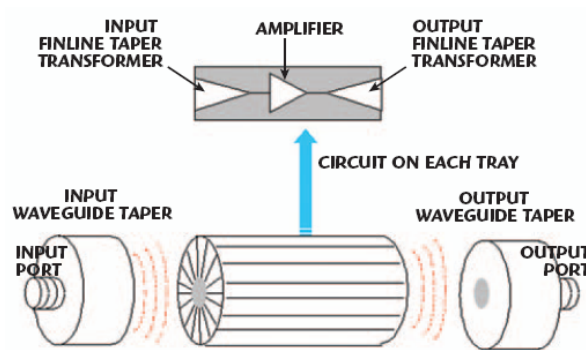


Fig1.36. The concept of a coaxial waveguide spatial N-way power combining[21].

In recent years a coaxial waveguide spatial power combiner that works from 4 ~17 GHz is proposed in [21]. 32 MMIC are placed around the centre conductor. Fig1.37 shows the schematic of this combiner. This combiner consists of an array of finlines, that act as a wide band antenna, and a transition from 50 Ohm N-type connector to finlines. The finline structure can be easily analyzed with a modern electromagnetic (EM) simulator software. MMIC amplifiers are also placed in the middle of each element of the array as shown in Fig1.38.

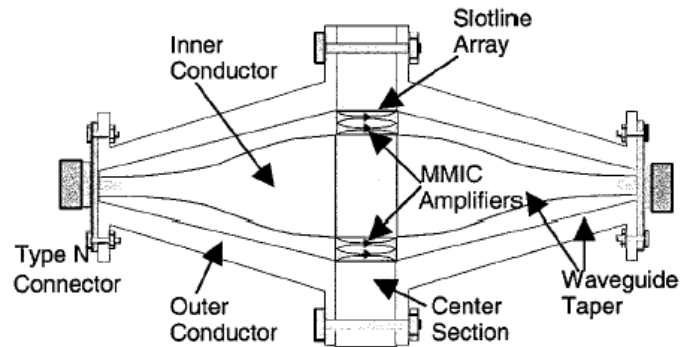


Fig1.37. Schematic of an oversized coaxial waveguide combiner [21].

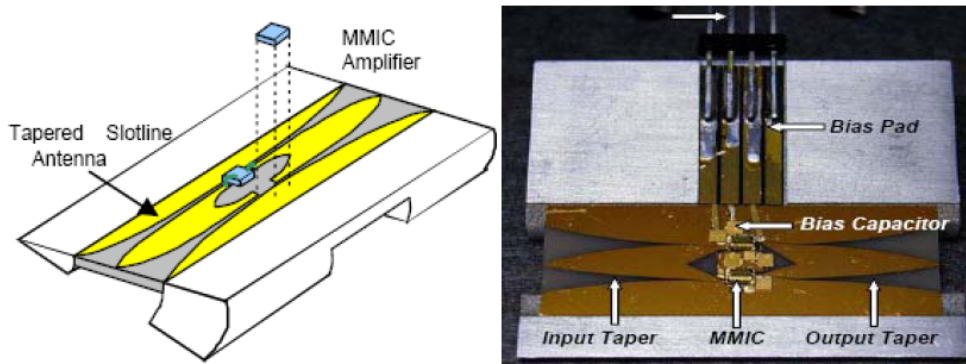


Fig1.38. Tray design for the modular spatial coaxial combining system [21].

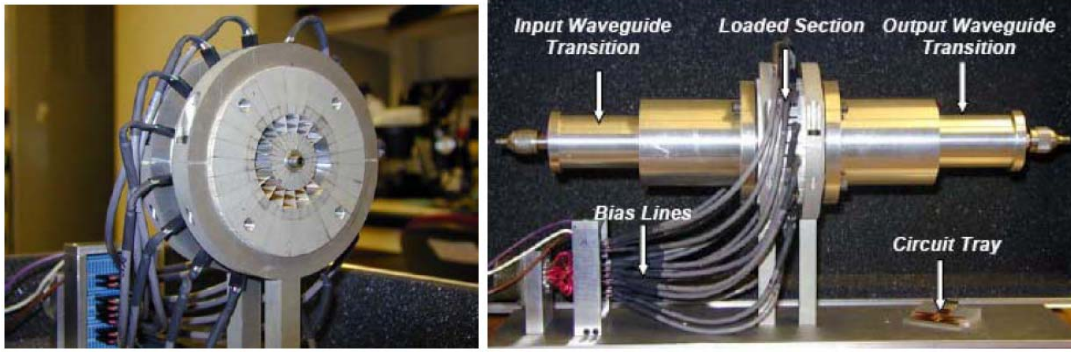


Fig1.39. Some pictures of coaxial waveguide spatially power combining [21].

Fig1.39 shows the total combiner system. The total loss of the combiner including ohmic and mismatch losses is nearly constant 2 dB over the band. (See Fig1.40). This corresponds to 1-dB output loss and, hence, 80% combining efficiency. In Fig1.41, the measured return loss is plotted and is better than 9 dB.

Some commercial amplifiers are proposed by CAP Wireless [25] that uses this method. A 45 W, 6 to 18 GHz power amplifier and a 10 W, 2 to 20 GHz amplifier are some products from this company.

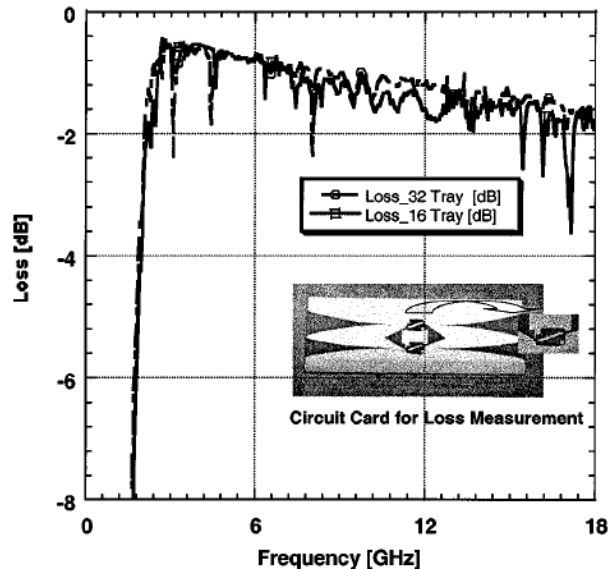


Fig1.40. Dissipative loss for 16- and 32-tray combiners with 50-Ohm microstrip through line in place of the active device [21].

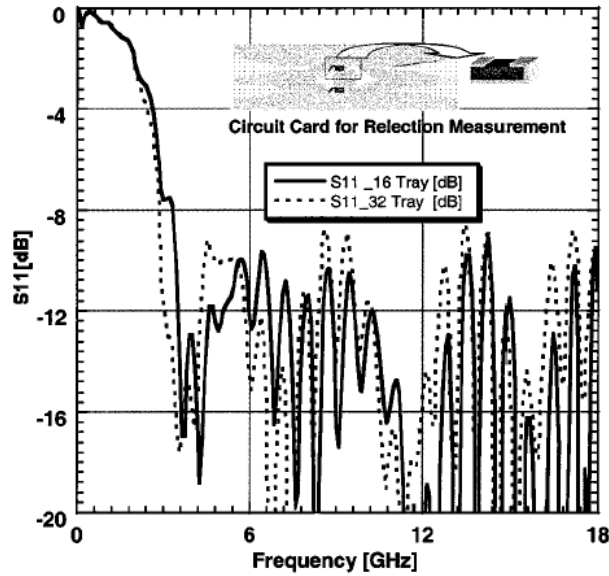


Fig1.41. Output return loss measurement for 16- and 32-tray combiner [21].

#### Comparison between tray and tile:

As illustrated in Fig1.31 the tile architecture probably has the greatest sensitivity to the design and manufacturing. Moreover, the small cell sizes limit the gain and power of the total system. On the other hand, because the tray architecture decouples the direction of the electrical circuit from the plane of the array, it has larger space for larger MMIC chips and consequently it can provide a higher output power. Also, the tray architecture seems to provide the greatest isolation between active circuits. The tray architecture also facilitates the use of a backside metal fixture for thermal management.

In summary the advantages of tray against tile are:

- better thermal management
- wider bandwidth
- higher gain and output power

Table 1.1 summarizes the specifications of tray and tile architectures.

	Tile	Tray
Bandwidths	narrow	Medium (Waveguide up to 4 GHz) (Coaxial up to 18 GHz )
Thermal Transfer	Medium	Good
Output Power	Up to 60 Watt	Up to 150 Watt (Waveguide) Up to 50 Watt (Coaxial)
Isolation	Medium	Good
Sensitivity	High	Medium
Complexity	High	Medium

Table 1.1 Comparison between tray and tile architectures.

## ***1.5 Comparison between N-way combining methods***

Various types of combiners were discussed in this chapter. Now we should compare them and select a proper candidate to our design. These combiners can be compared for the parameters such as bandwidth, efficiency, output power, cost, size, weight and heat transfer capability. Efficiency of combiner is related to its insertion loss. However in a power amplifier system other parameters like phase balancing can affect the efficiency but in our comparison, efficiency is only related to the combiner insertion loss.

Table 1.2 compares nine parameters of various types of combiners. Our goal is to design a wideband, compact and low cost combiner. The coaxial tray combiner [21] is very wideband but it is very bulky and is expensive to build. The conical radial power combiner is a compact and high efficient approach and in the first step we make some modification on the proposed structure in [16], but its bandwidth is limited and we couldn't extend it significantly. In appendix A.1 the results is presented.

Another choice is the microstrip radial power combiner that provides a compact and low cost solution for radial power combiners, but its bandwidth is limited in the previous works [10,17,18]. However, we have tried to overcome this problem and have presented a microstrip power combiner that works from 2 to 17 GHz.

	Type	Input number	Power Watt	Bandwidth	RBW %	Efficiency %	Heat Transfer	Complexity	Size	Cost
1	Binary	max 8	100	Up to mm Wave	100	60	Very good	Very low	Medium	Very low
2	Tile SPC	36	25	Up to mm Wave	30	55	Low	High	Low	High
3	Waveguide Tray SPC	32	150	X & Ku Band	40	75	Good	Medium	Medium	Medium
4	Coaxial Tray SPC	32	45	2~20 GHz	100	80	Medium	Medium	High	Medium
5	Microstrip RPC	30	100	Up to mm Wave	25	90	Very good	Low	Low	Low
6	Waveguide RPC	32	150	X & Ku & K & Ka	15	90	Very good	Medium	Medium	Medium
7	Conical RPC	30	100	X & Ku Band	60	95	Very good	Medium	Low	Medium

SPC: Spatial Power Combiner

RPC: Radial Power Combiner

RBW: Relative Bandwidth

Table 1.2 Comparison table between various types of power combiners.

## 2 Radial Power Combiner Modeling Methods

Several analysis methods can be used to evaluate radial power combiners. In cavity radial power combiners, the eigenmode method [31] is mostly preferred and in microstrip radial combiners, planar methods [17] are mostly used. However an N-way power combiner can be considered an (N+1) port network in general. The scattering matrix of such a network has several useful properties, which are worth contemplating, and will be investigated in the next section.

### 2.1 Scattering matrix properties of lossless N-way power combiner

Kagan [26] used basic principles to derive expressions for the magnitudes of the S-parameters of a symmetrical N-way combiner. In general an N-way power combiner is an (N+1) port network with N equal outputs. If we assume the N outputs are symmetrical and the input port (port 1) is fully matched, based on experience and experimental results (see section 3.3), it can be shown that  $S_{ij} \cong S_{23}$   $i, j \geq 2, i \neq j$  then

$$S = \begin{bmatrix} 0 & S_{12} & S_{12} & S_{12} & \cdots & S_{12} \\ S_{12} & S_{22} & S_{23} & S_{23} & \cdots & S_{23} \\ S_{12} & S_{23} & S_{22} & \cdots & \cdots & S_{23} \\ S_{12} & S_{23} & S_{23} & & & \\ \cdots & \cdots & \cdots & \cdots & \cdots & S_{23} \\ S_{12} & S_{23} & S_{23} & S_{23} & \cdots & S_{22} \end{bmatrix} \quad (2-1)$$

Which is a scattering matrix of the (N+ 1)<sub>th</sub> order. Since the device is lossless, the matrix is unitary. Therefore,

$$N|S_{12}|^2 = 1 \quad (2-2)$$

$$|S_{12}|^2 + |S_{22}|^2 + (N-1)|S_{23}|^2 = 1 \quad (2-3)$$

$$S_{12}S_{22}^* + (N-1)S_{12}S_{23}^* = 0. \quad (2-4)$$

The solution to this simultaneous equation indicates that:

$$|S_{12}|^2 = \frac{1}{N} \quad (2-5)$$

$$|S_{23}|^2 = \frac{1}{N^2} \quad (2-6)$$

$$|S_{22}| = \frac{N-1}{N}. \quad (2-7)$$

Now it can be concluded that the VSWR into any output port and the isolation between any two output ports are

$$VSWR_{(N \neq 1)} = \frac{1 + |S_{22}|}{1 - |S_{22}|} = 2N - 1 \quad (2-8)$$

$$Isolation_{(MN)} = 10 \log \frac{1}{|S_{23}|^2} = 20 \log N \quad (M \neq 1) \quad (N \neq 1) \quad (M \neq N) \quad (2-9)$$

And finally the coupling between the input and any output port is

$$Coupling_{1N} = 10 \log \frac{1}{|S_{12}|^2} = 10 \log N \quad (2-10)$$

It can be seen that when multi-outputs are required, say 8 or more, you can obtain some degree of isolation between the output ports.

## 2.2 Eigenvalue Equation Analysis

In the Kagan's equations [26], it's assumed that the input to the combiner was perfectly matched and also  $S_{ij} = S_{23}$  for  $i, j \geq 2, i \neq j$ . But in more general case, this assumption is not valid and we can employ the Eigenvalue Equation Method discussed in [27] to determine the scattering parameters of a general N-way power combiner. This method uses the geometrical symmetries of the divider to reduce the number of unknown parameter.

In a general N-way radial power combiner, N ports are symmetrically spaced  $360/N$  degrees around the axis coinciding with the inner conductor of the coaxial line as shown in Fig2.1. This N-way combiner can be in various forms such as microstrip, coaxial or waveguide type. By considering the symmetries of the structure, the Eigenvalue Equation Method gives the S-parameters of the combiner in terms of its eigenvalues. Because there are fewer unknown eigenvalues than S-parameters, we are able to determine

- (1) If all the combiner's ports can be matched perfectly,
- (2) If not all the ports can be matched, then how well a given port can be matched, and
- (3) The values of the other S-parameters.

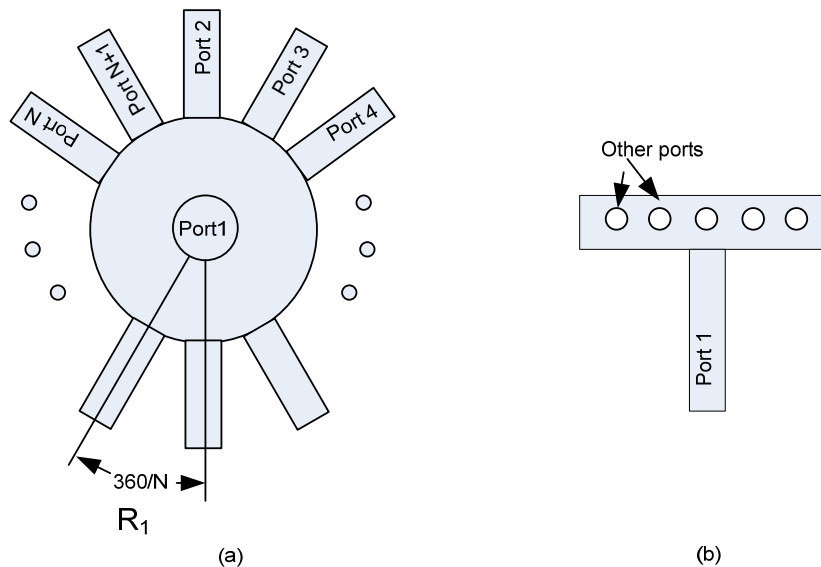


Fig2.1. A general N-way radial power combiner, (a) Top view (b) Side view.  $R_1$  is the  $360/N$  degree rotational operator.

In an N-way radial power combiner, we assume,  $S_{11} = \alpha$ ,  $S_{1n} = S_{n1} = \beta$ ,  $S_{ii, i \neq 1} = \gamma$  and other scattering matrix element are denoted by  $\eta$ , so the general scattering matrix for N way radial combiner can be written as follow[28]:

$$S_N = \begin{bmatrix} \alpha & \beta & \beta & \beta & \cdots & \beta & \cdots & \beta & \cdots & \beta & \beta \\ \beta & \gamma & \eta_m & \eta_{m-1} & \cdots & \eta_2 & \eta_1 & \eta_2 & \cdots & \eta_{m-1} & \eta_m \\ \beta & \eta_m & \gamma & \eta_m & \cdots & \eta_3 & \eta_2 & \eta_1 & \cdots & \eta_{m-2} & \eta_{m-1} \\ \beta & \eta_{m-1} & \eta_m & \gamma & \cdots & \eta_4 & \eta_3 & \eta_2 & \cdots & \eta_{m-3} & \eta_{m-2} \\ \vdots & \vdots \\ \beta & \eta_3 & \cdots & \eta_{m-1} & \eta_m & \gamma & \eta_m & \eta_{m-1} & \cdots & \eta_1 & \eta_2 \\ \beta & \eta_2 & \cdots & \eta_{m-2} & \eta_{m-1} & \eta_m & \gamma & \eta_m & \cdots & \eta_2 & \eta_1 \\ \beta & \eta_1 & \cdots & \eta_{m-3} & \eta_{m-2} & \eta_{m-1} & \eta_m & \gamma & \cdots & \eta_3 & \eta_2 \\ \beta & \eta_2 & \cdots & \eta_{m-4} & \eta_{m-3} & \eta_{m-2} & \eta_{m-1} & \eta_m & \cdots & \eta_4 & \eta_3 \\ \vdots & \vdots \\ \beta & \eta_{m-1} & \eta_{m-2} & \cdots & \eta_1 & \eta_2 & \eta_3 & \cdots & \eta_m & \gamma & \eta_m \\ \beta & \eta_m & \eta_{m-1} & \cdots & \eta_2 & \eta_1 & \eta_2 & \cdots & \eta_{m-1} & \eta_m & \gamma \end{bmatrix} \quad (\text{N even})$$

$$S_N = \begin{bmatrix} \alpha & \beta & \beta & \beta & \cdots & \beta & \cdots & \beta & \cdots & \beta & \beta \\ \beta & \gamma & \eta_m & \eta_{m-1} & \cdots & \eta_1 & \eta_1 & \eta_2 & \cdots & \eta_{m-1} & \eta_m \\ \beta & \eta_m & \gamma & \eta_m & \cdots & \eta_2 & \eta_1 & \eta_1 & \cdots & \eta_{m-2} & \eta_{m-1} \\ \beta & \eta_{m-1} & \eta_m & \gamma & \cdots & \eta_3 & \eta_2 & \eta_1 & \cdots & \eta_{m-3} & \eta_{m-2} \\ \vdots & \vdots \\ \beta & \eta_3 & \cdots & \eta_{m-1} & \eta_m & \gamma & \eta_m & \eta_{m-1} & \cdots & \eta_1 & \eta_2 \\ \beta & \eta_2 & \cdots & \eta_{m-2} & \eta_{m-1} & \eta_m & \gamma & \eta_m & \cdots & \eta_1 & \eta_1 \\ \beta & \eta_1 & \cdots & \eta_{m-3} & \eta_{m-2} & \eta_{m-1} & \eta_m & \gamma & \cdots & \eta_2 & \eta_1 \\ \beta & \eta_1 & \cdots & \eta_{m-4} & \eta_{m-3} & \eta_{m-2} & \eta_{m-1} & \eta_m & \cdots & \eta_3 & \eta_2 \\ \vdots & \vdots \\ \beta & \eta_{m-1} & \eta_{m-2} & \cdots & \eta_1 & \eta_1 & \eta_2 & \cdots & \eta_m & \gamma & \eta_m \\ \beta & \eta_m & \eta_{m-1} & \cdots & \eta_2 & \eta_1 & \eta_1 & \cdots & \eta_{m-1} & \eta_m & \gamma \end{bmatrix} \quad (\text{N odd})$$

(2-11)

Where N is even,  $m = N/2$ , where N is odd  $m = (N - 1)/2$ .

For example an 8-way radial power combiner scattering matrix is given by

$$S_{N=8} = \begin{bmatrix} \alpha & \beta \\ \beta & \gamma & \eta_4 & \eta_3 & \eta_2 & \eta_1 & \eta_2 & \eta_3 & \eta_4 \\ \beta & \eta_4 & \gamma & \eta_4 & \eta_3 & \eta_2 & \eta_1 & \eta_2 & \eta_3 \\ \beta & \eta_3 & \eta_4 & \gamma & \eta_4 & \eta_3 & \eta_2 & \eta_1 & \eta_2 \\ \beta & \eta_2 & \eta_3 & \eta_4 & \gamma & \eta_4 & \eta_3 & \eta_2 & \eta_1 \\ \beta & \eta_1 & \eta_2 & \eta_3 & \eta_4 & \gamma & \eta_4 & \eta_3 & \eta_2 \\ \beta & \eta_2 & \eta_1 & \eta_2 & \eta_3 & \eta_4 & \gamma & \eta_4 & \eta_3 \\ \beta & \eta_3 & \eta_2 & \eta_1 & \eta_2 & \eta_3 & \eta_4 & \gamma & \eta_4 \\ \beta & \eta_4 & \eta_3 & \eta_2 & \eta_1 & \eta_2 & \eta_3 & \eta_4 & \gamma \end{bmatrix}$$

Now, we call  $R_1$  the  $360/N$  degree rotational operator (see Fig2.1). If  $I_n$  and  $V_n$  ( $n = 1, 2, \dots, N+1$ ) represent the mode voltage and current at each of the combiner's ports, the rotational operator does not affect the voltage and current at port 1, but it rotates the voltages and currents of ports 2, 3, ...,  $N$  counter-clockwise to the next port. Under this  $360/N$  degree rotation, the  $N$ -way combiner's electrical behavior remains unchanged. Because of this rotational symmetry, there are a number of field excitations in the combiner which satisfy Maxwell's equations. These excitations satisfy the eigenvalue equation of the  $N$ -way combiner:

$$\mathbf{R}_1 \mathbf{a}_k = r_k \mathbf{a}_k \quad (2-12)$$

Where

$$R_1 = \begin{bmatrix} 1 & 0 & 0 & \dots & \dots & 0 & 0 \\ 0 & 0 & 0 & 0 & \dots & 0 & 1 \\ 0 & 1 & 0 & 0 & \dots & 0 & 0 \\ \dots & 0 & 1 & 0 & \dots & \dots & \dots \\ \dots & 0 & 0 & \dots & \dots & 0 & \dots \\ 0 & 0 & 0 & 0 & \dots & 0 & 0 \\ 0 & 0 & 0 & \dots & 0 & 1 & 0 \end{bmatrix} \quad (2-13)$$

$a_k$  is the  $k_{th}$  eigenvector or electromagnetic field excitation corresponding to the  $k_{th}$  eigenvalue  $r_k$ .

An important property of  $R_1$  is that it commutes with the scattering matrix of the combiner/divider [27]. Now, by solving equation (2-12) it can be found that

$$|\mathbf{R}_1 - r_k \mathbf{I}| = 0 \quad (2-14)$$

Where matrix I is the identity matrix. The solutions to equation (2-14) are

$$r_1 = r_2 = 1, r_3 = e^{j2\pi/N} \dots \text{ and } r_k = e^{j2(k-2)\pi/N}, \dots, r_{N+1} = e^{j2(N-1)\pi/N} \quad (2-15)$$

Using these eigenvalues, we get the orthogonal eigenvectors and these eigenvectors are also eigenvectors of the S matrix [28].

For example for the four-way radial power combiner if we assume scattering matrix as follow,

$$S = \begin{bmatrix} \alpha & \beta & \beta & \beta & \beta \\ \beta & \gamma & \eta_2 & \eta_1 & \eta_2 \\ \beta & \eta_2 & \gamma & \eta_2 & \eta_1 \\ \beta & \eta_1 & \eta_2 & \gamma & \eta_2 \\ \beta & \eta_2 & \eta_1 & \eta_2 & \gamma \end{bmatrix}$$

Then from [28] we have,

$$\alpha = \frac{1}{2}(s_1 + s_2)$$

$$\gamma = \frac{1}{8}(s_1 + s_2 + 4s_3 + 2s_4)$$

$$\beta = \frac{1}{4}(s_1 - s_2)$$

$$\eta_1 = \frac{1}{8}(s_1 + s_2 - 4s_3 + 2s_4)$$

$$\eta_2 = \frac{1}{8}(s_1 + s_2 - 2s_4)$$

Where  $s_i, i=1,2,3,4$  are the eigenvalues of S matrix.

From these equations we can see that the Eigenvalue Equation Method uses the geometrical symmetries of the divider to reduce the number of unknown parameters from five S parameters to four eigenvalues. In fact we can always adjust one of the port

reference planes as to make one of the eigenvalues equal to +1, so there are only three unknown parameters which allow us to determine whether the ports can be matched.

Now if we follow through with the analysis in [28], we get the scattering matrix for a N-way power combiner.

For an 8-way radial power combiner following equation can be written

$$\alpha = \frac{1}{2}(s_1 + s_2)$$

$$\gamma = \frac{1}{16}(s_1 + s_2 + 4s_3 + 4s_4 + 4s_5 + 2s_6)$$

$$\beta = \frac{\sqrt{2}}{8}(s_1 - s_2)$$

$$\eta_1 = \frac{1}{16}(s_1 + s_2 - 4s_3 + 4s_4 - 4s_5 + 2s_6)$$

$$\eta_2 = \frac{1}{16}(s_1 + s_2 - 2\sqrt{2}s_3 + 2\sqrt{2}s_5 - 2s_6)$$

$$\eta_3 = \frac{1}{16}(s_1 + s_2 - 2\sqrt{2}s_4 + 2s_6)$$

$$\eta_4 = \frac{1}{16}(s_1 + s_2 + 2\sqrt{2}s_3 - 2\sqrt{2}s_5 - 2s_6)$$

As application now we use this theory to see why all four ports of the three-way combiner cannot be matched perfectly. For N = 3, the scattering matrix is as follow:

$$s = \begin{bmatrix} \alpha & \beta & \beta & \beta \\ \beta & \gamma & \eta & \eta \\ \beta & \eta & \gamma & \eta \\ \beta & \eta & \eta & \gamma \end{bmatrix}$$

$$\alpha = \frac{1}{2}(s_1 + s_2)$$

$$\gamma = \frac{1}{6}(s_1 + s_2 + 4s_3)$$

$$\beta = \frac{\sqrt{3}}{6}(s_1 - s_2)$$

$$\eta = \frac{1}{6}(s_1 + s_2 - 2s_3)$$

To perfectly match all four ports we set  $\alpha = \gamma = 0$ .

Thus, we must set  $s_1 = -s_2$  and  $s_3 = 0$ . Consequently,  $\eta = 0$  also, leaving only  $\beta$  nonzero, a violation of conservation of power. Though we cannot match all four ports, we can match perfectly the coaxial port (port 1). In this case,  $\alpha = 0$  so that  $s_1 = -s_2$ . Then, if we apply conservation of power and the unitary principle, we obtain the following matrix for the three-way divider:

$$s = \frac{1}{3} \begin{bmatrix} 0 & \sqrt{3} & \sqrt{3} & \sqrt{3} \\ \sqrt{3} & 2 & -1 & -1 \\ \sqrt{3} & -1 & 2 & -1 \\ \sqrt{3} & -1 & -1 & 2 \end{bmatrix}$$

Where, we have adjusted the position of the reference planes on the ports such that the S-parameters are pure real.

### ***2.3 Planar analysis for microstrip radial power combiner***

Microstrip radial power combiners have a junction between the common port and other N ports. This junction is the most important part of the combiner, therefore, its behavior must be analyzed in more details. However, junction analysis methods depend on the dimension and type of the combiner. For instance, microstrip radial power combiners can be analyzed by a planar method, because of their planar structure.

A theoretical analysis based on the planar circuit approach which uses the two-dimensional impedance Green's function to derive the multiport impedance matrix is presented in [17]. Fig2.2 shows the general N-way microstrip disc with central axial port. If the center conductor diameter of the coaxial port ( $2r_c$ ) is much smaller than the diameter of the disk ( $2a$ ), the Green's function of the circular disk geometry has been used otherwise Green's function of annular ring geometry must be used [27]. However, the fringing field at the disk circumference can be accounted by replacing the physical disk by a larger disk surrounded by a perfect magnetic wall.

The effective radius of this large disk is given by [29]:

$$a_e = a \sqrt{1 + \frac{2d}{\pi \epsilon_r a} \left[ \ln \left( \frac{\pi a}{2d} \right) + 1.7726 \right]} \quad (2-16)$$

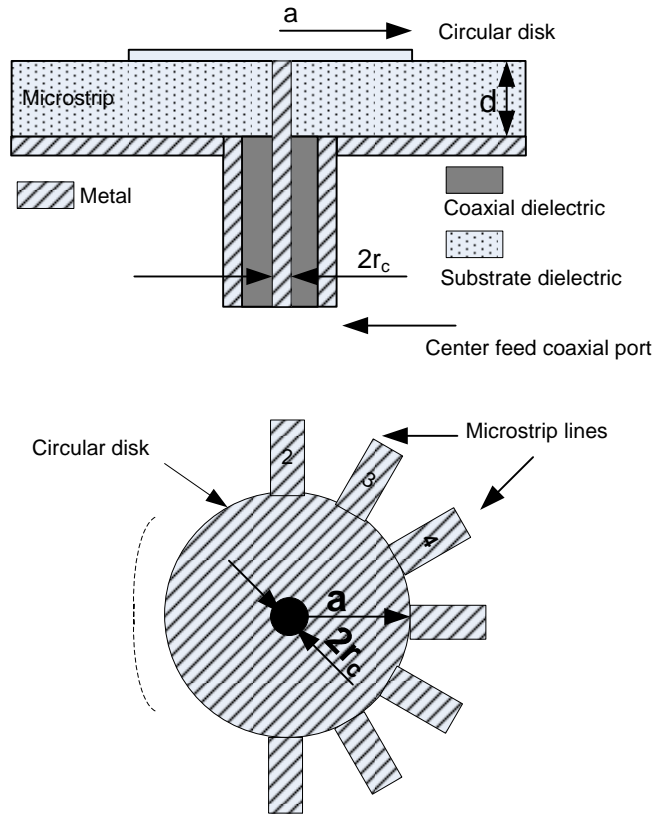


Fig2.2. General N-way microstrip disc junction with the central axial port.

In (2-16)  $a$  represents the physical radius,  $d$  is the substrate thickness, and  $\epsilon_r$ , is the relative dielectric constant of the substrate under the disk. This radius can be implemented for more accurate response in disk analysis.

### Z-Matrix of multiport disk [17]

The two-dimensional impedance Green's function for a circular segment with magnetic walls is available from [30, p. 249]. This Green's function has been used to derive the impedance matrix for the center-fed (N+1) port circular microstrip structure shown in Fig2.3. The elements of the Z-matrix are obtained as follows [17]:

$$Z_{ij} = \frac{1}{W_i W_j} \int_{W_i} \int_{W_j} G(s_i / s_j) ds_i ds_j \quad (2-17)$$

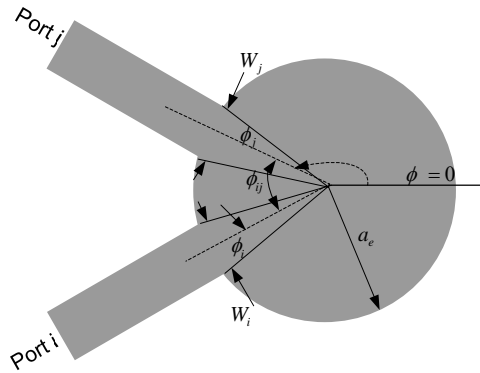


Fig2.3. Parameters of the circumferential ports.

Where  $W_i$  and  $W_j$  represent the effective widths of ports  $i$  and  $j$ , respectively, and  $ds_i$ ,  $ds_j$  are incremental distances along the port widths [30]. The Green's function of  $G$  in (2-17) is presented in [17].

The impedance matrix obtained from [17] and is then converted into the more familiar S-matrix representation.

A ten way microstrip radial power combiner is analyzed by this method in [17]. Fig2.4 shows the simulation and measurement. This combiner is narrowband due to its large circular patch at the central junction.

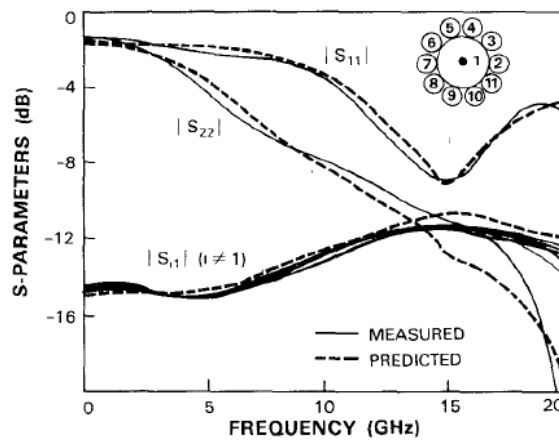


Fig2.4. Theoretical and experimental results for the ten-way radial power combiner [17].

## 2.4 Equivalent model analysis for junction

One efficient approach to design a structure with a non-planar junction is equivalent model method. In this method, the behavior of junction is modeled by the equivalent circuit. Several papers present the equivalent circuits for the microstrip to coaxial junction such as [10]. Because this method is a simple and time efficient method, we select it to design and analyze our combiner and therefore this method will be described in the next chapter.

## 2.5 Cavity type combiner analysis methods

Several literatures have described field matching analysis techniques which can provide fast and accurate designs using software written for PCs. A full wave analysis is used to obtain an admittance matrix of the complete  $(N+1)$  port structure in [31]. This method can be applied for a probe excited radial power combiners.

To analyze the power divider/combiner, the admittance matrix, rather than the scattering matrix approach is chosen. However, once the admittance matrix parameters are known, conversion to the scattering parameters is straightforward.

In an  $N$ -way radial power divider/combiner (see Fig2.5), when the peripheral probes are fed in the same way or are terminated in identical loads, the admittance matrix parameters of the device are defined by the following equations

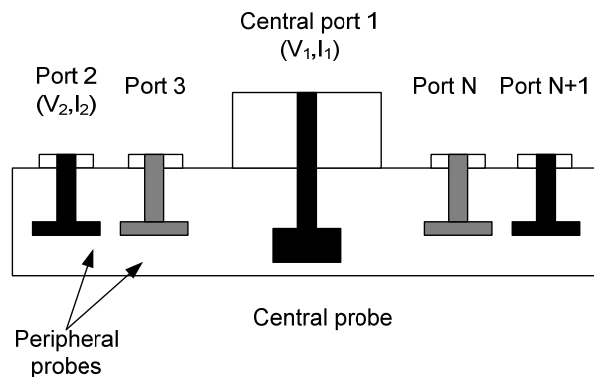


Fig2.5. An  $N$ -way radial cavity power divider/combiner.

$$\begin{aligned}
I_1 &= Y_{1,1}V_1 + (Y_{1,2} + Y_{1,3} + \dots + Y_{1,N+1})V_2 \\
I_2 &= Y_{2,1}V_1 + (Y_{2,2} + Y_{2,3} + \dots + Y_{2,N+1})V_2
\end{aligned}
\tag{2-18}$$

Which can be rewritten in the form:

$$\begin{aligned}
I_1 &= Y_{1,1}V_1 + N Y_{1,2} V_2 \\
I_2 &= Y_{2,1}V_1 + Y'_{2,2} V_2
\end{aligned}
\tag{2-19}$$

Where  $Y'_{2,2} = Y_{2,2} + Y_{2,3} + \dots + Y_{2,N+1}$ ,  $V_1$  is the voltage applied in the port 1 (the central probe),  $V_2$  is the voltage applied in the port 2 (the peripheral probes), and  $I_1$ ,  $I_2$  are the resulting currents in port 1 and 2.

Equations (2-18) and (2-19) show that in order to obtain the admittance matrix for the symmetric radial power combiner/divider for the case when the peripheral probes are loaded or energized identically, two field problems have to be solved: 1) when the central probe is energized by voltage  $V_1$  and the peripheral probes are short-circuited; and 2) when the peripheral probes are energized by the same voltage  $V_2$  and the central probe is short-circuited. Assuming that the parameters  $Y_{1,1}$ ,  $Y_{1,2}$ ,  $Y_{2,1}$  and  $Y'_{2,2}$  are found, the input admittance seen at the central probe can be determined by using standard circuit analysis.

### 3 Design and Optimization of Microstrip 8-Way Radial Power Combiner

Several types of radial power combiners were introduced in chapter 1, many of which are designed to work in limited bandwidths. Although a 4-17GHz power combiner using an oversized coaxial waveguide was developed by York group [21], but that structure is bulky and expensive. Our selected candidate, however, was the conical radial power combiner [16] (see Fig3.1). We applied some modifications to this combiner to improve its bandwidth (see Appendix A), but it did not extend to our desired range (2 GHz to 17 GHz). This was because of the narrowband behavior of the input probes. Although the conical radial power combiner is more compact than the coaxial waveguide combiner, it needs high-accuracy manufacturing process and may not be a cost effective solution. Microstrip radial power combiners are better choices to satisfy both cost and bandwidth requirements. Several types of microstrip combiners are presented in the literature [17, 10], but they do not provide a wideband frequency range. However, by modifying the microstrip radial power combiner, we have finally reached our goal, which is to have an 8-way radial power combiner with a bandwidth of 2 -17 GHz. In the first section of this chapter, we have explored several characteristic of the combiner scattering matrix. In the following sections, the design and optimization process is described and finally the measurement data in comparison to the simulation data is presented.

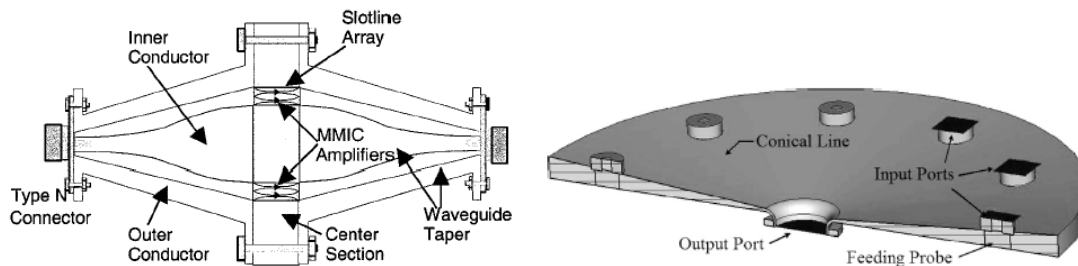


Fig3.1. Bulky coaxial waveguide combiner (left) [21] and not fully wideband conical radial power (right) [16].

### 3.1 8-way radial power combiner scattering matrix properties

The general properties of an N-way combiner were discussed in the previous chapter. To study the further details, consider a 9 port network as shown in Fig3.2. Ports are spaced 45 degrees apart and due to the structure symmetry, following equations can be written:

$$S_{11}=\alpha$$

$$S_{1n}=S_{12}=\beta \quad n=3\sim 9$$

$$S_{n,n+1}=S_{n+1,n+2}=\zeta_{23} \quad n=2\sim 7$$

$$S_{n,n+2}=S_{n+1,n+3}=\zeta_{24} \quad n=2\sim 6$$

$$S_{n,n+3}=S_{n+1,n+4}=\zeta_{25} \quad n=2\sim 5$$

$$S_{n,n+4}=S_{n+1,n+5}=\zeta_{26} \quad n=2\sim 4$$

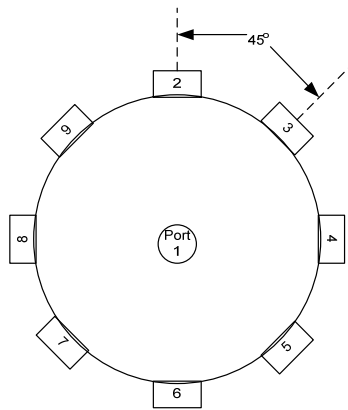


Fig3.2. General 8-way radial power combiner and its port configuration. Ports are spaced 45 degrees apart.

Considering the structure symmetry and the reciprocal property of the network, the whole scattering matrix can be written as follows:

$$\begin{bmatrix} \alpha & \beta \\ \beta & \gamma & \zeta_{23} & \zeta_{24} & \zeta_{25} & \zeta_{26} & \zeta_{25} & \zeta_{24} & \zeta_{23} \\ \beta & \zeta_{23} & \gamma & \zeta_{23} & \zeta_{24} & \zeta_{25} & \zeta_{26} & \zeta_{25} & \zeta_{24} \\ \beta & \zeta_{24} & \zeta_{23} & \gamma & \zeta_{23} & \zeta_{24} & \zeta_{25} & \zeta_{26} & \zeta_{25} \\ \beta & \zeta_{25} & \zeta_{24} & \zeta_{23} & \gamma & \zeta_{23} & \zeta_{24} & \zeta_{25} & \zeta_{26} \\ \beta & \zeta_{26} & \zeta_{25} & \zeta_{24} & \zeta_{23} & \gamma & \zeta_{23} & \zeta_{24} & \zeta_{25} \\ \beta & \zeta_{25} & \zeta_{26} & \zeta_{25} & \zeta_{24} & \zeta_{23} & \gamma & \zeta_{23} & \zeta_{24} \\ \beta & \zeta_{24} & \zeta_{25} & \zeta_{26} & \zeta_{25} & \zeta_{24} & \zeta_{23} & \gamma & \zeta_{23} \\ \beta & \zeta_{23} & \zeta_{24} & \zeta_{25} & \zeta_{26} & \zeta_{25} & \zeta_{24} & \zeta_{23} & \gamma \end{bmatrix} \quad (3-1)$$

Only 7 parameters are unknown and this can be used to simplify the network analysis. As is seen in the below scattering matrix, if we neglect  $\alpha$ , the second row contains all unknown parameters.

Un Known parameters

$$\begin{bmatrix} \alpha & \beta \\ \beta & \gamma & \zeta_{23} & \zeta_{24} & \zeta_{25} & \zeta_{26} & \zeta_{25} & \zeta_{24} & \zeta_{23} \\ \beta & \zeta_{23} & \gamma & \zeta_{23} & \zeta_{24} & \zeta_{25} & \zeta_{26} & \zeta_{25} & \zeta_{24} \\ \beta & \zeta_{24} & \zeta_{23} & \gamma & \zeta_{23} & \zeta_{24} & \zeta_{25} & \zeta_{26} & \zeta_{25} \\ \beta & \zeta_{25} & \zeta_{24} & \zeta_{23} & \gamma & \zeta_{23} & \zeta_{24} & \zeta_{25} & \zeta_{26} \\ \beta & \zeta_{26} & \zeta_{25} & \zeta_{24} & \zeta_{23} & \gamma & \zeta_{23} & \zeta_{24} & \zeta_{25} \\ \beta & \zeta_{25} & \zeta_{26} & \zeta_{25} & \zeta_{24} & \zeta_{23} & \gamma & \zeta_{23} & \zeta_{24} \\ \beta & \zeta_{24} & \zeta_{25} & \zeta_{26} & \zeta_{25} & \zeta_{24} & \zeta_{23} & \gamma & \zeta_{23} \\ \beta & \zeta_{23} & \zeta_{24} & \zeta_{25} & \zeta_{26} & \zeta_{25} & \zeta_{24} & \zeta_{23} & \gamma \end{bmatrix}$$

Since the device is lossless, the matrix is unitary. Therefore,

$$|\alpha|^2 + N|\beta|^2 = 1 \quad (3-2)$$

$$|\beta|^2 + |\gamma|^2 + 2|\zeta_{23}|^2 + 2|\zeta_{24}|^2 + 2|\zeta_{25}|^2 + |\zeta_{26}|^2 = 1 \quad (3-3)$$

$$\alpha\beta^* + \beta\gamma^* + 2\beta(\zeta_{23}^* + \zeta_{24}^* + \zeta_{25}^* + \zeta_{26}^* / 2) = 0 \quad (3-4)$$

If we assume that  $\zeta_{23}$ ,  $\zeta_{24}$ ,  $\zeta_{25}$ , and  $\zeta_{26}$  are experimentally small (see section 3.3) and all equal to one another, then above equations can be written as follow:

$$|\beta|^2 + |\gamma|^2 + (N-1)|\zeta_{23}|^2 = 1 \quad (3-5)$$

$$\alpha\beta^* + \beta\gamma^* + (N-1)\beta\zeta_{23}^* = 0 \quad (3-6)$$

If the input port is considered to be fully matched then  $\alpha=0$ , which leads to:

$$|\beta| = \sqrt{\frac{1}{N}} \quad (3-7)$$

$$|\gamma| = \frac{N-1}{N} \quad (3-8)$$

$$|\zeta_{23}| = \frac{1}{N} \quad (3-9)$$

Therefore, for  $N=8$ , i.e. 8-way power combiner, the theoretical scattering matrix parameters can be written as follow:

$$|\beta| = \sqrt{\frac{1}{8}} = 0.35 \text{ } \equiv \text{ } -9\text{dB}$$

$$|\gamma| = \frac{N-1}{N} = \frac{7}{8} \text{ } \equiv \text{ } -1.15\text{dB}$$

$$|\zeta_{23}| = \frac{1}{N} = \frac{1}{8} \text{ } \equiv \text{ } -18\text{dB}$$

VSWR for input ports  $=2N-1=17$

The parameter  $\beta$  presents the coupling and is equal to  $10\log N=9\text{dB}$  and  $\zeta_{23}$  is the isolation and equals to  $20\log N=18\text{dB}$ .

It is desired that all of the port be matched which is not possible and therefore usually the common port will be matched. This issue is not a serious problem in radial power combiners as we will show in the next chapter.

### 3.2 A design method for microstrip radial power combiner

A few analysis methods were presented in the previous chapter but due to the simple concept and time efficient process, the equivalent model is the preferred method to design and analyze the microstrip radial power combiners. In this method, the behavior of junction is modeled by equivalent circuit as shown in Fig3.3 which helps us to predict the behavior of the total combiner. This section presents a straightforward method [10] to design and analyze the radial microstrip combiners which will be followed by a full 3D simulation by HFSS software. Finally, based on the full wave simulation, an optimization process completes the design procedure.

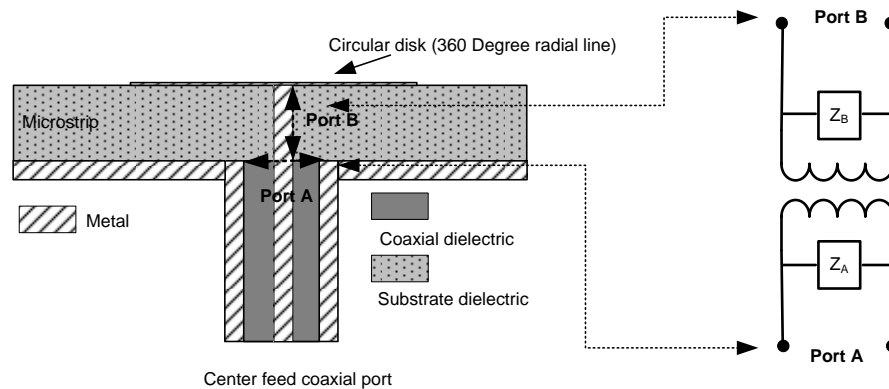


Fig3.3. The equivalent circuit model for the junction of coaxial and microstrip patch.

Generally, each microstrip radial power combiner consists of three main sections:

- 1) The common port transition or launcher
- 2) The non-planar junction
- 3) The N-way planar splitter/combiner

The launcher section (see Fig3.4.) is a coaxial line feeding a radial line. The splitting or combining path (the radial line) is a low-loss parallel plate transmission line with a central-point excitation, out of which energy expands uniformly in the dominant mode with an axial electric-field component. The radial line has relatively lower loss compared

to a microstrip line (in our case, roughly one-third of the loss of a 50 ohm microstrip line). However, it is extremely important to symmetrically feed the radial line to prevent the propagation of higher order modes. Mechanical stability, feed symmetry, and proper selection of the outer diameter of the coaxial line launcher are key factors in achieving balanced feed and uniformity. Propagation of higher order modes will, besides increasing the insertion loss, severely imbalance the amplitude and phase between individual peripheral ports of the N-way combiner. It should be noted that dominant mode propagates radially and higher order modes propagate circumferentially. The dominant mode provides in-phase balanced signal for all ports, while higher order modes change their polarity periodically in the circumferential direction every  $\pi/n$  angle (where n is the mode number), and cause severe phase imbalance. The disc is branched into microstrip lines, comprising the divider/combiner section. Microstrip lines are used to feed individual amplifiers in divider applications or come from amplifiers in combiner applications and are relatively lossy; hence, their lengths should be kept as short as possible to maximize the combining efficiency.

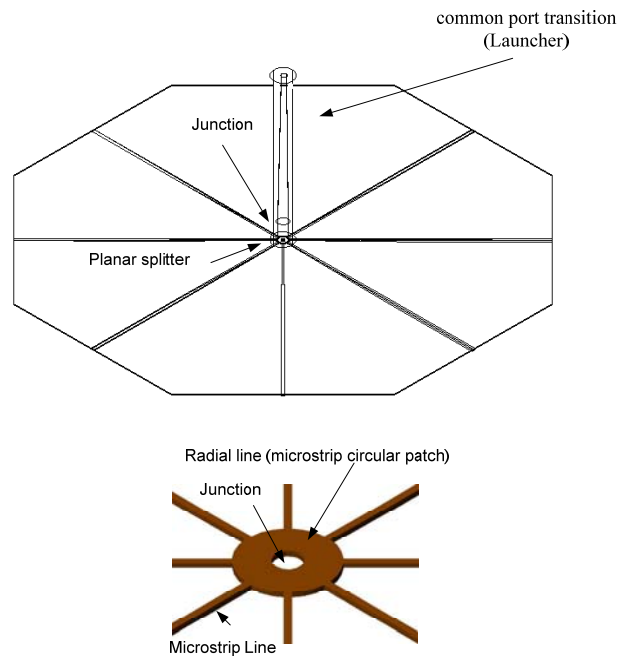


Fig3.4. A model for the coaxial/radial line structure. Each microstrip radial power combiner consists of three main sections: the common port transition or launcher, the non-planar junction and the N-way planar splitter/combiner.

### 3.2.1 Splitting/combining pad design

A general n-way power divider/combiner is a network with N+1 ports. If N 50 ohm ports join with each other, the total impedance of combined lines will be 50/N ohm. The next step is to match 50/N ohm section to the 50 ohm output. Indeed, at the first glance, N-way power combiner design is only a matching problem, but as we will see in the coming sections, it is not so simple.

A transmission line model of general N-Way power combiner is sketched in Fig3.5 .  $Z_0$  is the port impedance,  $Z_1$  is the transmission line impedance and  $Z_c$  is the impedance of the common junction.  $Z_{in}$  is the impedance of the microstrip lines at the junction point. It must be noted that  $Z_1$  is not constant and changes gradually from  $Z_0$  to  $Z_{in}$  to provide a better matching performance. In the output section,  $Z_{lc}$  is the output line impedance and it changes from  $Z_c$  to  $Z_0$ .

Now suppose that N=8, and  $Z_1=50$  ohm, consequently  $Z_c$  becomes 6.25 ohm, and it is needed to match 6.25 ohm to 50 ohm in a bandwidth of 2 ~17 GHz. In this case the impedance matching factor is equal to 8 requiring a long matching network besides being a difficult task to perform. So we came up with the idea of increasing the common junction impedance  $Z_c$  to create lower impedance matching factor. For this purpose, it is needed to increase the  $Z_1$  impedance near the junction i.e.  $Z_{in}$  . However, by this method, we have two matching networks, one in the input lines and the other in the output line.

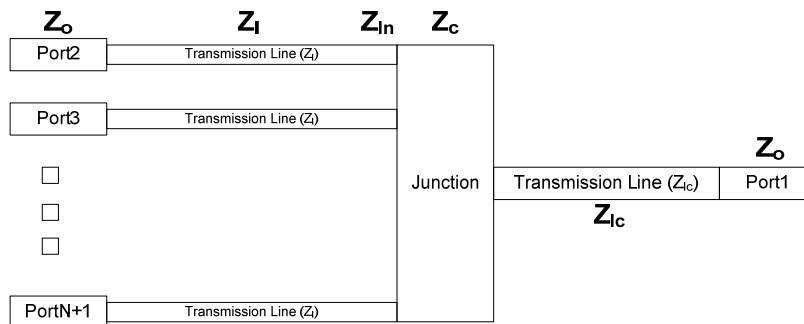


Fig3.5. A transmission line N-Way power combiner.

Maximum value of  $Z_{in}$  - we name it  $Z_{in,max}$  - depends on the height and the minimum feasible dimension of the microstrip line. For example, by selecting RT/D 5870 (with

thickness equal to 12 mil and  $\epsilon_r = 2.2$ ), the minimum feasible track widths is about 0.1 mm, consequently the  $Z_{ln,max}$  would equal to 137 ohm [36]. On the other hand, it's better to have thicker tracks because the narrow tracks can limit the maximum power at the junction. If the track width is selected to be 0.25mm,  $Z_{ln,max}$  will be 100 ohm. Moreover, by selecting  $Z_{ln,max} = 100$  ohm,  $Z_c$  becomes 12.5 ohm, therefore, in the first step we should match input lines to 100 ohm and on the other side, match 50 ohm output port to the 12.5 ohm junction impedance ( $Z_c$ ). In this case the impedance matching factor equals to 2 for input lines and equals to 4 for the output line.

One of the important parts of the combiner is the junction section. Because of the discontinuity at this section, other modes are excited and this can limit the bandwidth of the combiner. In the initial stages of our design, this junction effect is not taken into account but should definitely be considered as we proceed further in the analysis.

### Microstrip matching network

A broad band matching network is needed to match the input port to the high impedance side i.e.  $Z_{ln,max} = 100$  ohm, which is a simple task due to the small conversion ratio of 2. There are a few tapering methods for matching, but we select a linear matching network due to its simple design. For the linear matching network, as shown in Fig3.6, the microstrip length is selected as optimization parameter to have the best performance.

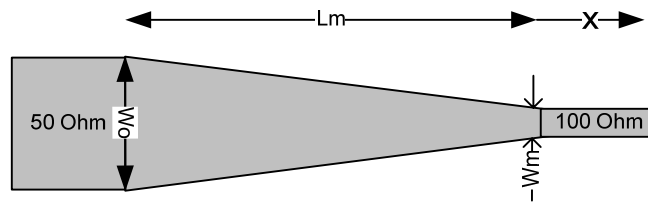


Fig3.6. A linear matching network in a two port microstrip line.

In the linear matching network we have:

$$Z(x) = \frac{(Z_{ln} - Z_0)}{L_m} x + Z_0 \quad (3-10)$$

Where  $Z_0$  is the port impedance,  $Z_{in}$  is the maximum impedance and  $L_m$  is the optimized length of the microstrip.

This matching circuit is analyzed by AWR Microwave Office, a high frequency design software, for the best matching performance. It is obvious that by increasing  $L_m$ , the reflection decreases but the microstrip loss and the combiner dimension increases as well. For three different lengths the transition return loss is sketched at Fig3.7 . In this step we cannot define the exact value of  $L_m$ , because it must be optimized with other parameters, however, we can tell a length greater than 25mm is a good transition and may be suitable for our final goal.

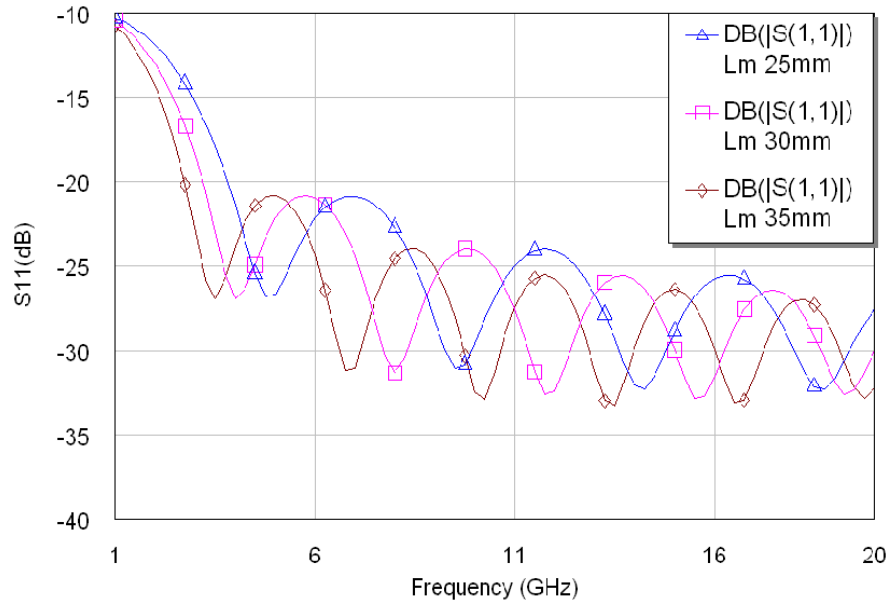


Fig3.7. Simulation results for linear microstrip impedance transformer (50 ohm to 100 ohm) for three different lengths.

Now eight microstrip lines can be combined at a common junction and it is helpful to understand the combiner behavior. For this purpose, AWR Microwave Office is used to model this network. Fig3.8 shows the eight taper lines that are connected to a common junction. This junction is considered to be ideal without physical dimension. The simulated common port return loss is sketched in Fig3.9.

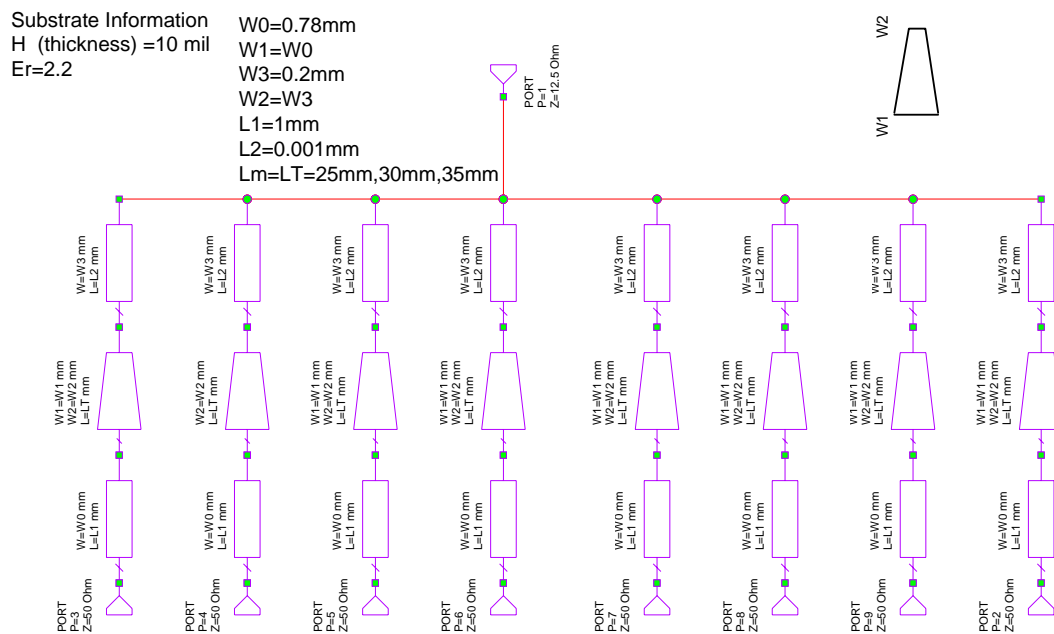


Fig3.8. Eight taper lines that are connected to the junction point.

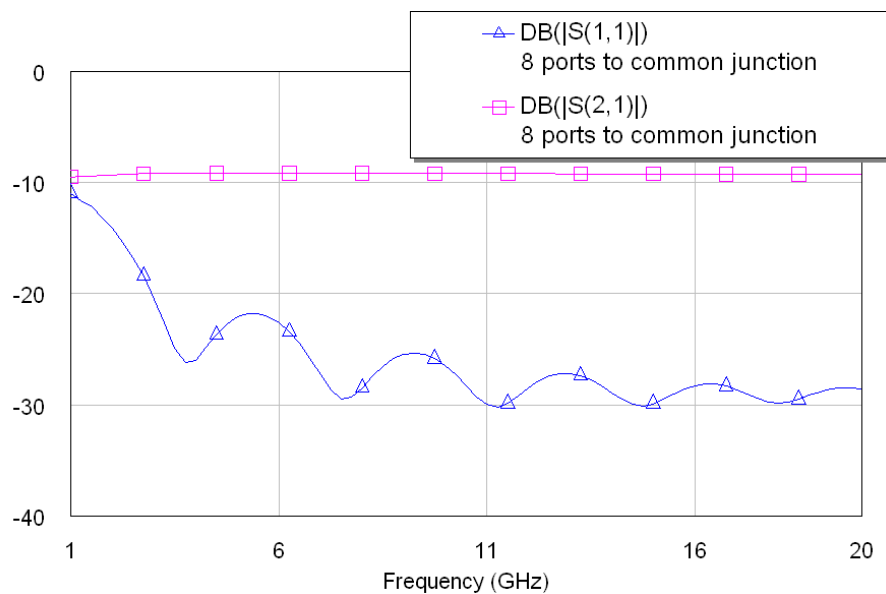


Fig3.9. AWR Microwave Office simulation results for ideally connected taper lines.

It is not possible to design a planar radial power combiner because the common port must be perpendicular to the common junction. So we have to add a coaxial transmission line to match the common junction to the output port. However to have a prediction of the total combiner response, we added an ideal unphysical junction model followed by tapered microstrip line that matched the common junction to the 50 ohm port as shown in Fig3.10. This circuit presents a simple eight way combiner and is compared with the previous model in Fig3.11. However these results are not close to real cases and some mismatch effects are not considered. For more accurate response, a 3D full wave simulation should be done.

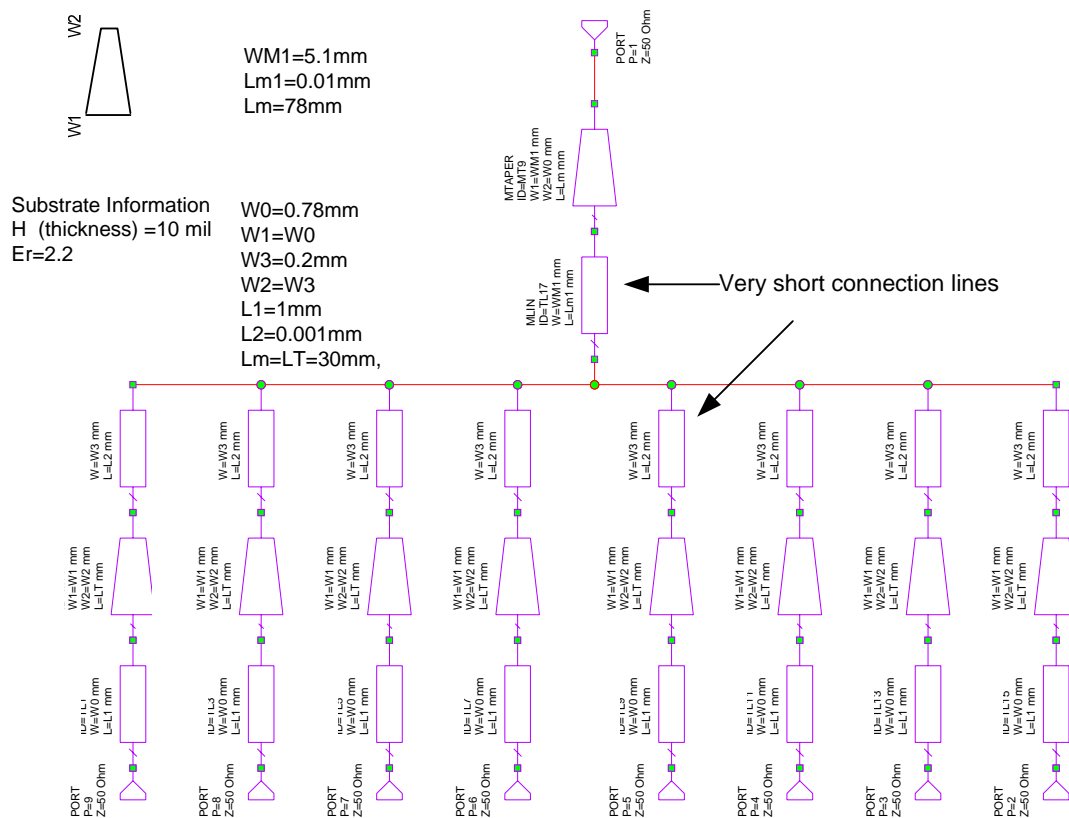


Fig3.10. A simple 8 way combiner with the output matching.

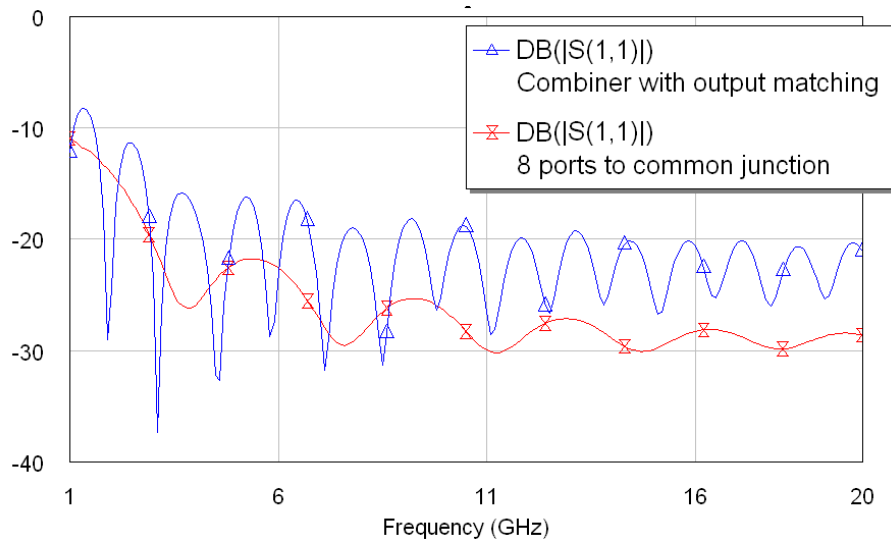


Fig3.11. Simulation results for a simple 8-way combiner with output matching section (Fig3.10 ) and without matching section ( Fig3.8 ).

### 3.2.2 The junction analysis

Junction is a critical part for the radial power combiners. In the junction microstrip lines are connected in a single point which is located at the center of structure. As mentioned before, eight 100 ohm microstrip lines are connected in the junction, therefore the junction impedance is equal to 12.5 ohm. On the other hand the common port is perpendicular to the junction plane. Fig3.12 shows a general junction structure that can be located at the center of combiner. The inner conductor of the coaxial line is connected to the circular microstrip disk.

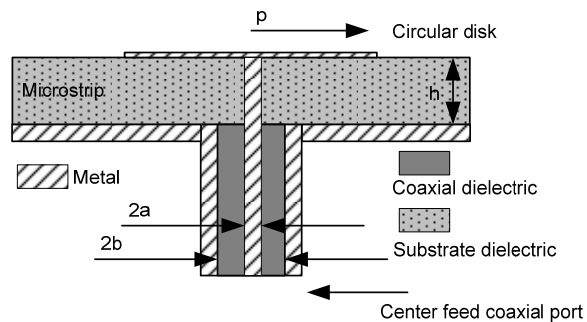


Fig3.12. The junction and coaxial contact, “p” is the circular radius and “h” is the substrate thickness, “b” and “a” are the outer and inner radius of coaxial conductors respectively.

In general, the input impedance of the radial line is complex, but for a long radial line with a relatively large input radius, the imaginary part can be neglected. And the real impedance can be written as follow [10]:

$$Z_{j,Re} = \frac{h}{2\pi b} \sqrt{\frac{\mu}{\epsilon_r \epsilon_0}} \quad (3-11)$$

Where  $b$  is outer diameter of coaxial line as shown in Fig3.12. Suppose the microstrip substrate is RT/D 5880 with 12mil thickness and  $\epsilon_r$  equal 2.2 and the coaxial line with  $b$  equal to 2.1mm, therefore from (3-11),  $Z_{j,Re}$  will be equal to 5.5ohm. This impedance is low and creates negative effect in the matching network and consequently it can decrease the bandwidth. Based on this fact, it is recommended not to have a large circular microstrip patch (or radial line) at junction position. On the other hand when  $p$  decreases, the imaginary part cannot be neglected and more accurate model is needed. In [10, 32], as shown in Fig3.13, a practical equivalent model for the radial line junction is presented, which will be explained in the following section.

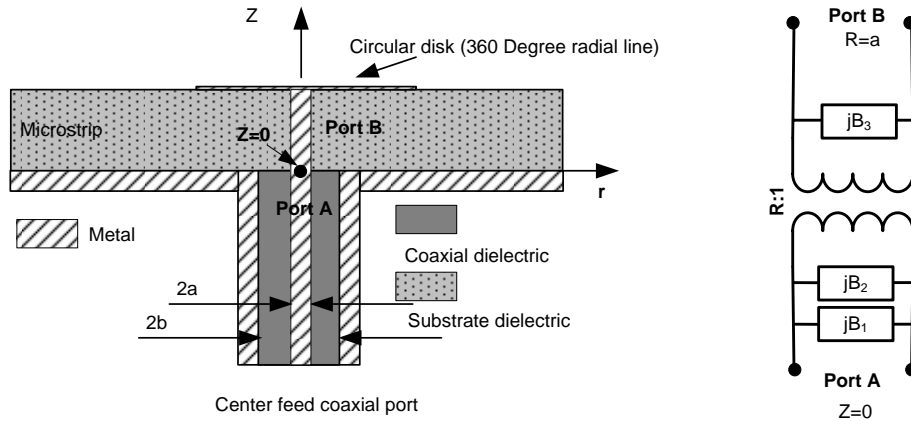


Fig3.13. The equivalent model for the junction.

### Microstrip to coaxial junction equivalent model [32]

The radial-line/coaxial-line junction shown in Fig3.12 is used in a wide variety of applications including antenna feeds and power combiners. In the design of such devices, one usually needs to find the input impedance of the central port when other ports are

terminated. We will show that if the electrical dimensions are very small (i.e.  $ka$ ,  $kb$  and  $kh \ll 1$ ,  $k = 2\pi/\lambda$ ,  $a$ ,  $b$ , and  $h$  are shown in Fig3.12) the impedance seen at the coaxial junction and in the radial line are the same. However, in many practical cases the junction parameters are not small (with the effect of the cutoff modes on the input impedance being significant), and a simple equivalent circuit interrelating the radial and coaxial lines (at appropriate planes) would be extremely useful.

Consider  $h=0.305\text{mm}$  as an example; in the 17GHz frequency,  $\lambda \approx 12\text{mm}$  and  $k=0.52$ , and  $kh=0.13$ . If we chose  $b=2.1\text{mm}$  and  $a=1.5\text{mm}$ , we would have:  $kb=1.1$ ,  $ka=0.78$ . On the other hand for 2GHz frequency we have,  $kh=0.01$ ,  $kb=0.1$  and  $ka=0.08$ , that means for low frequency and high frequency we have different impedances at the junction point. Determination of the equivalent circuit may be approached by considering the input admittance at the coaxial port (hereinafter at  $z = 0$ ) for two different radial line loads, namely a perfect match, and a short circuit at  $r = c$  ( $c > b$ ) [32] and the equivalent model at Fig3.13 can be written as follow [32].

$$B_1 = -\frac{2\pi}{\eta_0 \ln(b/a)} \cot(kh) \quad (3-12)$$

$$B_2 = \frac{4\pi}{kh\eta_0 \ln^2(b/a)} \sum_{m=1}^{\infty} \frac{1}{q_m^2} \frac{K_0(q_m kb)}{K_0(q_m ka)} \cdot (I_0(q_m ka) \cdot K_0(q_m kb) - I_0(q_m kb) \cdot K_0(q_m ka)) \quad (3-13)$$

$$B_3 = \frac{2\pi ka}{\eta_0 kh} \cdot \frac{J_1(ka)Y_0(kb) - J_0(kb)Y_1(ka)}{J_0(ka)Y_0(kb) - J_0(kb)Y_0(ka)} \quad (3-14)$$

$$R = \frac{(2/\pi) \ln(b/a)}{J_0(ka)Y_0(kb) - J_0(kb)Y_0(ka)} \quad (3-15)$$

Where

$$q_m = \sqrt{\left(\frac{m\pi}{kh}\right)^2 - 1}$$

and  $k = 2\pi/\lambda$ ,  $\eta_0$  is the intrinsic impedance of free space, and  $J_0, J_1, Y_0, Y_1, I_0$ , and  $K_0$  are Bessel functions and modified Bessel functions of the first and second kinds. The above parameters were deduced analytically, using the TEM approximation for the electric field in the coaxial aperture.

Only  $B_2$ , which relates to the susceptance contribution of the cutoff radial-line modes, is affected by the use of the TEM approximation, and this affection is not great anyways. The equivalent circuit shown in Fig3.13 with the parameters as above is quite an accurate model. In this model, it is assumed that the fields are rotationally symmetric and the dominant modes are the only propagating modes.

Now, suppose that the microstrip substrate is RT/D 5880 with thickness equal to 12mil and  $\epsilon_r$  equal to 2.2 and a coaxial line with  $b$  equal to 2.1mm, using equations (3-12) to (3-15) following results are obtained:

$R \approx 1$ ,  $B_2 \approx 0$  for frequencies of 2~18 GHz and  $B_1$  and  $B_3$  are plotted in Fig3.14 versus frequency for several junction dimensions.

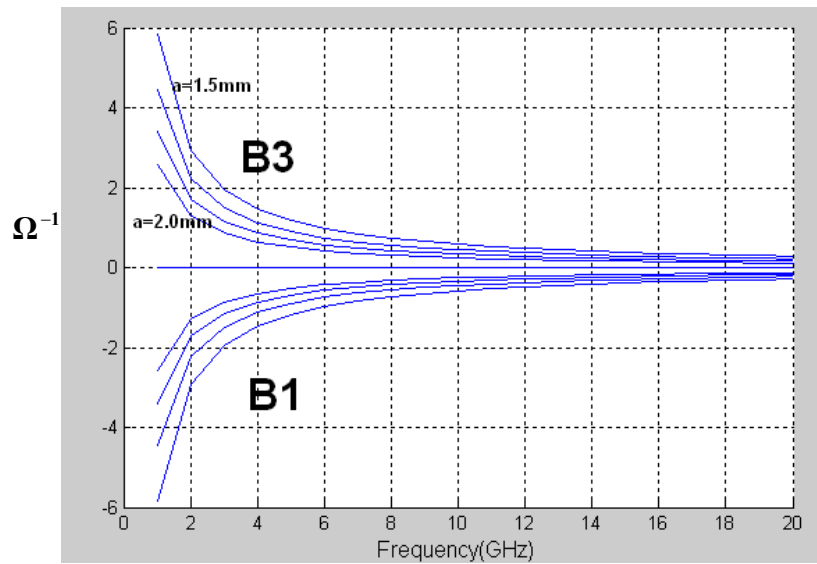


Fig3.14. Equivalent values of the junction for  $b=2.1\text{mm}$  and  $1.5\text{mm} < a < 2\text{mm}$ .

Now we can derive the impedance at the coaxial port of the junction:

$$Z_{jc} = \frac{1}{\frac{1}{R^2 Z_j} + j(B_1 + B_2 + \frac{B_3}{R^2})} \quad (3-16)$$

Where  $Z_{jc}$  is the impedance at the coaxial port,  $Z_j$  is the impedance of the radial line and  $B_1$ ,  $B_2$ ,  $B_3$ , and  $R$  are calculated based on equations (3-12) to (3-15). The normalized imaginary part of  $Z_{jc}$  is plotted versus frequency at Fig3.15. It can be seen that the ratio of imaginary part over real part of  $Z_{jc}$  increases with frequency, however it is small and can be neglected. Therefore based on the calculated data of Fig3.14 and Fig3.15 and the equation (3-16), we can write  $Z_{jc} \cong Z_j$  (The imaginary part of  $Z_j$  is also small and can be neglected [10]). From (3-12) to (3-16), it is also clear that if the electrical dimensions are very small (i.e.  $ka$ ,  $kb$  and  $kh \ll 1$ ,  $k = 2\pi/\lambda$ ), the impedance seen at the coaxial junction and at the radial line are the same. i.e.  $Z_{jc} = Z_j$

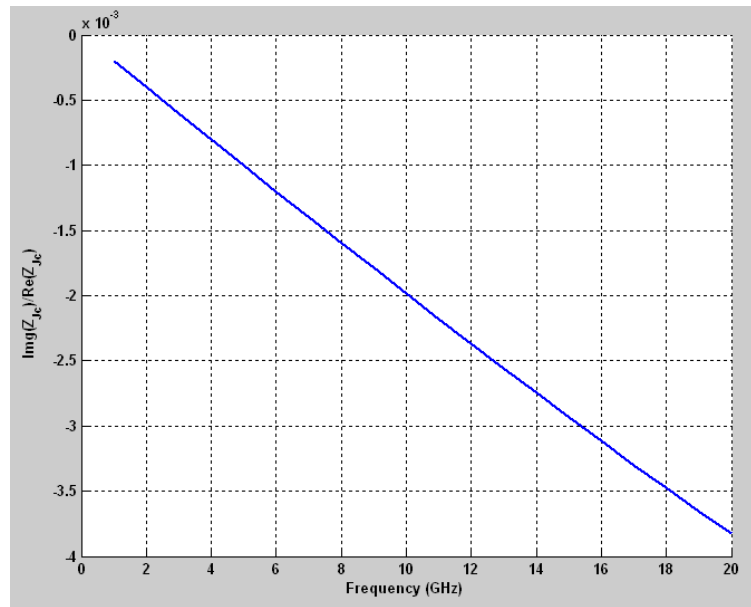


Fig3.15. Ratio of imaginary part over real part of  $Z_{jc}$  versus frequency for  $Z_j = 1$ .

Using the obtained equivalent model, the combiner circuits in Fig3.10 can be modified. Fig3.16 shows the modified results. It is obvious that the junction discontinuity has more effect in upper frequency band.

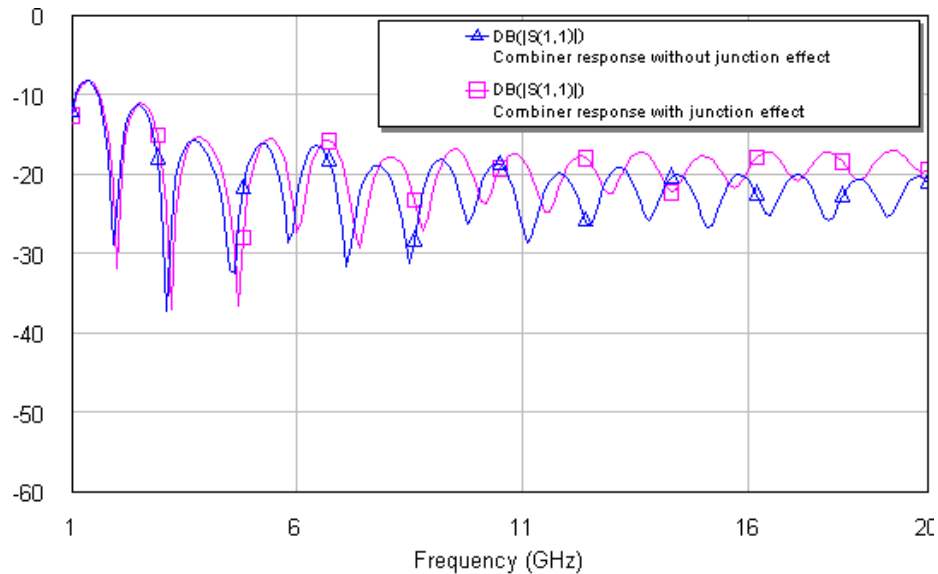


Fig3.16. Combiner response with and without junction effect. The junction is modeled by equivalent circuit model without optimization.

### A full wave junction analysis

The accurate response of the junction can be achieved by using a 3D software simulator like Ansoft HFSS. In this simulation the effect of higher order modes will be accounted and more accurate parameters will be obtained. Fig3.17 shows a view of junction in HFSS environment. In this model eight 100 ohm microstrip lines are connected to a central microstrip disk and the microstrip disk is connected directly to the inner conductor of a coaxial line. The coaxial port is also designed for 12.5 ohm characteristic impedance. The microstrip lines length is equal to 12mm and we add this extra length to draw the structure in HFSS. This extra length only affects on the phase response of the junction and can be compensated by a negative length in future simulation. The simulation result for this junction is shown in Fig3.18. However the junction optimization process will be done in section 3.3.

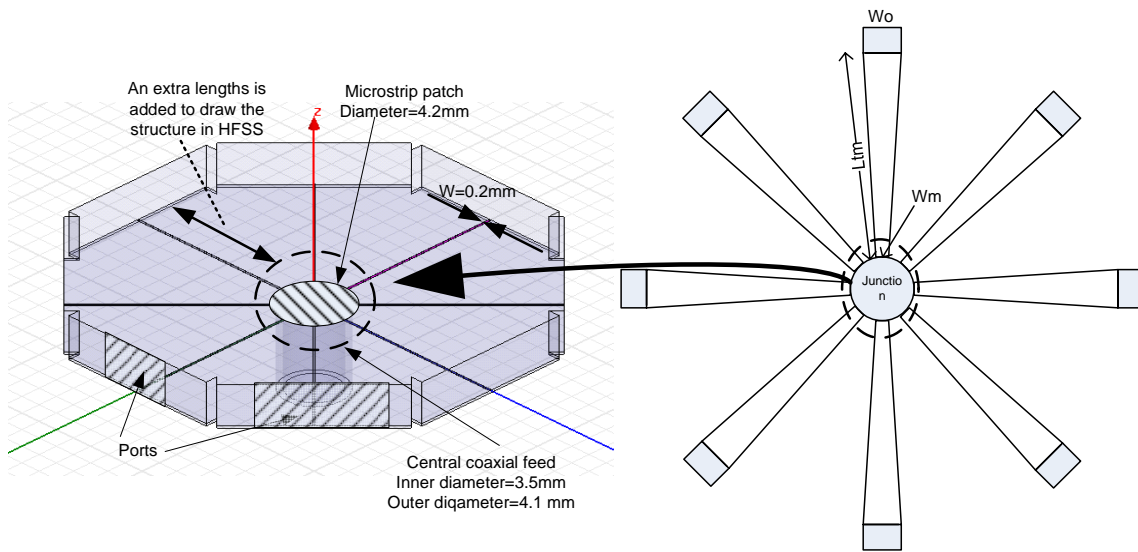


Fig3.17. HFSS model for the junction (left) Radial combiner top view (right).

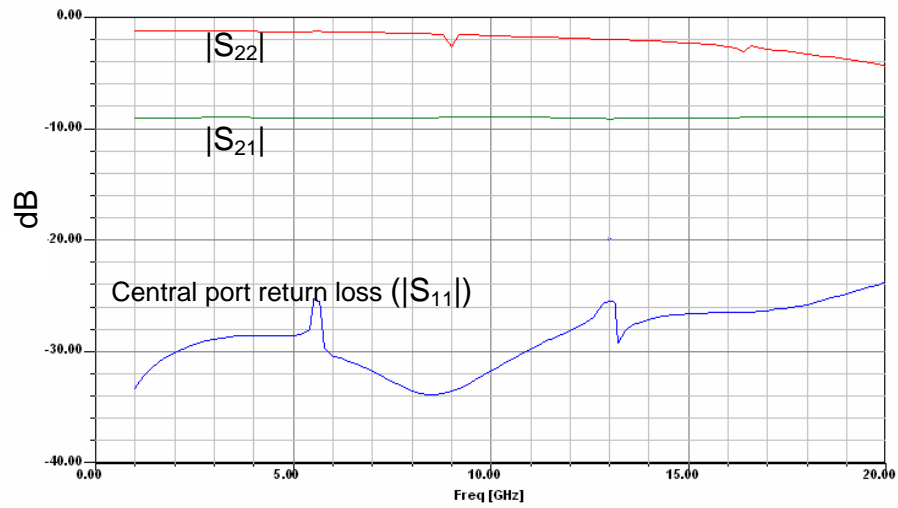


Fig3.18. Full wave simulation results for 8 way junction. Port (1) is considered as central port.

Now from the HFSS simulation results we can derive an accurate scattering matrix for the junction and place this model in the AWR Microwave Office combiner model as shown in Fig3.19. The full wave junction model degrades the ideal combiner response as shown in Fig3.20. This degradation is more noticeable in higher frequencies.

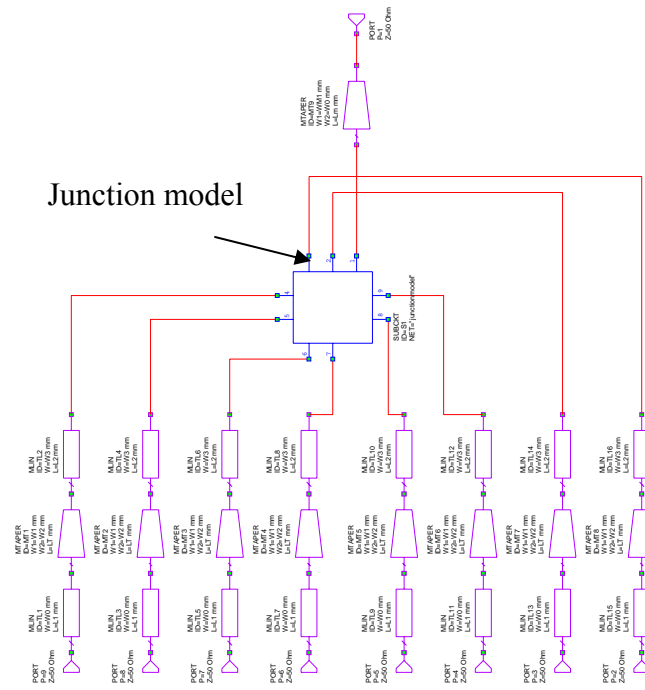


Fig3.19. Full wave junction model is inserted in Fig3.10 circuit.

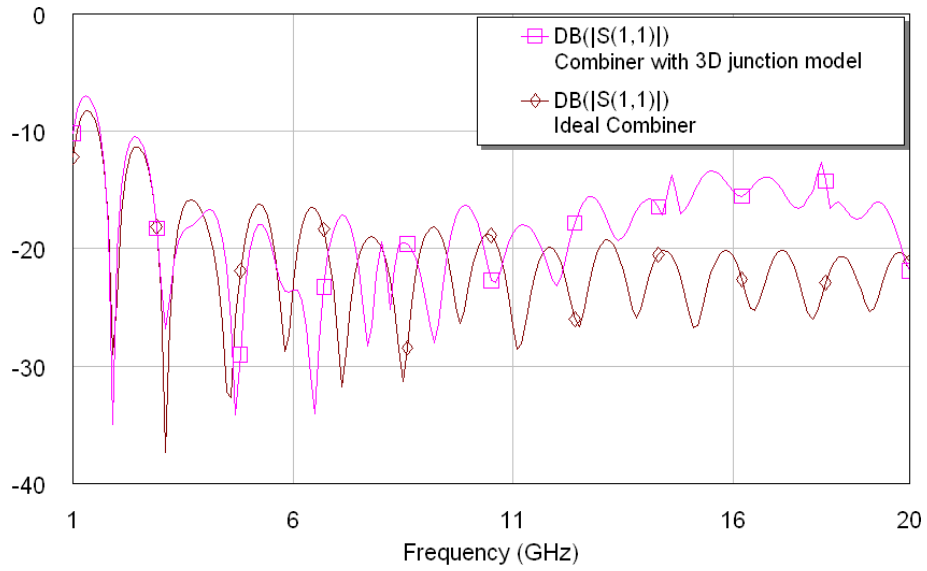


Fig3.20. Comparison between the ideal junction combiner (see Fig3.10) and the combiner with full wave junction model (see Fig3.19).

### 3.2.3 Design of output matching network

We use a coaxial transformer to provide an adequate impedance transformer over frequency range from 2 to 17 GHz. The initial transformer length is not optimum and may lead to a poor input matching due to the effect of junction discontinuity. Therefore a further optimization is necessary to improve the input matching section. We can utilize either the circuit or the HFSS models to implement the optimization analysis.

This section needs a matching network with the ratio of 4 (12.5 ohm to 50 ohm) in a wide frequency range (2~17GHz), so for simplicity a linear taper matching network is suggested as shown in Fig3.21:

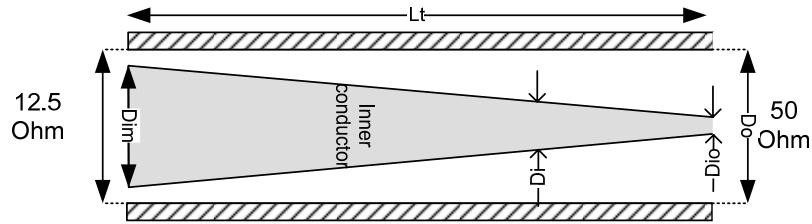


Fig3.21. Linear taper coaxial matching network.

Suppose that “Di” indicates inner diameter and outer diameter (Do) is constant and equal to 4.2mm. The impedance of coaxial line can be calculated from following equation,

$$Z_0 = \frac{1}{2\pi} \sqrt{\frac{\mu}{\epsilon}} \ln \frac{D_o}{D_i} \quad (3-17)$$

Therefore:

For  $Z_0=12.5$  ohm :  $D_{im}=3.5$  mm

For  $Z_0=50$  ohm :  $D_{io}=2$ mm

To achieve a low loss transformer, the dielectric of coaxial line is selected to be air i.e.  $\epsilon_r = 1$ .

We can also use a multi step matching network as shown in Fig3.22. This structure may be easier to fabricate, but for the same matching performance, in the multi step coaxial line we need greater  $L_t$  than the linear taper coaxial line.

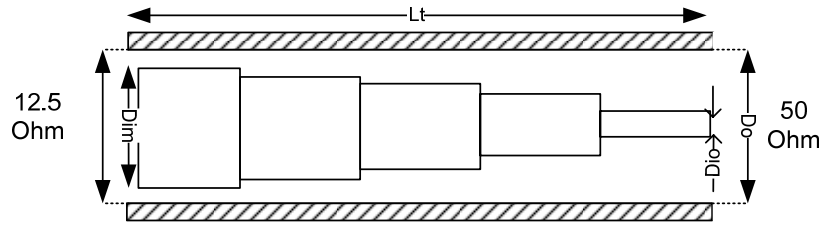


Fig3.22. Multi section impedance matching network.

For example we design two matching networks with equal length; one contains 5 sections and another have the linear taper as shown in Fig3.23. These two matching networks are simulated by HFSS and are compared in Fig3.24. For this case, it is obvious that the linear taper matching has better response compared to the step tapered matching.

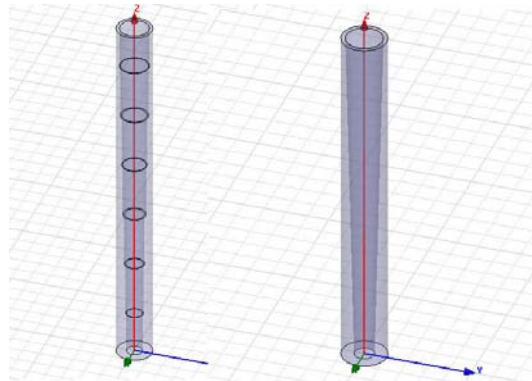


Fig3.23. linearly tapered and step tapered coaxial line with 30mm length.

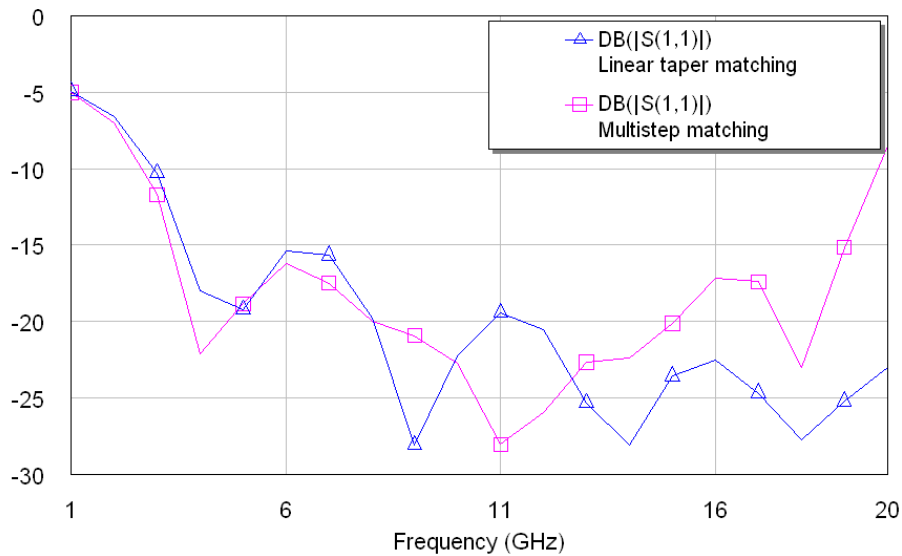


Fig3.24. Comparison between equal length linear and multi step taper coaxial lines.

### 3.3 Total structure Simulation

After the design of the constituting parts, it is necessary to simulate the whole structure. The proposed structure is shown in Fig3.25 . A Teflon transmission line is added right beneath the central microstrip patch to compensate for the junction reactance and also to provide easier mechanical montage. The length of this transmission line will be selected as one of the optimization parameters. To minimize the combiner loss, the length of this Teflon should be remained as low as possible.

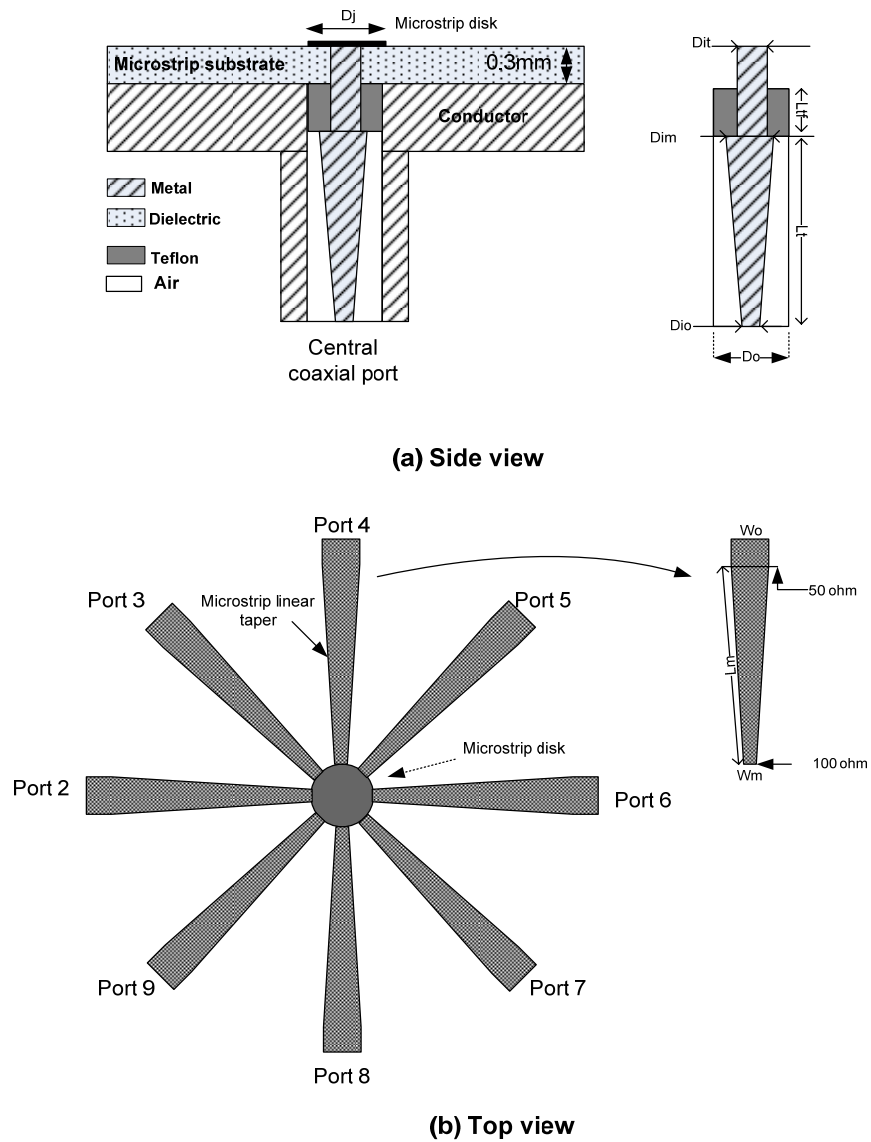


Fig3.25. A drawing of microstrip power combiner with its important parameters.

In our design some parameters are constant and some are variable and are considered as optimization parameters. The constant parameters and optimization parameters are as follow:

Constant dimension:

Microstrip height,  $h=0.305\text{mm}$ , microstrip conductor thickness equal to  $17\ \mu\text{m}$ , coaxial conductors diameter,  $D_{io}=2\text{mm}$ ,  $D_o=4.2\text{mm}$

Variable parameters (optimization parameters) are:

The microstrip taper length:  $L_m$  (The initial value  $L_m=25\text{mm}$ )

The coaxial length with Teflon dielectric:  $L_{tf}$  (The initial value  $L_{tf}=3\text{mm}$ )

The coaxial taper length:  $L_t$  (The initial value  $L_t=30\text{mm}$ )

The central conductor diameter at the junction:  $D_{it}$  (The initial value  $D_{it}=3\text{mm}$ )

The central conductor diameter right beneath Teflon:

$D_{im}$  (The initial value  $D_{im}=3.4\text{mm}$ )

The microstrip patch diameter:  $D_j$  (The initial value  $D_j=4.0\ \text{mm}$ )

Fig3.26 shows the designed combiner in HFSS software. This structure has an axial symmetry and this symmetry can be used to simplify the structure for the faster numerical simulation. Therefore the structure can be reduced to 1/8 as shown in Fig3.27. Using the structure symmetry, the simulation speed increases. Moreover it causes a better numerical convergence. Two perfect H symmetry planes are defined for the reduced structure. These H-plane walls are located in the two sides of the structure. Note that by this simplification we have only a two port network and only the two-port parameters, i.e. ports return loss and the common port coupling, can be calculated. So we can not use this simplified model to derive the other ports response.

### **The combiner Goal**

The most important parameter in the combiners design, with a certain medium and number of ports, is the common port return loss. Although other parameters such as insertion loss and isolation are important but they both depend on the factors; the combiner loss depends on the size and material and also the peripheral ports isolation depend on the number of combiner ports.

Our goal is to have at least 15dB of return loss at the common port. From the analytical calculations we remember that the isolations between peripheral ports for an 8-way

combiner are about 18dB, with each port having a return loss of about 1.5 dB. But the common port can be matched perfectly over our desired bandwidth.

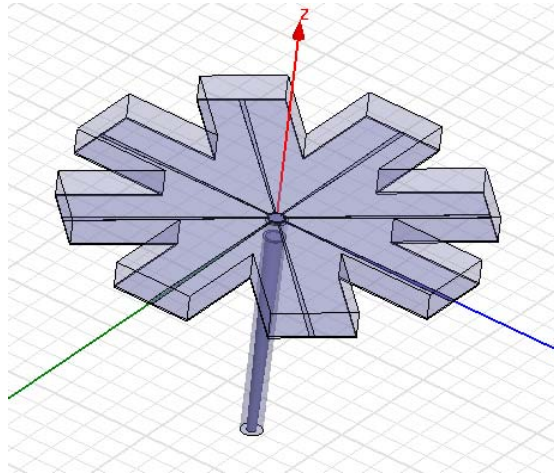


Fig3.26. Microstrip radial power combiner model in HFSS.

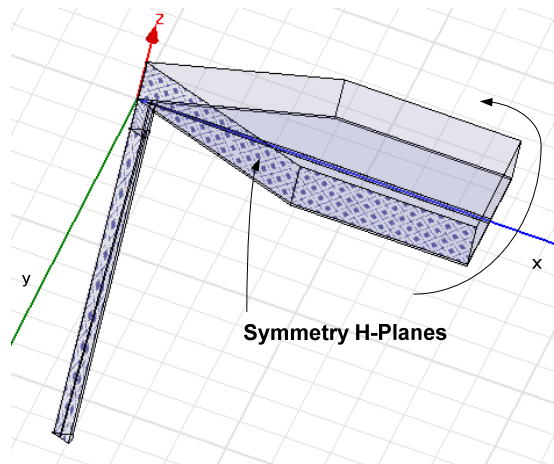


Fig3.27. Simplified structure using H-planes symmetry.

After the optimization process in Ansoft HFSS, following values are obtained.

The microstrip taper length:  $L_m=32$

The Teflon dielectric length:  $L_{tf}=4.25\text{mm}$

The coaxial taper length:  $L_t=41.25\text{mm}$

The central conductor diameter at the junction:  $D_{it}= 3.1$

The central conductor diameter after Teflon:  $D_{im}=3.5$

The microstrip patch diameter:  $D_j=3.9\text{mm}$

Fig3.28 shows the simulation results for the simplified two port structure. The total 9 ports scattering parameters are also simulated and are sketched in Fig3.29 to Fig3.32.

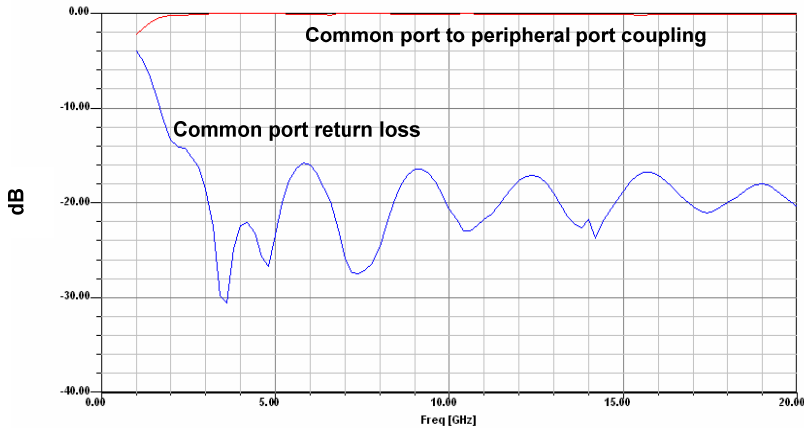


Fig3.28. HFSS simulation results for the simplified structure using H-plane symmetry.

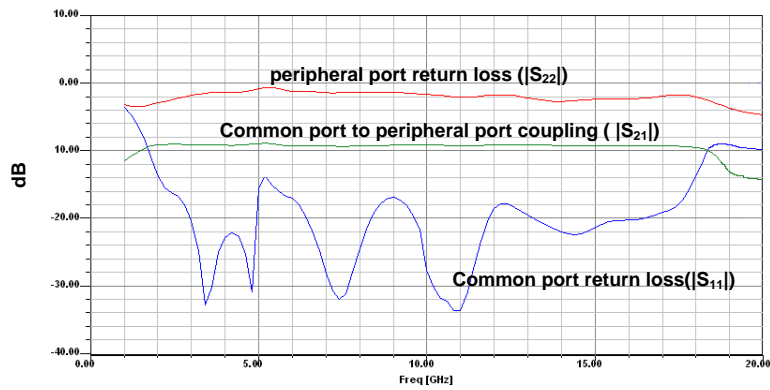


Fig3.29. Complete structure simulation results.

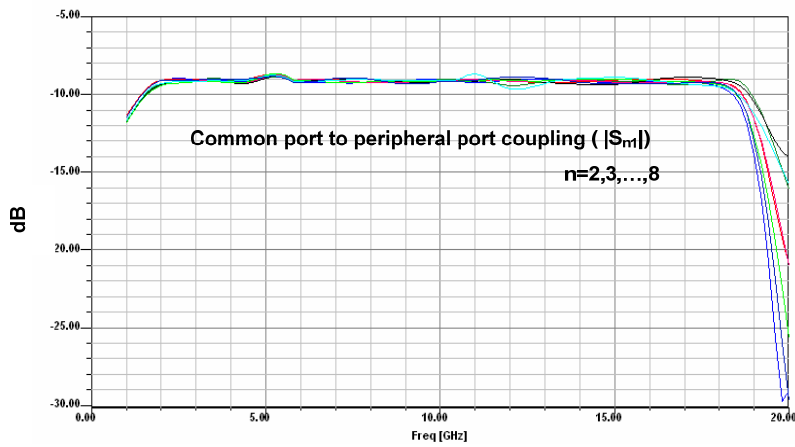


Fig3.30. Common port to other port coupling simulation results. In upper frequency ranges the structure is more sensitive to the HFSS mesh grids and numerical convergence and so there are some differences between the common ports to peripheral ports coupling in frequencies upper than 17 GHz

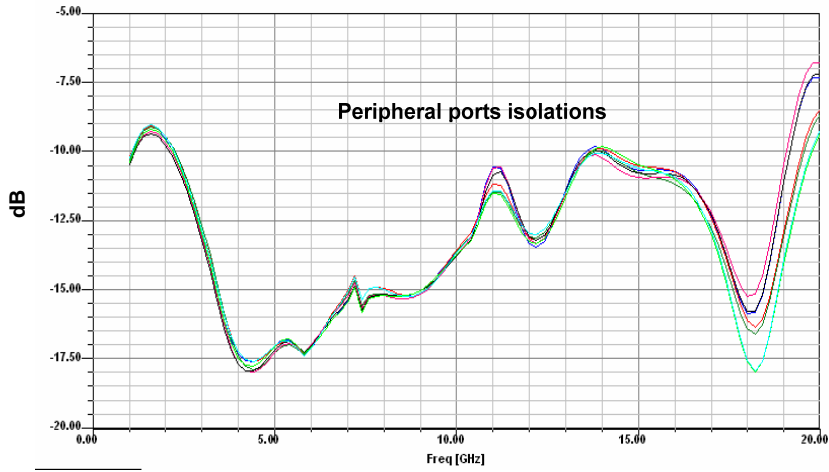


Fig3.31. Ports isolation simulation results ( $|S_{23}|$ ,  $|S_{34}|$ ,  $|S_{45}|$ ,  $|S_{56}|$ ,  $|S_{67}|$ ,  $|S_{78}|$ ,  $|S_{89}|$ ).

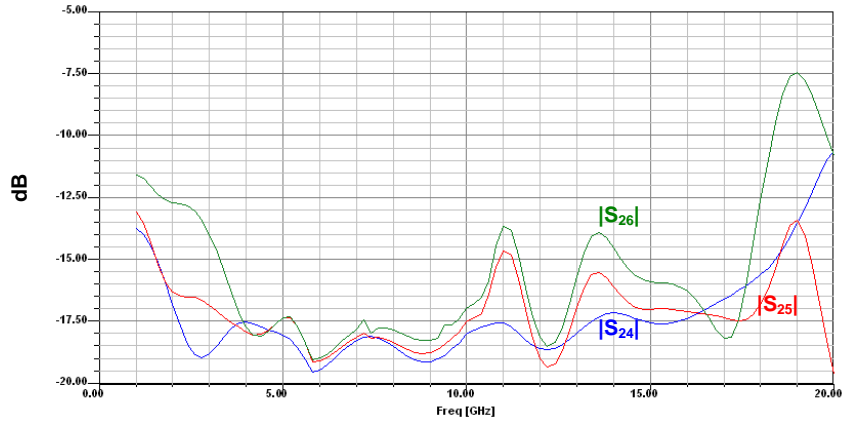


Fig3.32. Port isolation simulation results ( $|S_{24}|$   $|S_{25}|$   $|S_{26}|$ ).

By noting the simulation results and equations in section 3.1, following relations between scattering parameters can be verified, but with approximation,

$$S_{1n}=S_{12}=\beta \quad n=3\sim 9$$

$$S_{n,n+1}=S_{n+1,n+2}=\zeta_{23} \quad n=2\sim 7$$

$$S_{n,n+2}=S_{n+1,n+3}=\zeta_{24} \quad n=2\sim 6$$

$$S_{n,n+3}=S_{n+1,n+4}=\zeta_{25} \quad n=2\sim 5$$

$$S_{n,n+4}=S_{n+1,n+5}=\zeta_{26} \quad n=2\sim 4$$

However in upper frequency ranges the structure is more sensitive to the HFSS mesh grids and numerical convergence and so there are some differences between the common ports to peripheral ports coupling (see Fig3.30) and ports isolation (see Fig3.31) in frequencies upper than 17 GHz.

As the final simulation, it would be helpful to plot electrical fields in the combiner. Fig3.33 represents the electric field in the junction.

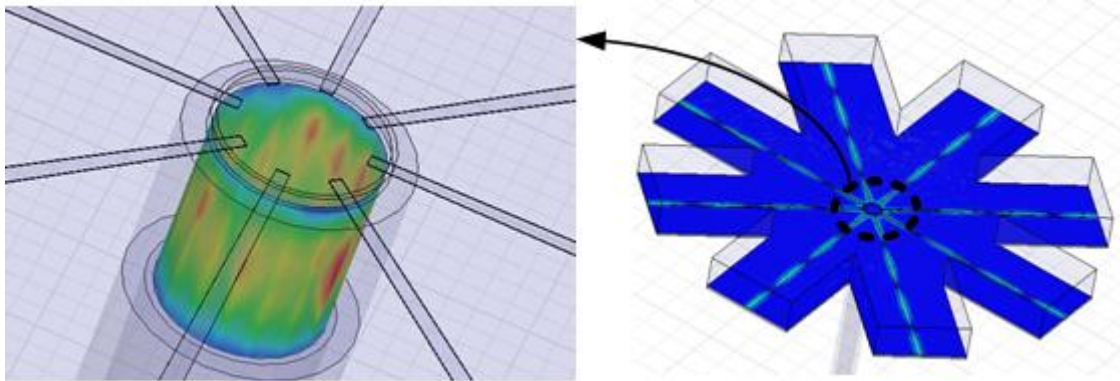


Fig3.33. The magnitude of the electric field in the combiner at 10GHz.

### **3.4 Mechanical structure**

The mechanical structure of the radial power combiner is presented in Fig3.34 and Fig3.35. This mechanical structure contains the launcher section, the combining plate, an upper housing, the coaxial inner conductor, the microstrip substrate and nine SMA connectors. Aluminum is used for this combiner however the inner conductor in the launcher section is made from Brass. Microstrip ground plane can be attached to Aluminum in two different ways; silver epoxy attachment [37] and soldering method. However in the soldering, Aluminum plate needs the silver or gold plating process.

SMA connectors are selected as output and input ports interface. One of the important sections of the combiner is the SMA to microstrip transition. It also should have a broadband behavior. For the better attachment, we used a four-hole version of SMA connector and the contact pad of the SMA connector was modified for better transition. Fig3.36 shows the modified cut on the SMA conductor and Fig3.37 shows the HFSS simulation result for this transition.

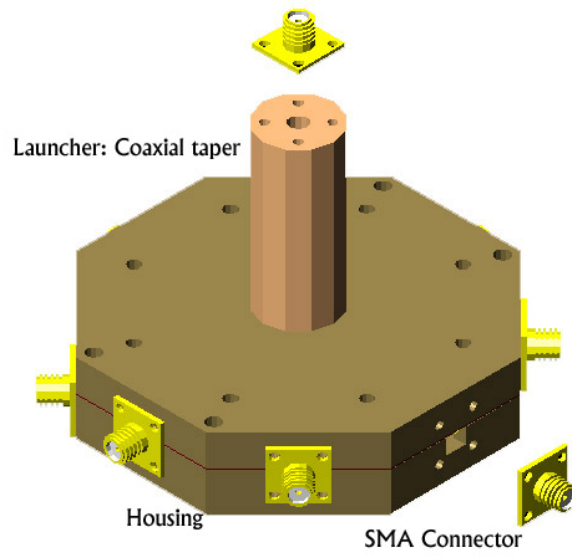


Fig3.34. A view of radial power combiner and its mechanical structure.

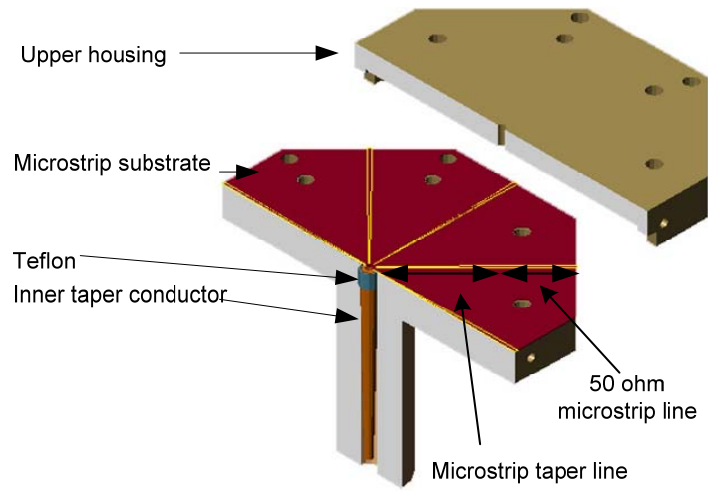


Fig3.35. A cut view of the radial power combiner.

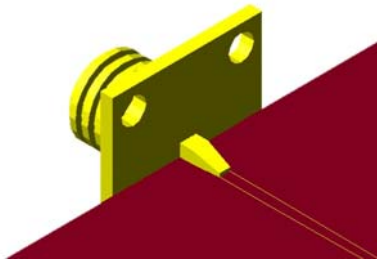


Fig3.36. Modified SMA connector contact to microstrip transition.

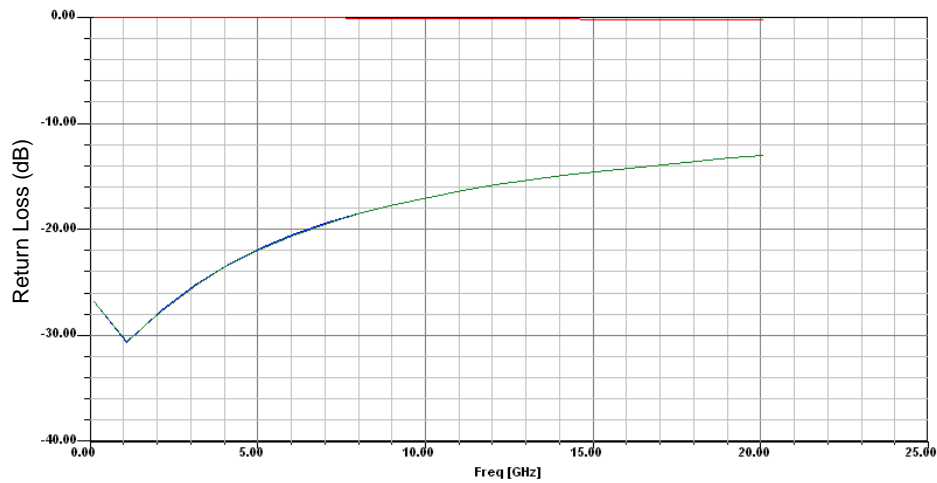


Fig3.37. HFSS simulation results for the modified SMA connector to microstrip transition.

Fig3.38 shows the upper cut view of the combiner. It shows some walls in upper housing. These walls are added to reduce the inner volume of the combiner and consequently decrease the simulation time. These walls also improve attachment strengths.

Fig3.39, Fig3.40 and Fig3.41 are photos of the manufactured microstrip radial power combiner.

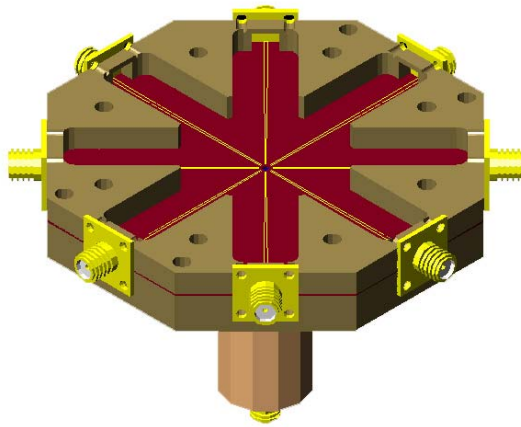
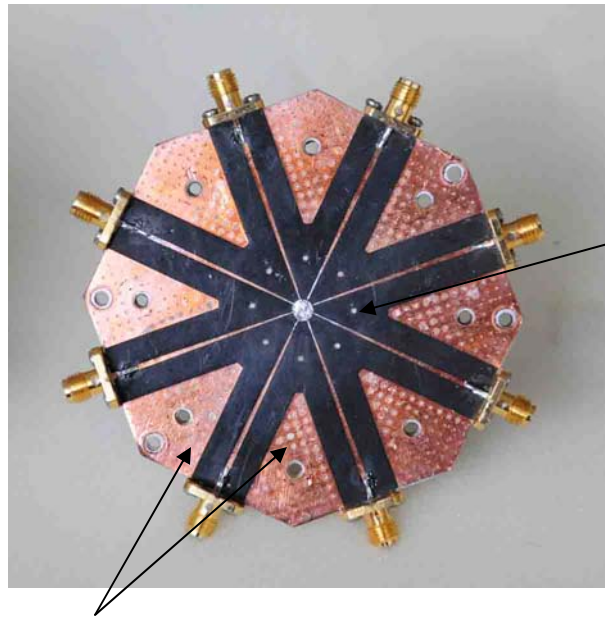


Fig3.38. Walls in the upper housing. This walls help in better attachment.



Walls are placed in these areas.

Fig3.39. Top view of the manufactured microstrip radial power combiner. Holes around the junction are provided to send out extra solder or epoxy in the attachment process.



Fig3.40. Bottom side of the manufactured microstrip radial power combiner.



Fig3.41. Tapered coaxial center conductor used for output matching.

### 3.5 Measurement results

Two identical combiners were manufactured by two different attachment methods. One by soldering and another by the silver epoxy method. The measured return losses are presented here but because of manufacturing tolerances we can not specify which method is better. The results are close to one another and both have relative good return loss, however the one with epoxy presents higher return loss. These combiners are measured from 1 to 20 GHz frequencies, by a HP network analyzer. To measure the common port return loss, the network analyzer was calibrated and connected to the common port. Other ports were connected to broadband match loads. Fig3.42 and Fig3.43 show the measured return loss for both silver epoxy and soldering attachment methods.

The measured minimum common port return loss is around 10 dB. The measurement results could be compared with the simulation results in Fig3.44. Due to the manufacturing tolerances, there are some differences between measured and simulated results.

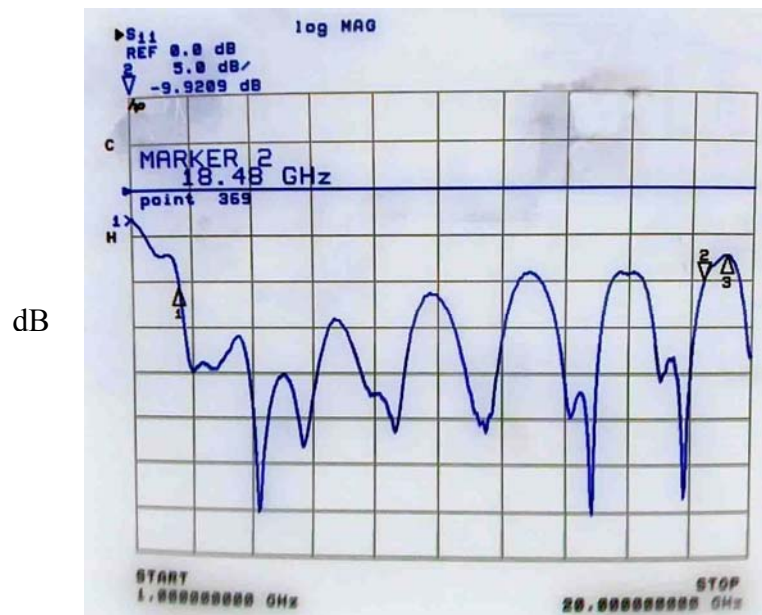


Fig3.42. Common port measured  $|S_{11}|$  in the epoxy attachment method.

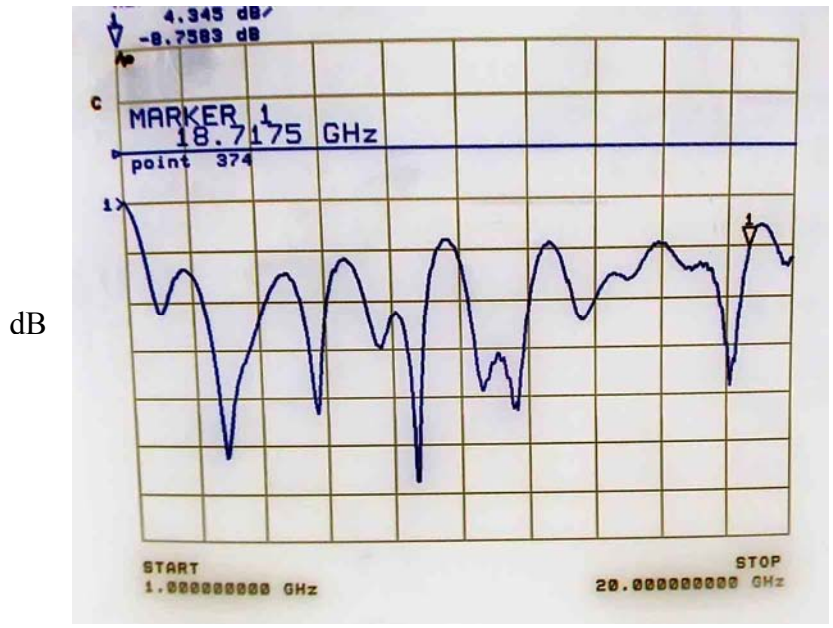


Fig3.43. Common port measured  $|S_{11}|$  in soldering attachment method.

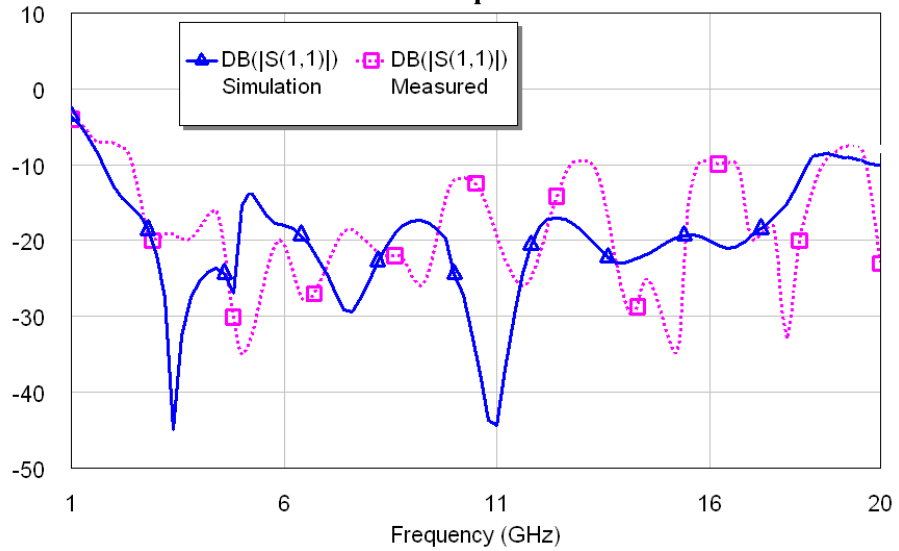


Fig3.44. Comparison between simulated and measured combiner response.

To find a combiner loss, we actually need two identical samples of that combiner. On the other hand, because of the manufacturing and montage tolerances, it is very difficult to build two identical combiners. However, with an approximation, we can connect these combiners back to back like Fig3.45 and measure the combiner insertion loss. In this case, the total loss contains the combiner loss plus the transmission line and SMA connector losses. In other word:

$$L_{Meas} = 2L_{ceff} + L_{coax} + 2L_{SMA} + 2L_{mic} \quad (3-18)$$

Where  $L_{Meas}$  is the measured loss and  $L_{ceff}$  is the effective loss of each combiner and  $L_{coax}$  is the loss for the coaxial transmission lines between two combiners,  $L_{SMA}$  is the loss of SMA connector and finally  $L_{mic}$  is the loss of the extra 50 ohm microstrip lines in the combiner before the linear tapered lines. If we want to integrate a MMIC amplifier into the combiner the extra microstrip line should be removed. Note that the losses before MMIC amplifiers are not critical because it does not affect the combiner efficiency which is why we are interested in the combiner effective loss ( $L_{ceff}$ ). Fig3.46 shows an example of a MMIC amplifier placement in a radial power combiner.  $L_{coax}$  depend on frequency and is between 0.1dB for lower frequencies to 0.5 dB for higher frequencies. Fig3.47 shows the measured insertion loss for two back to back combiners. From the measured result and the equation (3-18), we can write the non-effective combiner loss as follow:

$$L = L_{ceff} + L_{SMA} + L_{mic} \cong 0.5 \text{ dB} \quad 2\text{GHz} < \text{Frequency} < 8\text{GHz}$$

$$L = L_{ceff} + L_{SMA} + L_{mic} \cong 1.5 \text{ dB} \quad 8\text{GHz} < \text{Frequency} < 17\text{GHz}$$

From experimental results,  $L_{SMA} + L_{mic}$  is about 0.1 dB for lower frequencies and 0.5 dB for higher frequencies. Therefore we can write the effective combiner loss as follow:

$$L_{ceff} \cong 0.4 \text{ dB} \quad 2\text{GHz} < \text{Frequency} < 8\text{GHz}$$

$$L_{ceff} \cong 1.0 \text{ dB} \quad 8\text{GHz} < \text{Frequency} < 17\text{GHz}$$

There are also some resonance frequencies in the measured insertion loss. These resonance frequencies may be eliminated by a more accurate montage process.

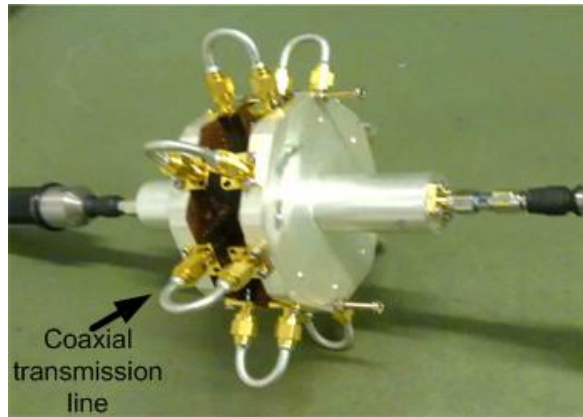


Fig3.45. Two combiners are connected back to back to measure the combiner loss.

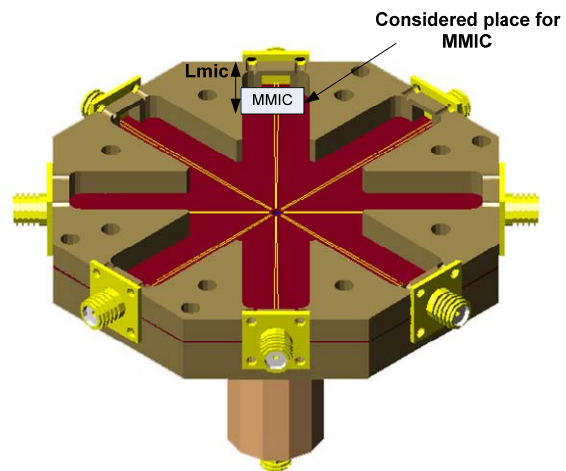


Fig3.46. MMIC placement in combiner.

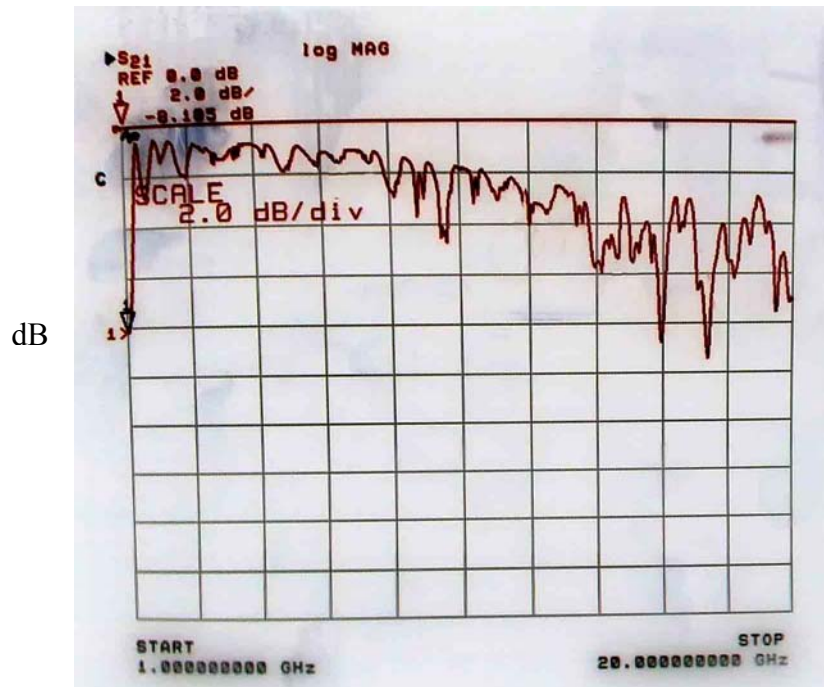


Fig3.47. Measured insertion loss for two back to back combiners.

## 4 Integration of Broadband Amplifiers into the Radial Power Combiner

N-way power combiners can be used in antenna feed systems and power amplifiers. This chapter is devoted to simulating the combination of eight broadband amplifiers with the designed radial power combiner.

### 4.1 Theory of combination

All ports of a lossless radial power combiner cannot be matched simultaneously. In an N-way combiner the common port is designed to be matched and other ports must have equal responses (magnitude and phase) relative to the common port. Although the common port return loss is good enough, poor matching for the other ports may seem undesirable for the input amplifiers. However, in one condition, non-matched ports can not be a problem for the amplifiers. For a deeper view into this matter, consider an N-way symmetric radial combiner as shown in Fig4.1:

We assume that port 1 is matched and there is no input from that port i.e.  $a_1^+ = 0$ , therefore:

$$a_k^- = \sum_{i=2}^N S_{ki} a_i^+ \quad (4-1)$$

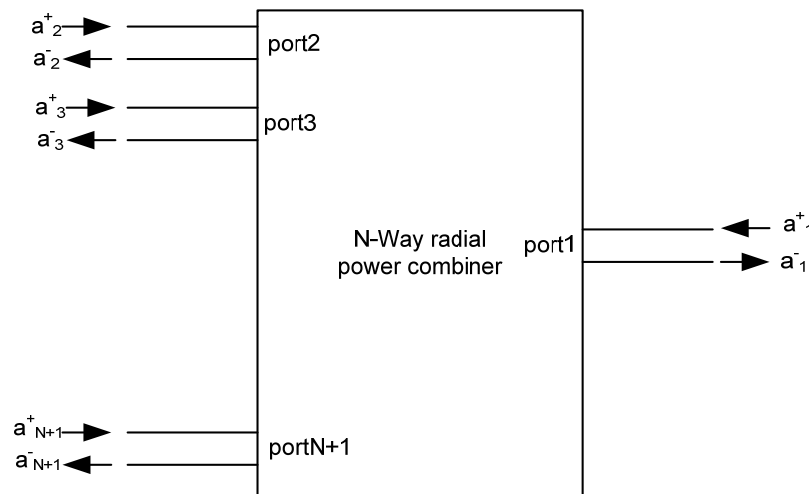


Fig4.1. General radial power combiner network.

Because all ports are in the same phase and same amplitude we can write  $a_i = a_2$ , where  $i=3, 4, \dots, N$ , and consequently,

$$a_k^- = a_2^+ \sum_{i=2}^N S_{ki} \quad k>1 \quad (4-2)$$

On the other hand in the N-way symmetric radial power combiner,  $\sum_{i=2}^N S_{ki} = 0$  [28], and that means  $a_k^- = 0$  i.e. there is no reflection from the other ports and the total power is the sum of the individual input ports.

For example for a 3-way power combiner the s parameter is as follow:

$$S = \frac{1}{3} \begin{bmatrix} 0 & \sqrt{3} & \sqrt{3} & \sqrt{3} \\ \sqrt{3} & 2 & -1 & -1 \\ \sqrt{3} & -1 & 2 & -1 \\ \sqrt{3} & -1 & -1 & 2 \end{bmatrix}$$

As it seen it is obvious that  $S_{22}+S_{23}+S_{24}=0$ .

### **Amplifier Efficiency**

Solid state power amplifiers (SSPA) are superior to tube amplifiers in size and scalability. However, a great challenge for SSPAs is efficiency. Three definitions of efficiency are commonly used. Drain efficiency is defined as the ratio of RF-output power to dc-input power, i.e.,  $\eta=P_o /P_{DC}$ . Power added efficiency (PAE) incorporates the RF-drive power by subtracting it from the output power, i.e.,  $\eta=(P_o-P_i )/ P_{DC}$  . PAE gives a reasonable indication of power amplifier performance when gain is high; however, it can become small for low gains. An overall efficiency such as  $\eta=P_o/(P_{dc}+P_{in})$  is usable in all situations.

Class A, B, AB and C amplifiers are widely used in PA designs, but their drain efficiency only ranges from 50% to around 85% theoretically. Innovative class D, E, and F amplifiers can improve the drain efficiency up to unit ideally.

Although there are some high efficiency class-E amplifier, it is still mandatory to use a class A amplifier for broader bandwidth applications. In the lossless situation, class A amplifiers have a drain efficiency of 50%. However, considering the lossy mechanism

inside the devices and the matching circuit, the power added efficiency is only around 30%. If the combiner has an output combining efficiency of 75%, the amplifier's overall PAE is only a little more than 20%. It means 4 times the output power is wasted in the form of heat. When there is no input signal to the amplifier, 5 times the rated power is converted into heat. A 50-watt output power rated amplifier must have the ability to dissipate more than 250 watt of heat effectively. As a modification, Class B push pull amplifiers will increase the efficiency decently while maintaining broad bandwidth.

### Linearity

Linearity is important for broadband communication systems. A two-tone intermodulation distortion (IMD) measurement is used to evaluate the linearity of the amplifiers. The IMD is a ratio of the strength of the third order component produced by two adjacent fundamental signals to the strength of one of the fundamental signals. The extrapolated cross point of the fundamental and the third order intermodulation component is known as the third order intercept point (IP3) (see Fig4.2). Although the power level of the fundamental carrier can never be equal to that of the third order intermodulation component because of saturation, it is an expression to represent the amplifier's linearity.

Compared to TWTAs that work in the saturation mode, solid-state amplifiers offer better linearity by operating at  $P_{1dB}$  point. To reach an IMD level of  $-25$  dBc (or power ratio of fundamental signal to IMD equal to 25dB), a typical TWTA needs to back off more than 7 dB from the rated single carrier output power. A solid-state amplifier only needs to back off around 2 to 3 dB from  $P_{1dB}$  to reach the same IMD level.

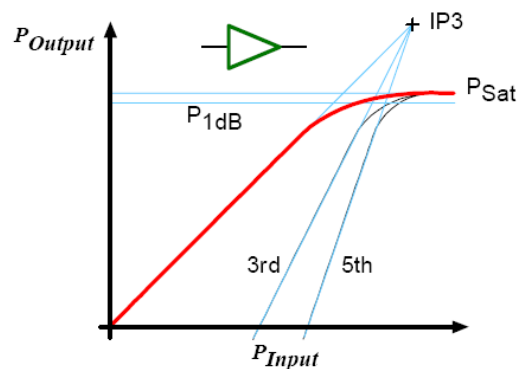


Fig4.2. Output power and harmonics and definition of IP3.

To evaluate the change of the IP3 point in power combining, we need to compare the third order intermodulation component (IM3) of a MMIC amplifier and the combiner. For a MMIC amplifier, we can express the fundamental and IM3 output power as

$$P_{out} = G_m P_{in} \quad (4-3)$$

$$IM3 = A \cdot P_{in}^3 \quad (4-4)$$

Where  $G_m$  is the gain of a MMIC amplifier, and  $A$  is the coefficient for IM3. The output IP3 (OIP3) is the output power at the IP3 point, where the linearly extrapolated fundamental output power  $P_{out} = IM3$ . The OIP3 of a MMIC amplifier is:

$$OIP3_m = \sqrt{\frac{G_m^3}{A}} \quad (4-5)$$

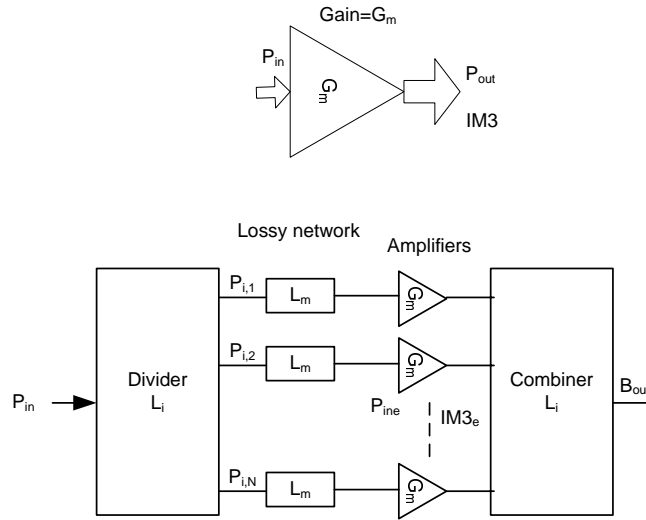


Fig4.3. Linearity analysis for the MMIC amplifier and the combiner.

For a combiner, we have

$$G_c = G_m L_i^2 L_m$$

$$P_{out} = G_c P_{in} = G_m L_i^2 L_m P_{in} \quad (4-6)$$

Where  $L_i, L_m$  are the loss of combiner and matching network respectively as shown in Fig4.3.

For each MMIC amplifier in the combiner, we have

$$P_{in,e} = \frac{P_{in} L_i L_m}{N} \quad (4-7)$$

$$IM3_e = A \cdot P_{in,e}^3 \quad (4-8)$$

Where, N is the number of channels in the combiner. We assume the divider and combiner have the same loss  $L_i$ . The  $IM3_e$  from each MMIC amplifier are added in the same way as the fundamental signal. The sum of the  $IM3_e$  at the output port is expressed in IM3 as

$$IM3 = N \cdot IM3_e \cdot L_i = N \cdot A \cdot P_{in,e}^3 L_i \quad (4-9)$$

Then we have

$$P_{out} = IM3 = N \cdot A \left( \frac{P_{in} L_i L_m}{N} \right)^3 L_i \quad (4-10)$$

$$OIP3_c = N \cdot L_i \sqrt{\frac{G_m^3}{A}} \quad (4-11)$$

Where,  $OIP3_c$  is the OIP3 of the combiner. Comparing equations (4-5) and (4-11), we conclude that

$$OIP3_c = N \cdot L_i \cdot OIP3_m \quad (4-12)$$

For an 8-channel combiner with a  $L_i$  of 1dB, the combiner will have a factor of 8 dB improvement in OIP3 over a MMIC amplifier. We note that the OIP3 has no relationship with the lossy matching network. We will observe the 8 dB improvement no matter whether we use the lossy matching network or not.

## 4.2 Simulations

It is helpful to integrate the measured scattering matrix of the amplifiers and the combiner to have a better estimation for the output power. For this purpose, a broad band amplifier with the part number of HMC463 [3] is selected from Hittite semiconductor.

The HMC463 is a GaAs MMIC PHEMT low noise distributed amplifier which operates between 2 GHz and 20 GHz. The amplifier provides 14 dB of gain, 2.5 dB noise figure and 19 dBm of output power at 1 dB gain compression while requiring only 60 mA from a +5V supply. Fig4.4 shows the gain and return loss for HMC463 die and Fig4.5 shows the measured response for HMC463 with SMA connectors.

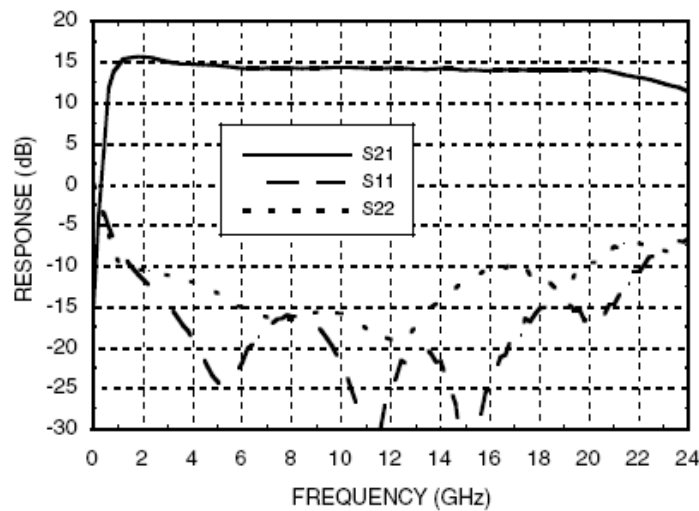


Fig4.4. Gain and return loss for HMC463 (die).

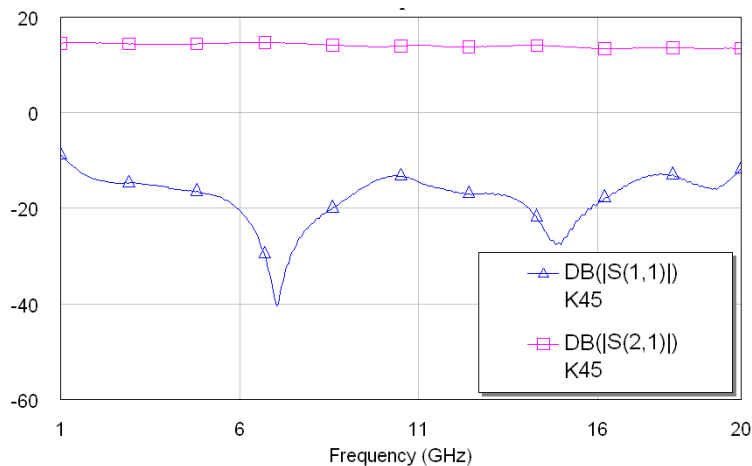


Fig4.5. The measured response for HMC463 with connectors.

Eight amplifier modules that contain one HMC463 each are measured. Responses of these amplifiers are shown in Fig4.6. As it is indicated, the phase and amplitude of eight amplifiers have more differences in higher frequency ranges.

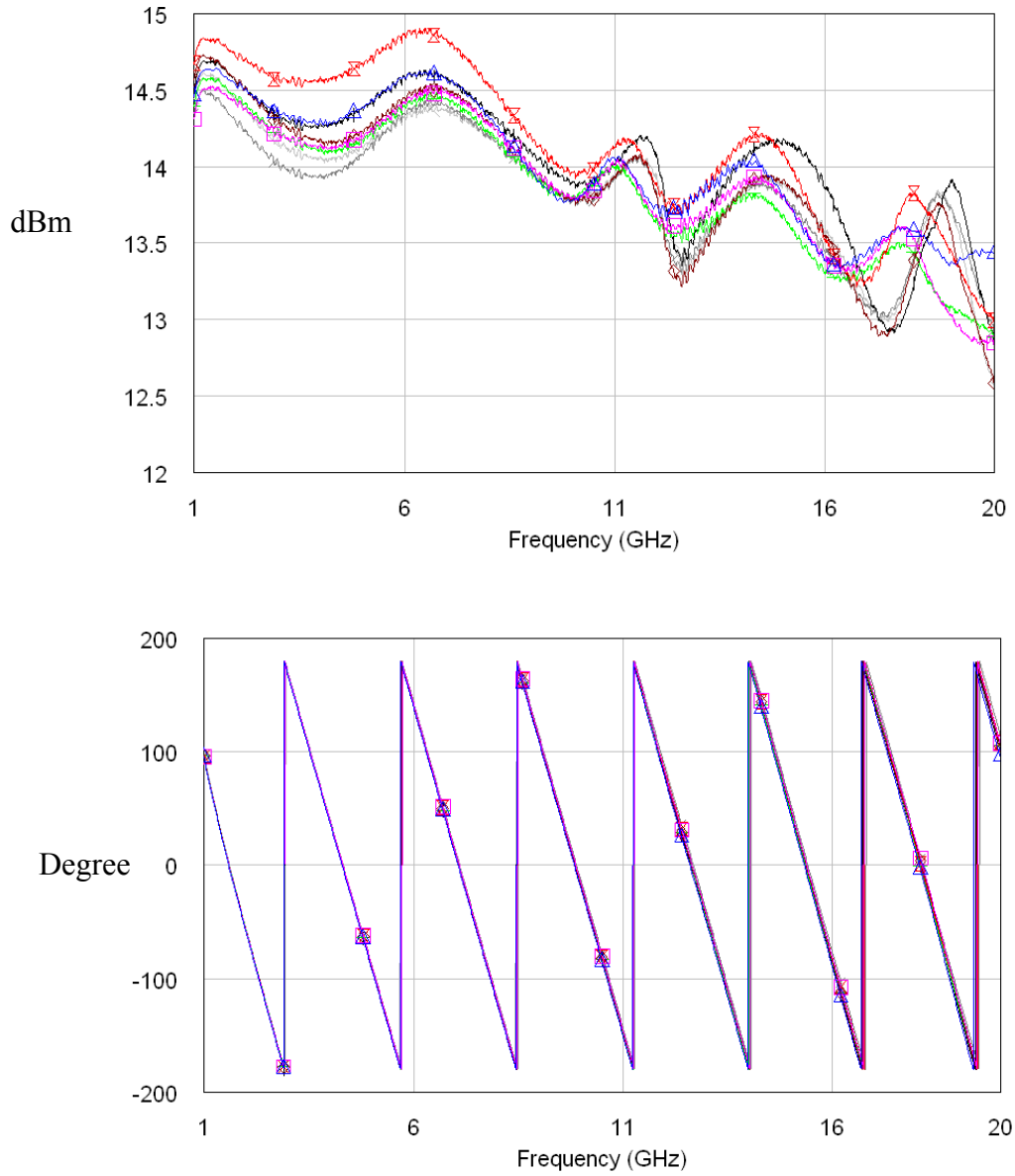


Fig4.6. The measured gain (Amplitude and phase) for eight amplifiers.

### Amplifiers combination in AWR Microwave Office software

To integrate measured amplifier responses into the simulated combiner model, we used the full 3D model of radial power combiner as shown in Fig4.7. The simulation results are sketched in Fig4.8.

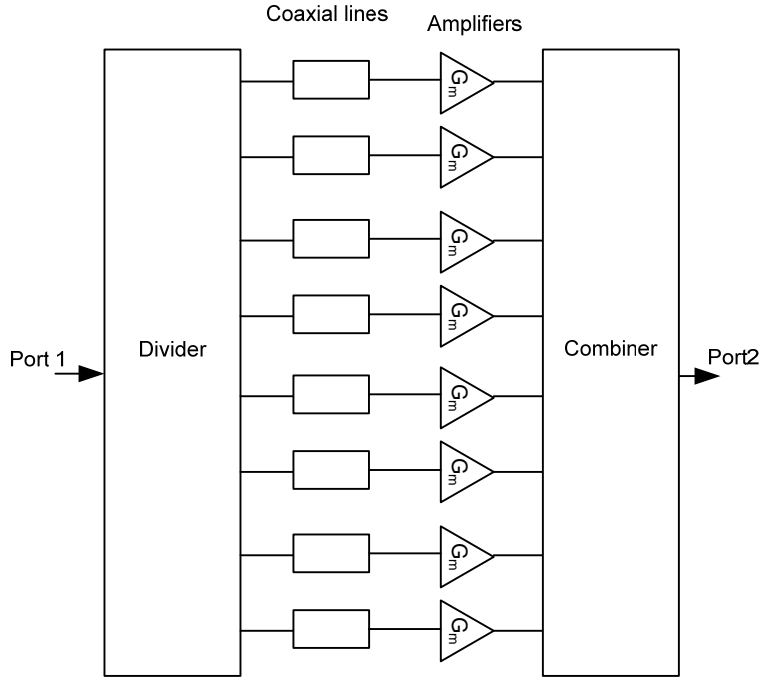


Fig4.7. Eight amplifiers are combined with 3D model of radial power combiner.

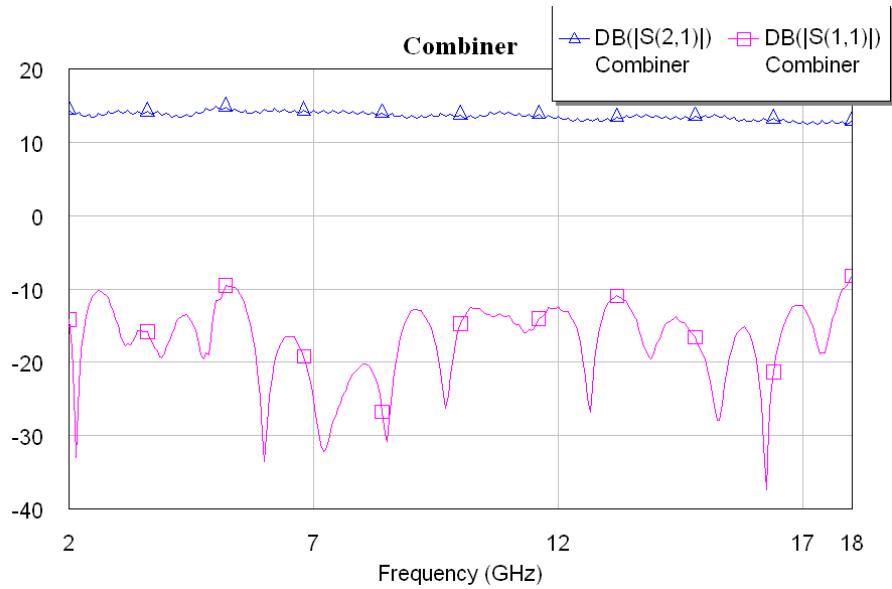


Fig4.8. Simulation results for the combined amplifiers.

Finally we measured the system, in its entirety, which is composed of eight broadband amplifier modules and two radial power combiner/divider. In a more practical situation, the MMIC amplifiers should be placed in the inner part of combiner. However it is useful to connect several modular amplifiers to the main combiner and then measure the system performance. Fig4.9 shows a photo of the composed system and Fig4.10 shows the measured results. The total loss in the proposed test setup includes combiner's loss, coaxial cables loss and the loss from RMS phase error. In Fig4.10, the total system loss has reached 4 dB in the upper frequency range. If we consider 1.5 dB of loss due to each combiner and 0.5 dB of loss due to coaxial line and SMA adaptor then 0.5 dB of losses is related to RMS phase error. However if we shorten the path between the MMIC amplifier and the junction as much as possible the combiner loss can be reduced to 1dB.

The measured maximum power for this system is shown in Fig4.11. For a bandwidth of 2~8 GHz near 1 W (30dBm) of power and in upper frequency range around 0.7 W (28dBm) is achieved.

There are also several resonance frequencies in the output of the system. These resonance frequencies can be created in any amplifier due to the reflection from the output port to the input port especially when interconnections are not matched perfectly. With an accurate montage and also adding absorber inside the combiner, resonance frequencies can be decreased.

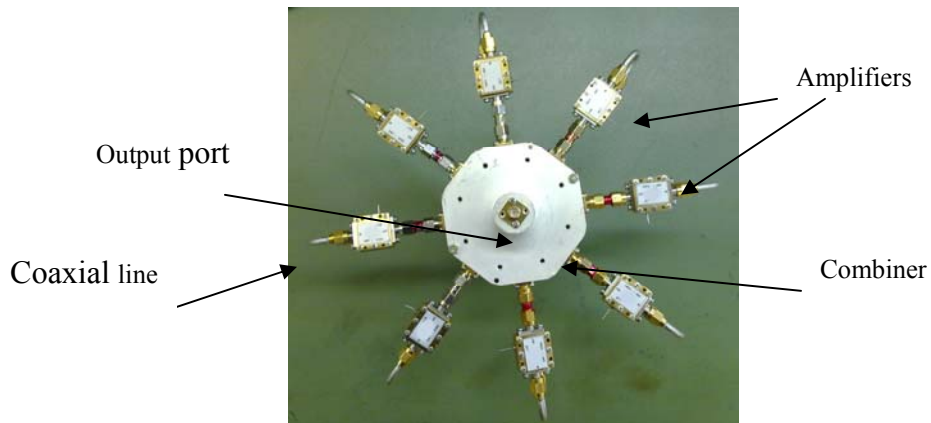


Fig4.9. Eight amplifiers are integrated into radial power combiner. The divider is placed behind the combiner.

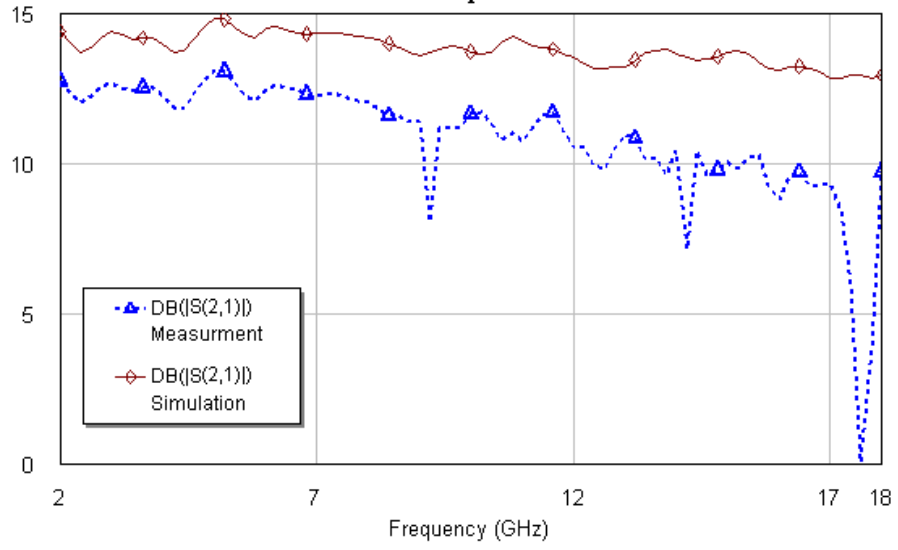


Fig4.10. Comparison between simulated and measured results for eight combined amplifier.

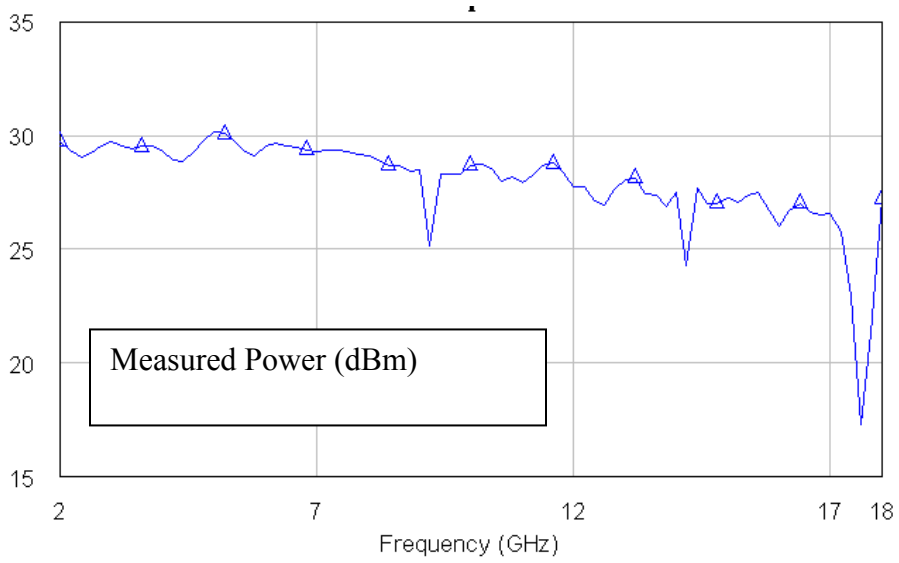


Fig4.11. Measured maximum output power for the combined amplifiers.

## 5 Conclusion

In this thesis, we discussed the modeling, fabrication and measurement results of a microstrip radial power combiner, and demonstrated a successfully realized, compact, highly efficient and low cost broadband power amplifier based on the proposed power combiner.

It is shown that power combining technique by a radial N-way structure is an effective approach to integrate a large quantity of devices over a broad bandwidth with high efficiency. This high power broadband amplifier design will enable industry to shift from traveling tube amplifiers to the solid-state amplifiers.

A simple technique has been presented for designing microstrip radial power combiners. The technique is general and may be applied to the design of similar N –way combiners. Due to the semi-TEM properties of microstrip lines, the design technique is reliable and can be applied to achieve a wide operating bandwidth. This is in contrast to the design of combiners which do not support a TEM transmission mode. Full-wave model optimization of the entire non-TEM structure is normally necessary to obtain wideband operation.

An eight-way microstrip combiner was constructed with excellent wideband performance, as well as having low loss. The structure is compact and lightweight and, therefore, is ideally suited for low cost applications. The measured return loss and insertion loss is better than 10dB and 1.5dB, respectively, over the full bandwidth.

These combiners are used to combine 8 broadband amplifiers to produce an output power around 0.7W. Moreover, if amplifiers are incorporated into the combiner the efficiency will be increased even more. In a further step, these amplifiers can be integrated inside the combiner. As another improvement, it is possible to use other optimized tapered forms instead of the linear tapered structures in the microstrip line and output coaxial line. Also, using a precise K connector, instead of ordinary SMA connector, increases the frequency bandwidth.

## Appendix A

Conical radial power combiner is one of our candidates for a broadband radial power combiner. This structure is compact and has high efficiency and in the first step we tried to make some modification on this structure [16]. In the modified structure, we used tapered excitation probes and tapered side walls as shown in Fig 5.2. Due to the abrupt transition between the input and the conical line, the bandwidth could not be extended as was desired and consequently we tried another configuration. In Fig 5.3, the simulation results are compared for both the original and the modified combiners.

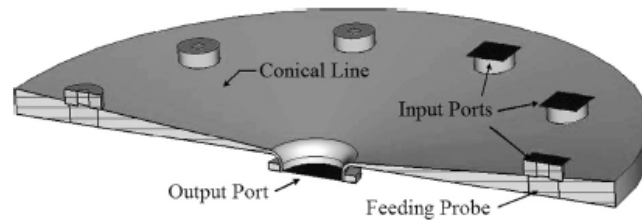


Fig 5.1. The original conical radial power combiner [16].

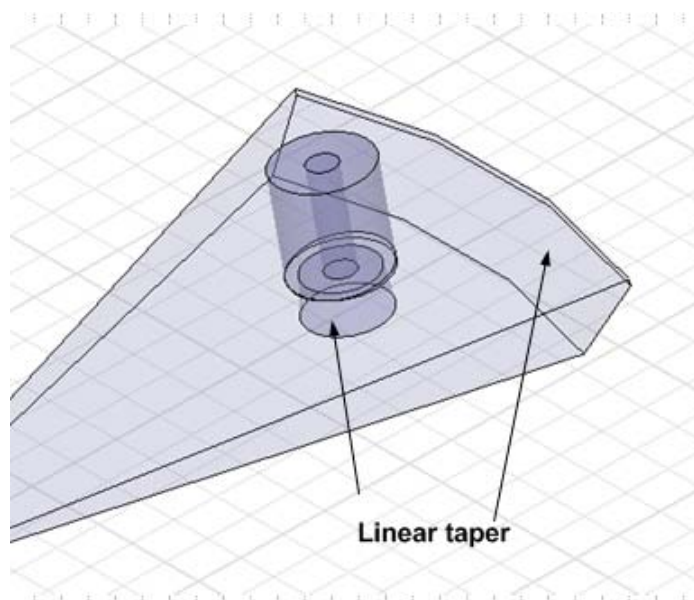


Fig 5.2. The modified conical radial power combiner.

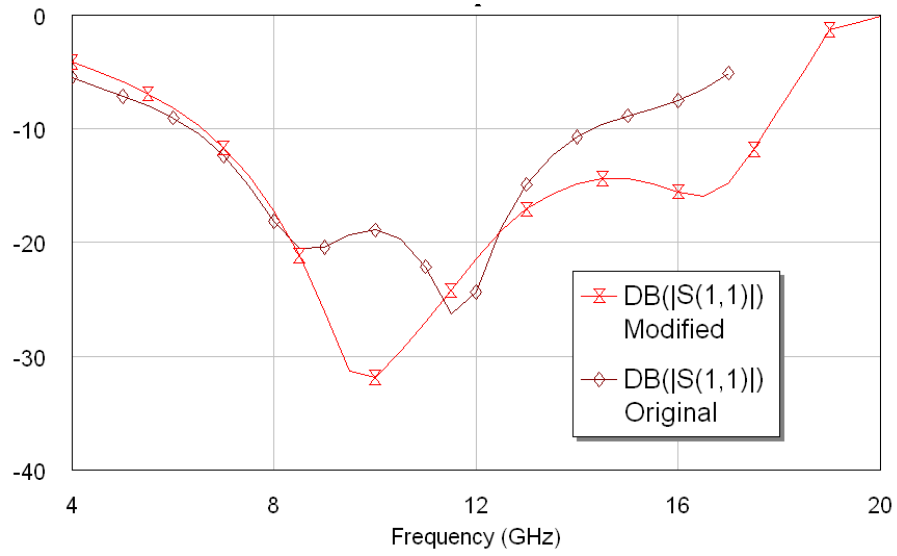


Fig 5.3. Simulation results for the original and the modified conical radial power combiner.

## References

- [1] Jia. P. CAP wireless Inc, "A 2 to 20 GHz high power amplifier using spatial power combining techniques" ,Microwave Journal, April 2005
- [2] J.W.Gewartowski , H.A.Watson "Principle of electron tubes " D.Van Nostran company, New York , 1966
- [3] K. J. Russel, "Microwave power combining techniques," IEEE Trans. Microwave Theory Tech., vol. MTT-27, no. 5, p. 472, May 1979.
- [4] M. Cicolani - A. Panariello , "Novel design technique for radial power combiners" European Microwave Conference, Oct 2000
- [5] P. Khan, L. Epp and A. Silva1, "A Ka-Band Wide-Bandgap Solid-State Power Amplifier", IPN Progress Report 42-163, November 15, 2005
- [6] E. Wilkinson, "An N-way hybrid power divider," IRE Trans. Microwave Theory Tech., vol. MTT-8, p. 116, Jan. 1960.
- [7] U. H. Gysel, "A new N-way power divider/combiner suitable for high-power applications, " in Proc. 1975 IEEE- MTT- S Int. Microwave Symp., IEEE Cat. No. 75CH0955-5, p. 116. May 1975.
- [8] N. Nagai et al., "New N-way hybrid power dividers", IEEE Trans. Microwave Theory Tech., vol. MTT-25, p. 1008, Dec. 1977.
- [9] Z. Galani and S. J. Temple. "A broadband planar N-way combiner/divider", IEEE MTT- S Int., Microwave Symp. June 1977.

- [10] A. E. Fathy, S.-W. Lee, and D. Kalokitis, "A simplified design approach for radial power combiners", IEEE Trans. Microwave. Theory Tech., vol. 54, no. 1, p. 247, Jan. 2006.
- [11] Lin Li and Ke Wu," Integrated Planar Spatial Power Combiner", IEEE Trans. Microwave Theory Tech. vol. 54, No. 4, p. 1470, April 2006
- [12] C. T. Rucker, "A multiple-diode high-average power avalanche-diode oscillator," IEEE Trans. Microwave Theory Tech., vol. MTT- 17, p. 1156, Dec. 1969.
- [13] K. Kurokawa, "An analysis of Rucker's multi device symmetrical oscillator", IEEE Trans. Microwave Theory Tech., vol. MTT- 18, p. 967, Nov. 1970.
- [14] J. M. Schellenberg and M. Cohn, "A wideband radial power combiner for FET amplifiers", IEEE Int. Solid State Circuits Conf., Dig. Tech. Papers, Feb. 1978.
- [15] Kaijun Song, Yong Fan, and Yonghong Zhang," Eight-Way Substrate Integrated Waveguide Power Divider With Low Insertion Loss", IEEE Trans. Microwave. Theory Tech., vol. 56, no. 6, p. 1473, June. 2008.
- [16] Dirk I. L. de Villiers, PieterW. "Design of Conical Transmission Line Power Combiners Using Tapered Line Matching Sections", IEEE Trans. Microwave. Theory Tech., vol. 56, no. 6, p.1478, June. 2008.
- [17] M. D. Abouzahra and K. C. Gupta, "Multiple-port power divider/combiner circuits using circular microstrip disk configurations", IEEE Trans. Microwave Theory Tech., vol. MTT-35, p. 1296, Dec. 1987.
- [18] Sushim Mukul Roy, Isaac Balbin, "Novel N - way Power Divider and Array configuration for RFID Readers operating at 5.8 GHz", 2008 IEEE International Conference on RFID ,The Venetian, Las Vegas, Nevada, USA, April 16-17, 2008

[19] Yung-Jinn Chen Ruey-Beei Wu, “A wide band multiport planar power divider design by radially combining matched sectorial components”, IEEE MTT- S Int., Microwave Symp. June 1997.

[20] CHENG Haifeng, ZHANG bin, “Design of C-Band Improved Radial Power Combiner” 9<sup>th</sup> international on solid state and integrated circuit technology, ICSICT, Oct 2008

[21] P. Jia, L.-Y. Chen, A. Alexanian, and R. A. York, “Multioctave spatial power combining in oversized coaxial waveguide”, IEEE Trans. Microwave Theory Tech., vol. 50, p. 1355, May 2002.

[22] Kim, M., “A grid amplifier”, IEEE Microwave and Guided Wave Letters, vol. 1. No.11, p.322. Nov.1991.

[23] J. Harvey ,E.R. Brown, D.B. Rutledge, R.A. York, “Spatial Power Combining for High power transmitter”, IEEE microwave magazine, p. 48, December 2000

[24] N.-S. Cheng, P. Jia, D. B. Rensch, and R. A. York, “A 120-W X-band spatially combined solid-state amplifier”, IEEE Trans. Microwave Theory and Techs., vol. 47, p. 2561, Dec1999

[25] CAP wireless Ins. , [www.capwireless.com](http://www.capwireless.com)

[26] H. Kagan, “N-Way power divider,” IRE Trans. Microwave Theory Tech., vol. MTT-9, p. 198, Mar. 1961.

[27] c. G. Montgomery, R. H. Dicke and E. M. Purcell, “Principles of Microwave Circuits” New York: McGraw-Hill, 1948, ch. 12.

- [28] Eric L. Holzman, "An Eigenvalue Equation Analysis of a Symmetrical Coax Line to N-Way Waveguide Power Divider", IEEE Trans. Microwave Theory Tech., vol. 42, p. 1162, July 1994
- [29] W. C. Chew and J. A. Kong, "Effects of fringing fields on the capacitance of circular microstrip disk", IEEE Trans. Microwave Theory Tech., vol. MTT-28, p. 98. Feb. 1980
- [30] K. C. Gupta et al., "Computer-Aided Design of Microwave Circuits". Dedham MA: Artech House, 1981, p. 249.
- [31] Marek E. Bialkowski, Vesa P. Waris," Electromagnetic Model of a Planar Radial-Waveguide Divider/Combiner Incorporating Probes", IEEE Trans. Microwave Theory Tech., vol. 41, NO. 6/7, p. 1126, July 1993
- [32] A. G. Williamson, "Radial line/coaxial line stepped junction", IEEE Trans. Microwave. Theory Tech., vol. MTT-33, no. 1, p. 56, Jan. 1985.
- [33] Pengcheng Jia, Lee-Yin Chen, Angelos Alexanian, Robert A. York, "Broad-Band High-Power Amplifier Using Spatial Power-Combining Technique", IEEE Trans. Microwave Theory Tech., vol. 51, No.12, p. 2469, Dec 2003
- [34] York, R.A., "Some considerations for optimal efficiency and low noise in large power Combiners", IEEE Trans. Microwave Theory Tech., vol42, No.8,. p. 1477, Aug 2001
- [35] L. D'Addario, "Combining Loss of a Transmitting Array due to Phase Errors", The Interplanetary Network Progress Report, 42-175, Nov2008
- [36] David M. Pozar, "Microwave Engineering" second edition, John Wiley 1998, p 161.

[37] Panacol-Elosol GmbH, “Elecolit 325 technical datasheet “ ,  
[http://www.panacol.de/fileadmin/panacol/pdf\\_en/pdf\\_elektronik\\_en/el325\\_gb.pdf](http://www.panacol.de/fileadmin/panacol/pdf_en/pdf_elektronik_en/el325_gb.pdf)

[38] Hittite Microwave Corporation, “HMC 463 datasheet”,  
[http://www.hittite.com/content/documents/data\\_sheet/hmc463.pdf](http://www.hittite.com/content/documents/data_sheet/hmc463.pdf)